Title
Effects of collisions and finite length on plasma waves in a single-species plasma column

Author
Anderson, Michael Wesley

Publication Date
2011

Peer reviewed|Thesis/dissertation

UNIVERSITY OF CALIFORNIA, SAN DIEGO

Effects of Collisions and Finite Length on Plasma Waves in a Single-Species Plasma Column

A Dissertation submitted in partial satisfaction of the
Requirements for the degree Doctor of Philosophy

in

Physics

by

Michael Wesley Anderson

Committee in charge:

Professor Thomas O'Neil, Chair
Professor Salah Baouendi
Professor Daniel Dubin
Professor Clifford Surko
Professor George Tynan

2011

The Dissertation of Michael Wesley Anderson is approved, and it is acceptable in quality and form for publication on microfilm:

Chair

University of California, San Diego

2011

TABLE OF CONTENTS

LIST OF FIGURES

ACKNOWLEDGEMENTS

I would like to thank my advisor, Tom O'Neil, for his generous involvement in my research. I always felt welcome in seeking his guidance, and it was often inspiring to watch Tom go to town on his whiteboard. What impressed me most was his ability to keep the ball rolling by pursuing one idea after another with intense focus, only resting his brain occasionally to ask me about surfing or pass on some physics lore. I hope that some of Tom's tenacious approach to problem-solving has rubbed off on me. It was fun working together.

My research also benefitted from many enlightening interactions with other members of UCSD's nonneutral plasma group. Dan Dubin was recruited to many discussions with Tom and me, and I appreciated his fresh insights and lucid explanations. I also enjoyed learning Mathematica from his book. Francois Anderegg took pains to explain experimental procedure to me and always treated me as an equal. Fred Driscoll patiently walked me through computer code and operating system issues and did his best to make sure I wasn't getting too comfortable in theoryland. Eric Bass helped me around many Mathematica-related obstacles. Jo Ann Christina did a lot of behind-the-scenes work booking flights and hotels for conferences and submitting abstracts.

I would also like to thank Roy Gould at Caltech for taking an interest in my research and for sharing some valuable thoughts.

In addition, I would like to thank the members of my thesis committee, Tom O'Neil, Dan Dubin, Salah Baouendi, Cliff Surko, and George Tynan, for their time and feedback.

Finally, I would like to thank my friends and family. Research has been a bit of an emotional rollercoaster for me, and I might not have made it to this point without these people. To Jack Quinn, Scott Stambach, and Zak Rangwala, thanks for taking my mind off of my work during frustrating times. Thanks to my parents, Austin and Marilyn, for their constant support, frequent pep talks, and sound advice. To my wife, Rae, thanks for being so unconditionally supportive, for inspiring me, and for brightening up each day.

Chapter 2, in part, is a reprint of the material as it appears in Physics of Plasmas. M. W. Anderson and T. M. O'Neil, *Physics of Plasmas* **14**, 052103 (2007). The dissertation author was the primary investigator and author of this paper.

Chapters 1, 3, and 4, in part, are a reprint of the material as it appears in Physics of Plasmas. M. W. Anderson and T. M. O'Neil, *Physics of Plasmas* **14**, 112110 (2007). The dissertation author was the primary investigator and author of this paper.

Some of the material in Chapter 5 is in preparation for publication. The dissertation author was the primary investigator and author of this material.

VITA

2003 Bachelor of Science, University of California, Los Angeles

2005 Master of Science, University of California, San Diego

2011 Doctor of Philosophy, University of California, San Diego

PUBLICATIONS

M. W. Anderson, T. M. O'Neil, D. H. E. Dubin, and R. W. Gould. "Degenerate mixing of plasma waves on a cold, finite-length, single-species plasma column." (*in preparation*)

M. W. Anderson and T. M. O'Neil. "Collisional damping of plasma waves on a pure electron plasma column." *AIP Conference Proceedings* **1114**, 114 (2009).

M. W. Anderson and T. M. O'Neil. "Collisional damping of plasma waves on a pure electron plasma column." *Physics of Plasmas* **14**, 112110 (2007).

M. W. Anderson and T. M. O'Neil. "Eigenfunctions and eigenvalues of the Dougherty collision operator." *Physics of Plasmas* **14**, 052103 (2007).

FIELDS OF STUDY

Major Field: Physics

Studies in Classical Mechanics
Professor Patrick Diamond

Studies in Classical Electrodynamics
Professor Thomas O'Neil

Studies in Quantum Mechanics
Professor Aneesh Manohar

Studies in Mathematical Physics
Professor Donald Fredkin

Studies in Statistical Mechanics
Professor Terrence Hwa

Studies in Plasma Physics
Professors Thomas O'Neil and Patrick Diamond

Studies in General Relativity
Professor Kenneth Intriligator

Studies in Quantum Field Theory
Professors Julius Kuti and Benjamin Grinstein

Studies in Nonlinear Dynamics
Professor Henry Abarbanel

Studies in Renormalization Group Theory
Professor Terrence Hwa

ABSTRACT OF THE DISSERTATION

Effects of Collisions and Finite Length on Plasma Waves in a Single-Species Plasma Column

by

Michael Wesley Anderson

Doctor of Philosophy in Physics

University of California, San Diego, 2011

Professor Thomas M. O'Neil, Chair

This dissertation discusses the effects of collisions and finite plasma length on Trivelpiece-Gould waves on a magnetized, single-species plasma column. Starting from Poisson's equation and a drift-kinetic equation with an energy- and momentum-conserving Fokker-Planck collision term, a dispersion equation is obtained for an azimuthally symmetric wave on an infinitely long column. The dispersion relation includes the effect of velocity-scattering collisions with impact parameters less than the cyclotron radius and recovers Landau damping as collisionality approaches zero. For wavenumbers such that $(k\lambda_D) << 1$—where $k \equiv (k_z^2 + k_\perp^2)^{1/2}$ is the total

wavenumber, k_z and $k_\perp$ are the wavenumbers along and transverse to the magnetic field, and λ_D is the Debye length—Landau damping is exponentially small, and the complex frequency of the wave is approximately $\omega \cong (k_z\omega_p / k)[1 + (3/2)(k\lambda_D)^2 \times$ $\times(1 + 10i\alpha/9)/(1 + 2i\alpha)]$, where ω_p is the plasma frequency, $\alpha \equiv k\nu_D/(k_z\omega_p)$ is a collisionality parameter, and ν_D is the collision frequency. When the Debye length is larger than the cyclotron radius, long-range interactions between particles on different field lines are also significant but cannot be treated by a Fokker-Planck collision operator. Fluid theory provides a simpler context for incorporating these long-range interactions, since their primary effect is the enhancement of transport across the magnetic field. Fluid analysis reveals that the damping rate obtained from kinetic theory corresponds to bulk viscosity and that viscous relaxation of radial shear in the parallel flow, due to long-range collisions, gives an important additional contribution to the damping rate. Lastly, azimuthally symmetric normal modes are calculated for a cold, finite-length plasma column. The dispersion equation $\omega = k_z\omega_p/(k_z^2 + k_\perp^2)^{1/2}$ for Trivelpiece-Gould waves on a cold, strongly magnetized plasma has the property that two waves with wavenumbers $(k_z, k_\perp)$ and $(k_z', k_\perp')$ have the same frequency if $k_z/k_\perp = k_z'/k_\perp'$. Such degenerate waves are mixed upon reflection at the ends of the plasma column, and consequently each normal mode involves many such waves. The modes often exhibit sharp features along resonance cones with slope $dz/dr = \pm(\omega_p^2/\omega^2 - 1)^{1/2}$.

Chapter 1

Background and Summary of Results

This dissertation presents theoretical studies of plasma waves—more precisely, Trivelpiece-Gould (TG) waves—on a magnetized single-species plasma column [1]. The results should be relevant to nonneutral plasmas confined in a Penning-Malmberg trap [2]. Two problems are considered.

Chapters 2-4 examine the effect of collisions on an azimuthally symmetric TG wave propagating along an infinitely long plasma column [3]. Chapter 2 introduces a simple Fokker-Planck operator devised by J. P. Dougherty to treat like-particle collisions [4, 5]. In Chapter 3, the Dougherty collision model enables the derivation of a kinetic dispersion relation that includes collisions with impact parameter smaller than the cyclotron radius. When the phase velocity is much larger than the thermal velocity, the dispersion equation yields a simple formula for the complex frequency of the wave. In Chapter 4, this formula is interpreted using simpler fluid models, and bulk viscosity is identified as the damping mechanism. Fluid theory also provides a framework for considering the effect of collisions with impact parameter larger than the cyclotron radius. These collisions lie outside the scope of the Fokker-Planck theory but nonetheless transport momentum across the magnetic field, contributing to the damping of the wave [5, 6].

Chapter 5 deals with the effects of finite plasma length. Azimuthally symmetric modes of oscillation are calculated for a cold finite-length plasma column.

Similar mode calculations have been carried out in past work [7-9], but here a novel finding is presented: each mode is a mixture of multiple degenerate standing waves, often exhibiting sharp features along "resonance cones" corresponding to the frequency of the mode [10]. The observed mixing is a low-temperature phenomenon, requiring that the cold-fluid dispersion relation be valid even for wavelengths much smaller than the dimensions of the plasma. In this regime, Landau damping is exponentially small, so the modes are damped by viscosity. Perturbation theory yields a formal expression for the viscous damping rate when the damping is sufficiently weak.

1.1 Collisional Effects

1.1.1 Kinetic Theory with Collisional Velocity Scattering

Theoretical studies of the collisional damping of electron plasma waves in an electron-ion plasma date back to the pioneering work of Lenard and Bernstein and extend into recent literature [11-14]. Using a simple Fokker-Planck collision operator, now called the Lenard-Bernstein (LB) collision operator, Lenard and Bernstein solved the linearized Boltzmann and Poisson equations for the electrons to obtain a dispersion relation for the complex wave frequency, ω. The dispersion relation admits a discrete infinity of roots, the least damped of which corresponds to the Landau (or Bohm-Gross) root of collisionless theory [15]. Lenard and Bernstein focused on the least damped root, finding the collisional damping decrement $\mathrm{Im}(\omega) = -\nu_{LB}/2$, where ν_{LB}

is a generic collision frequency that appears in the LB collision operator. (Actually, the ½ was omitted in the final step of the analysis, and the omission was corrected only recently [13].) Recent work also showed that there is a complete set of kinetic eigenfunctions corresponding to the discrete infinity of roots, and these eigenfunctions replace the continuum of Van-Kampen eigenfunctions of collisionless theory [12, 14, 16].

The LB collision operator conserves particle number but not momentum or energy. However, failure of the electron collision operator to conserve momentum and energy is acceptable for an electron-ion plasma, since momentum and energy can be transferred from the electrons to the ions by collisions. Indeed, the damping of electron plasma waves in an electron-ion plasma involves just such a transfer of momentum (and, to a lesser extent, energy). The oscillating electrons are slowed by collisions with the relatively immobile ions, and this friction damps the wave.

In contrast, in a single-species plasma, the damping mechanism described above is irrelevant, since there is no heavier background species. By default, the collisional damping of plasma waves in the single-species plasma must result from collisions between like particles. Therefore, the failure of the LB operator to conserve momentum and energy disqualifies it from describing damping in the single-species plasma. Dougherty has introduced a modification of the LB operator that conserves momentum and energy as well as particle number, and we will use Dougherty's collision operator [4, 5, 17, 18].

The advantage of the LB and Dougherty operators is that they are analytically tractable. For example, the Hermite polynomials form a complete set of eigenfunctions of the 1-D LB operator, and this set is a convenient basis for expansion of the velocity distribution when collisions are described by the LB operator [12]. Here we use an analogous set of orthogonal functions as a basis for expansion of the velocity distribution.

Following Trivelpiece and Gould [1], we consider plasma waves on an infinitely long, magnetized plasma column of uniform density surrounded by a coaxial cylindrical conductor. For simplicity, we limit the discussion to azimuthally symmetric waves. We also take the magnetic field to be sufficiently large that the drift approximation is justified. Accordingly, we describe the plasma dynamics with a drift kinetic equation that includes Dougherty's collision term—hereafter referred to as the Dougherty kinetic equation. This treatment accounts for collisions with impact parameters ρ satisfying $b < \rho < r_c$, where $b \equiv q^2 / T$ and $r_c \equiv (T/m)^{1/2} / \Omega_c$ are, respectively, the classical distance of closest approach and the cyclotron radius for a thermal particle (q and m are the charge and mass of a single particle, T is the plasma temperature, and Ω_c is the cyclotron frequency). Here we have implicitly assumed that $r_c >> b$; this ordering is typical of experiments on nonneutral plasmas. Interactions with impact parameters $\rho > r_c$ lie beyond the scope of a Fokker-Planck collision operator; however, these interactions are considered later in the context of fluid theory.

The linearized Dougherty kinetic equation and Poisson's equation yield a dispersion relation for the complex wave frequency [3]. Like the LB dispersion relation, this dispersion relation admits a discrete infinity of roots for each wavenumber. We focus on the least damped root, which corresponds to the Landau root of collisionless theory.

For wavelengths much larger than the Debye length, the least damped root of the dispersion equation is given by the simple approximate expression

$$\omega \cong \frac{k_z \omega_p}{k}\left[1+\frac{3}{2}(k\lambda_D)^2\left(\frac{1+10i\alpha/9}{1+2i\alpha}\right)\right], \tag{1.1}$$

where $\omega_p \equiv (4\pi q^2 n_0 / m)^{1/2}$ and $\lambda_D \equiv [T_0/(4\pi q^2 n_0)]^{1/2}$ are the plasma frequency and the Debye length of the unperturbed plasma (n_0 and T_0 being the unperturbed density and temperature), k_z and $k_\perp$ are the wavenumbers along and transverse to the magnetic field, $k = \sqrt{k_z^2 + k_\perp^2}$ is the total wavenumber, ν_D is a generic collision frequency that appears in the Dougherty collision operator, and $\alpha \equiv \nu_D k/(k_z \omega_p)$ is a parameter characterizing the strength of collisionality. Note that the ratio of the phase velocity to the thermal speed, $v_{th} \equiv (T_0/m)^{1/2}$, is approximately $\mathrm{Re}(\omega)/(k_z v_{th}) \cong (k\lambda_D)^{-1} >> 1$. For wavelengths comparable to the Debye length (*i.e.*, $k\lambda_D \sim 1$), the phase velocity is closer to the thermal velocity. In this case, the dispersion relation must be solved numerically, and Landau damping is recovered in the limit $\alpha \to 0$.

For weak collisionality (*i.e.*, $\alpha << 1$), Eq. (1.1) reduces to

$$\mathrm{Re}(\omega) \cong \frac{k_z \omega_p}{k}\left[1+\frac{3}{2}(k\lambda_D)^2\right] \tag{1.2}$$

$$\mathrm{Im}(\omega) \cong -\frac{4}{3}\nu_D (k\lambda_D)^2. \tag{1.3}$$

Equation (1.2) is the well-known result from collisionless theory for the frequency of a TG wave on a single-species plasma column [19]. Equation (1.3) gives the collisional damping rate. Note that the damping rate is suppressed by the small factor $(k\lambda_D)^2 << 1$; this suppression is a reminder that the dominant damping mechanism in an electron-ion plasma—electron-ion friction—is not available in the single-species plasma.

According to Eq. (1.1) the ordering $k_z / k_\perp << 1$ implies that $\mathrm{Re}(\omega) << \omega_p$. This is the typical wavenumber ordering for plasma wave experiments on a long column, and we assume this ordering here. In fact, this ordering is implicit in our use of a Fokker-Planck collision operator, since the derivation of such an operator requires the Bogoliubov hypothesis [20], $|\omega| << \omega_p$.

A weakly damped solution to the dispersion equation exists even in the limit of strong collisionality (*i.e.*, $\alpha >> 1$). In this limit, Eq. (1.1) reduces to

$$\mathrm{Re}(\omega) \cong \frac{k_z \omega_p}{k}\left[1+\frac{5}{6}(k\lambda_D)^2\right] \tag{1.4}$$

$$\mathrm{Im}(\omega) \cong -\frac{1}{3}\left(\frac{\mathrm{v}_{th}^2}{\nu_D}\right)k_z^2. \tag{1.5}$$

Here, we implicitly assume that the plasma is weakly correlated (*i.e.*, $\nu_D << \omega_p$) even though the wave dynamics are strongly collisional, and this is possible since $\mathrm{Re}(\omega) << \omega_p$.

Note that the Bohm-Gross correction to the real part of the frequency—that is, the term $(3/2)(k\lambda_D)^2$ in the bracket of Eq. (1.2)—has been replaced by $(5/6)(k\lambda_D)^2$ in Eq. (1.4). This change, which emerges automatically from kinetic theory, has a simple explanation based on the adiabatic law of compression [21]. The numerical coefficient of the Bohm-Gross term is $(d+2)/(2d)$, where d is the number of degrees of freedom that share the compressive energy. For weak collisionality, there is negligible equipartition, so $d = 1$ and $(d + 2)/(2d) = 3/2$; whereas, for strong collisionality, there is nearly complete equipartition, so $d = 3$ and $(d + 2)/(2d) = 5/6$.

1.1.2 Fluid Theory with Collisional Transport and Temperature Isotropization

While the kinetic dispersion equation (1.1) is valid from the limit of weak collisionality to the limit of strong collisionality, its physical interpretation in each these limits is not immediately clear. Fortunately, fluid models provide a complementary approach to the kinetic theory in these limits, provided that resonant particle effects are negligible.

First consider the limit of strong collisionality. Here a dispersion relation can be obtained from Poisson's equation plus the linearized equations of motion for the plasma density, flow velocity, and temperature, with collisional effects contained in

the viscosity and heat conduction terms. For wavelengths much larger than the Debye length $(i.e., k\lambda_D << 1)$, the fluid dispersion relation recovers Eq. (1.4) for the real part of the wave frequency. As a first approximation, the damping rate is given by [3]

$$\mathrm{Im}(\omega) \cong -\left(\frac{2}{3}\zeta_{\parallel}k_z^2 + \frac{1}{2}\zeta_{\perp}k_{\perp}^2\right), \tag{1.6}$$

where $\zeta_{\parallel}$ and $\zeta_{\perp}$ are the coefficients of kinematic viscosity for transport of axial momentum along and across the magnetic field, respectively. The contribution to the damping from heat conduction is of higher order in the small parameter $k\lambda_D$. If the second term on the right-hand side of Eq. (1.6) is ignored, the kinetic expression (1.5) is recovered by the substitution $\zeta_{\parallel} = \zeta_D \equiv \mathrm{v}_{th}^2/(2\nu_D)$, where ζ_D is the kinematic viscosity predicted by the Dougherty operator. In other words, the kinetic damping formula (1.5) corresponds to the dissipation of the compressive flow by bulk viscosity.

However, there is no justification for ignoring the contribution to the damping from cross-field viscosity. Typical experiments on single-species plasmas are characterized by the ordering $r_c << \lambda_D$, and in this regime the cross-field kinematic viscosity is roughly [6]

$$\zeta_{\perp} \cong \nu_c \lambda_D^2, \tag{1.7}$$

where $\nu_c \equiv q^4 n_0/(m^{1/2}T_0^{3/2})$. Comparison of the two terms in the expression (1.6) using this estimate indicates that transport of axial momentum across the magnetic field is the dominant damping mechanism in the limit of strong collisionality. The estimate (1.7) is based on collisions between particles on different field lines—that is, collisions with impact parameter ρ satisfying $r_c << \rho < \lambda_D$. These collisions can only

be described by a nonlocal collision operator and thus lie outside the scope of the Dougherty operator or any other Fokker-Planck operator.

In the limit of weak collisionality, a fluid model can still be used if the phase velocity of the wave is much larger than the thermal velocity. In particular, the ordering $\mathrm{Re}(\omega)/k_z >> \mathrm{v}_{th}$ implies that the particles comprising a given fluid element do not disperse on the timescale of the wave and also that the number of resonant particles is exponentially small. However, this fluid model must allow for two distinct temperatures, $T_\parallel$ and $T_\perp$, corresponding to the parallel and cyclotron degrees of freedom, since the timescale for exchange of energy between these degrees of freedom is longer than the wave timescale. We assume that the collisional relaxation of the two temperatures is governed by the equation [22]

$$\frac{dT_\parallel}{dt} = \nu_{\parallel,\perp}(T_\perp - T_\parallel), \tag{1.8}$$

which defines the equipartition rate, $\nu_{\parallel,\perp}$. Meanwhile, the total internal energy of a fluid element increases as it is compressed by the wave, evolving in time as

$$\frac{d}{dt}\left(\frac{1}{2}T_\parallel + T_\perp\right) = -\frac{T_\parallel}{n}\frac{dn}{dt}. \tag{1.9}$$

The parallel flow and the density evolve according to Euler's equation (with pressure $p = nT_\parallel$) and the continuity equation, respectively. Together with Poisson's equation, these fluid equations admit a weakly damped wave with super-thermal phase velocity for wavenumbers such that $k\lambda_D << 1$. As a first approximation, the real part of the wave frequency is given by Eq. (1.2) and the damping rate by

$$\mathrm{Im}(\omega) \cong -\nu_{\parallel,\perp}(k\lambda_D)^2. \tag{1.10}$$

Equation (1.3) is recovered by the substitution $\nu_{\parallel,\perp} = \nu_{\parallel,\perp}^{(D)} \equiv 4\nu_D/3$, where $\nu_{\parallel,\perp}^{(D)}$ is the equipartition rate predicted by Dougherty's collision operator.

While the kinetic derivation of the damping formula (1.3) for weak collisionality obscures the underlying damping mechanism, comparison with the two-temperature fluid model suggests a physical interpretation for the kinetic result. The parallel temperature of a given fluid element oscillates as it compresses and expands in the presence of the passing wave. However, because of the weak collisional coupling between parallel and perpendicular degrees of freedom, the oscillation in the parallel temperature leads the compression/decompression cycle by a small phase. As a result, the pressure is greater (on average) during compression than during decompression, so positive net work is done on the fluid element at the expense of the wave energy. The dissipation is equivalent to a high-frequency bulk viscosity.

The long-range collisions with impact parameters $\rho >> r_c$ have little effect on temperature isotropization, since the cyclotron adiabatic invariant inhibits the transfer of energy between perpendicular and parallel degrees of freedom by such collisions [23]. However, as in the limit of strong collisionality, these collisions contribute to the wave damping by transporting momentum across the magnetic field. The nature of this transport is the same regardless of the strength of collisionality, so the second term in the damping formula (1.6)—with cross-field viscosity again given by Eq. (1.7)—still gives a reasonable estimate of this contribution even when collisions are weak.

1.2 Finite-Length Effects

Figure 1.1 shows a schematic diagram of a single-species plasma that is confined in a Penning-Malmberg trap [2]. A conducting cylinder is divided into three sections, and the plasma resides in the central grounded section, with radial confinement provided by a uniform axial magnetic field ($\vec{B} = B\hat{z}$) and axial confinement by voltages applied to the end sections of the cylinder. These plasmas routinely come to a state of thermal equilibrium in the trap and are routinely cooled to the cryogenic temperature range [24]. The plasma configuration is then particularly simple; the density is constant out to some surface of revolution and there drops to zero [25]. Chapter 5 discusses the normal modes of plasma oscillation for these cold equilibrium plasmas. Of course, cold-fluid theory provides a good description of these modes.

At first glance, the problem sounds straightforward: find the longitudinal modes of oscillation of a uniformly magnetized, uniform-density, bounded plasma in cold-fluid theory. However, we will see that the problem is subtle and that there is some confusion in the literature.

The origin of the difficulty is the peculiar dispersion relation for plasma waves in a cold magnetized plasma,

$$\omega = \frac{k_z \omega_p}{\sqrt{k_z^2 + k_\perp^2}}, \tag{1.11}$$

where ω is the wave frequency, ω_p is the plasma frequency in the unperturbed plasma, k_z is the wavenumber along the magnetic field, and $k_\perp$ is the wavenumber transverse to the field. Note that a wave with wavenumbers $(k_z, k_\perp)$ has the same frequency as a wave with wavenumbers $(k_z', k_\perp')$ if $k_z'/k_\perp' = k_z/k_\perp$; thus, each wave has the same frequency as infinitely many other waves. Upon reflection from the boundaries, an incident wave typically mixes with other waves sharing the same frequency, and consequently each normal mode is a complicated many-wave structure.

A toy problem illustrates the issues. Consider a 2-D slab of uniform-density plasma that occupies the domain given by $0 \le x \le a$ and $0 \le z \le b$, and assume a strong magnetic field in the *z*-direction. The potential for a mode oscillating with frequency ω satisfies the equation

$$\frac{\partial^2 \delta\varphi_\omega}{\partial x^2} + \left(1 - \frac{\omega_p^2}{\omega^2}\right)\frac{\partial^2 \delta\varphi_\omega}{\partial z^2} = 0. \tag{1.12}$$

Suppose that the plasma is bounded on all sides by a perfect conductor so that the potential is zero at the boundaries. In this case, a set of normal modes and frequencies is given by

$$\delta\varphi_\omega(x,z) = \sin\left(\frac{m\pi x}{a}\right)\sin\left(\frac{n\pi x}{b}\right) \tag{1.13}$$

$$\omega_{mn} = \frac{\omega_p(n\pi/b)}{\sqrt{(m\pi/a)^2 + (n\pi/b)^2}} \tag{1.14}$$

where *m* and *n* are integers. For any mode (m,n) there are an infinite number of exactly degenerate modes (m',n'), where $n'/m' = n/m$. Each mode can be

decomposed into a pair of waves propagating in opposite directions along the magnetic field and reflecting at the boundaries, but for this particular geometry there is no mixing since the sine functions are orthogonal on the boundary surfaces. However, if the boundary were deformed, the orthogonality would be destroyed and reflections would mix degenerate modes, yielding more complicated many-wave modes.

It is interesting to construct an alternate representation of the degenerate modes [26]. For any frequency, the mode equation (1.12) admits characteristic solutions of the form $\delta\varphi_\omega = \delta[z \pm (\omega_p^2/\omega^2 - 1)^{1/2} x + c]$, where c is an arbitrary constant. These solutions can be thought of as a line or ray at slope $dz/dx = \pm(\omega_p^2/\omega^2 - 1)^{1/2}$. For the mode frequencies in Eq. (1.14), an assembly of such rays can be arranged end to end so that the assembly closes on itself. The sign of the ray changes upon reflection from the boundary so that the boundary condition on the wall is satisfied. Figure 1.2 shows a parallelogram-shaped assembly for the degenerate mode frequency corresponding to $n/m = 1$. There are an infinite number of such parallelograms with sides of different lengths, and this set is an alternative representation of the sinusoidal degenerate modes of Eq. (1.13) for which $n/m = 1$. Similar ray-like representations can be constructed for any other set of degenerate modes—that is, for any other value of the ratio n/m. Interestingly, if the rectangular plasma boundary is deformed slightly, all of the degenerate sinusoidal modes are mixed, but a given ray-like mode is only modified if the boundary is changed at the points at which the ray makes contact.

This picture is modified somewhat in cylindrical geometry. For example, for a uniform-density plasma bounded by a cylindrical conducting wall at $r = a$ and flat

conducting walls at $z = 0$ and $z = b,$ the mode degeneracies are only approximate. Furthermore, the ray-like solutions are replaced by more complicated functions that are peaked along resonance cones with slope [10] $dz / dr = \pm(\omega_p^2 / \omega^2 - 1)^{1/2}$. A crucial difference is that the cylindrical functions are not entirely localized along these cones. Nevertheless, the basic ideas illustrated by the rectangular toy problem persist. In numerical studies of the normal modes for a long, cylindrical plasma column in a Penning-Malmberg trap, we will find complicated many-wave normal modes, with the waves often adding to produce conical structures with slope $dz / dr = \pm(\omega_p^2 / \omega^2 - 1)^{1/2}$.

However, we emphasize that the mixing is a low-temperature phenomenon, requiring that the cold-fluid dispersion relation be valid for axial and transverse wavelengths much shorter than the dimensions of the plasma. The condition for validity of the cold-fluid dispersion relation is that $(k_\perp^2 + k_z^2)^{1/2} \lambda_D << 1;$ otherwise, kinetic effects such as Landau damping modify the dispersion relation, spoiling the degeneracy that underlies the mixing. Thus, in sufficiently warm plasmas, no mixing should be observed.

With this background, we now return to the discussion of normal modes for a cold equilibrium plasma in a Penning-Malmberg trap. An important difference between this problem and the toy problem is that vacuum separates the plasma from the conducting wall. For the simple case of a mode with azimuthal mode number zero, the mode equation is given by

$$\frac{1}{r}\frac{\partial}{\partial r} r \frac{\partial \delta\varphi_\omega}{\partial r} + \frac{\partial}{\partial z}\left[1 - \frac{\omega_p^2(r,z)}{\omega^2}\right]\frac{\partial \delta\varphi_\omega}{\partial z} = 0, \qquad (1.15)$$

where $\omega_p^2(r,z) = 4\pi q^2 n(r,z)/m$ inside the plasma and $\omega_p^2(r,z) = 0$ in the vacuum. The mode potential vanishes on the trap wall and as $z \to \pm\infty$.

Historically, two geometrical limits have been emphasized. In the first limit, pioneered by the atomic physics community, the plasma is small compared to the radius of the cylindrical conductor and resides in a quadratic trap potential. The surface of revolution defining the shape of the plasma is then spheroidal [27]. Using spheroidal coordinates, Dubin found exact analytic expressions for the normal modes, and images of the modes in Be+ plasmas corroborated the theory [28, 29]. Of course, the Dubin modes have many near degeneracies, and one expects that a deformation of the spheroidal boundary will mix these modes.

In the second limit, more familiar to plasma physicists, the plasma is long compared to the radius of the conducting cylinder and takes the shape of a finite-length cylinder with rounded ends. The more complicated shape of these longer plasmas prevents an analytic description of the modes. However, the solution by Trivelpiece and Gould for waves on a cold, magnetized, infinitely long plasma cylinder provides a useful benchmark for theoretical studies of modes on the finite-length plasma cyliners [1]. Previous theory has argued that, to a good approximation, each mode is a single standing TG wave with the axial wavenumber quantized to fit the length of the plasma column. Moreover, for the case of warm plasmas with significant kinetic effects, experimental observations are consistent with this simple picture [30]. In contrast, our numerical solution based on cold-fluid theory shows that

each mode involves many TG waves, which often add to produce conical structures at the expected slope, $dz/dr = \pm(\omega_p^2/\omega^2 - 1)^{1/2}$.

The dispersion relation for the TG waves is given by Eq. (1.11), but with the transverse wavenumber $k_\perp$ quantized to discrete values, each corresponding to a different solution to the ODE for the radial dependence of the wave. Upon reflection at the end of the column, a given TG wave reflects not only into its backward-propagating counterpart but also into other waves with different radial wavefunctions [7]. Note that when ω and $k_\perp$ are specified, Eq. (1.11) chooses the value of k_z. The value of k_z is important in determining the extent to which a wave participates in the mode. If, after a complete circuit of two reflections, the wave adds in phase with itself (say, to produce a standing wave), then that wave will tend to play a significant role in the mode. Such approximate standing waves here play the role of the exactly degenerate modes in the toy problem.

The numerical method is easiest to understand for the idealized case where the plasma column has flat ends—that is, where the plasma is a perfect right circular cylinder as shown in Fig. 1.3(*a*). This is probably the simplest generalization of the toy problem. The dashed lines in the figure divide the confinement region axially into a central region where the plasma resides and two adjacent vacuum regions. Following Prasad and O'Neil [7], we expand the mode potential in the central region in an infinite sum of TG waves, all having the same frequency, ω—the unknown frequency of the mode—but different axial and transverse wavenumbers, k_z and $k_\perp$. These waves all satisfy the mode equation for a mode with frequency ω as well as the

boundary condition on the wall, and they are known analytically. In the vacuum region $z > L/2,$ we expand the mode potential in an infinite series of cylindrical harmonics of the form $J_0(\chi_{0n} r/R)\exp[-\chi_{0n}(z-L/2)/R],$ where R is the radius of the conducting cylinder, χ_{0n} is the n^{th} zero of the Bessel function $J_0(x),$ and n is a positive integer. For the vacuum region $z < -L/2,$ there is simply a sign change in the argument of the exponential (and an overall sign change in the case of odd modes). The three series satisfy the mode equation in the three regions as well as the boundary conditions on the wall and at $z \to \pm\infty,$ and the numerical task is to find a frequency ω and choose the coefficients in the series so that the solutions match properly across the surfaces separating these regions. The mode potential and the normal component of the electric displacement vector must be continuous across these surfaces.

For the simple case of flat ends, the matching task is facilitated by the orthogonality of both the Bessel functions to one another and the TG radial wavefunctions to one another on the flat matching surfaces [the dashed lines in Fig. 1.3(*a*)]. Note that the Bessel functions are not orthogonal to the TG radial wavefunctions; indeed, it is this lack of orthogonality that gives rise to the mixing upon reflection. Each TG wave couples to many vacuum solutions, and these couple back to different TG waves. In contrast to the toy problem, the plasma ends need not be deformed to get wave mixing.

Of course, for numerical implementation of the matching, the three series are truncated at a finite number of terms, and here a difficulty arises for the idealization of

a flat end. We do not find convergence of the solution, in that TG waves of arbitrarily large wavenumber appear to participate significantly in each mode.

Figure 1.3(*b*) shows a more realistic plasma with rounded (spheroidal) ends that fit smoothly onto the central cylindrical section of the plasma. Here, the matching surfaces that separate the central region containing the plasma from the adjacent vacuum regions are no longer flat but extend outward to follow the end-shape of the plasma [the dashed curves in Fig. 1.3(*b*)]. Again we expand the mode potential in three series for the three regions, but here we lose the orthogonality of the Bessel functions and of the TG radial wavefunctions on the matching surfaces. The matching is carried out by choosing the frequency and the coefficients in the series to minimize the mean-square error in matching at a large number of sample points on the matching surface. Fortunately, the rounding of the ends suppresses the coupling to large-wavenumber components, and we find convergent solutions.

By taking the central cylindrical section of the plasma to be arbitrarily small, a spheroidal plasma is obtained, as illustrated in Fig. 1.3(*c*). For the spheroidal plasma, if the radius of the conducting cylinder is much larger than the dimensions of the plasma, Dubin's analysis of the modes of a cold plasma spheroid should be applicable [28]. Indeed, in this limit we obtain modes that resemble the Dubin modes (although, unfortunately, convergence is too slow to resolve fine-scale details of the modes in this limit).

As mentioned earlier, one advantage of the numerical method is that it explicitly identifies the extent to which each TG wave participates in a given normal

mode. Also, use of the known TG wave solutions and vacuum solutions effectively reduces the dimension of the numerical task. Matching on the boundary surface involves N unknowns; whereas, a numerical solution on a grid spanning r and z would involve N^2 unknowns.

A signature of the predicted wave-mixing is that the least damped modes of the cold plasma cylinder damp more quickly than one would expect based on the assumption that the mode is a single standing TG wave. The reason for the enhanced damping is that the viscous momentum flux underlying the damping is intensified by the presence of steep momentum gradients—*i.e.*, high wavenumbers—in the mixed mode. We investigate viscous damping in the limit where viscous effects can be treated as a perturbation to Eq. (1.15). To first order in viscosity, each mode damps with a rate given by a quadratic form that acts on the zero-order (inviscid) mode. We evaluate this expression for one of the numerically calculated modes and compare with the rate obtained by approximating the mode as a single TG wave. The single-wave approximation underestimates the damping rate by roughly an order of magnitude.

1.3 Acknowledgements

Chapter 1 is a reprint, in part, of the material as it appears in Physics of Plasmas. M. W. Anderson and T. M. O'Neil, *Physics of Plasmas* **14**, 112110 (2007). The dissertation author was the primary investigator and author of this paper.

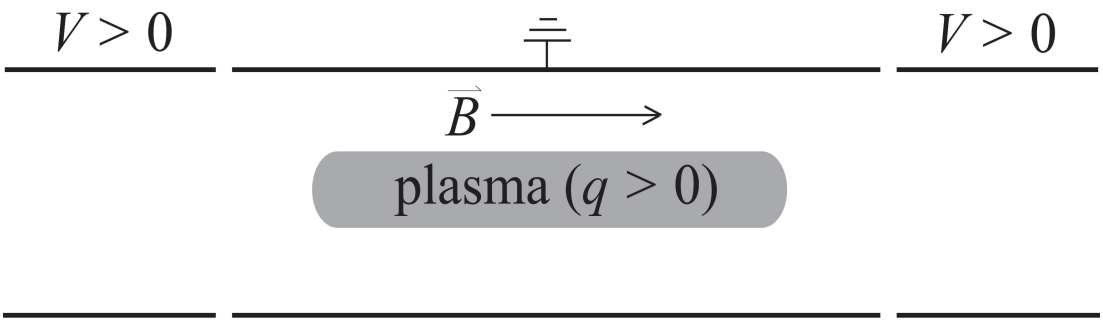

Figure 1.1. Schematic diagram of a finite-length single-species plasma column confined in a Penning-Malmberg trap. Axial confinement is electrostatic, provided by an electric potential, V, applied to the outer cylindrical electrodes; radial confinement is provided by an axial magnetic field. The confinement scheme depicted here is for positively charged particles.

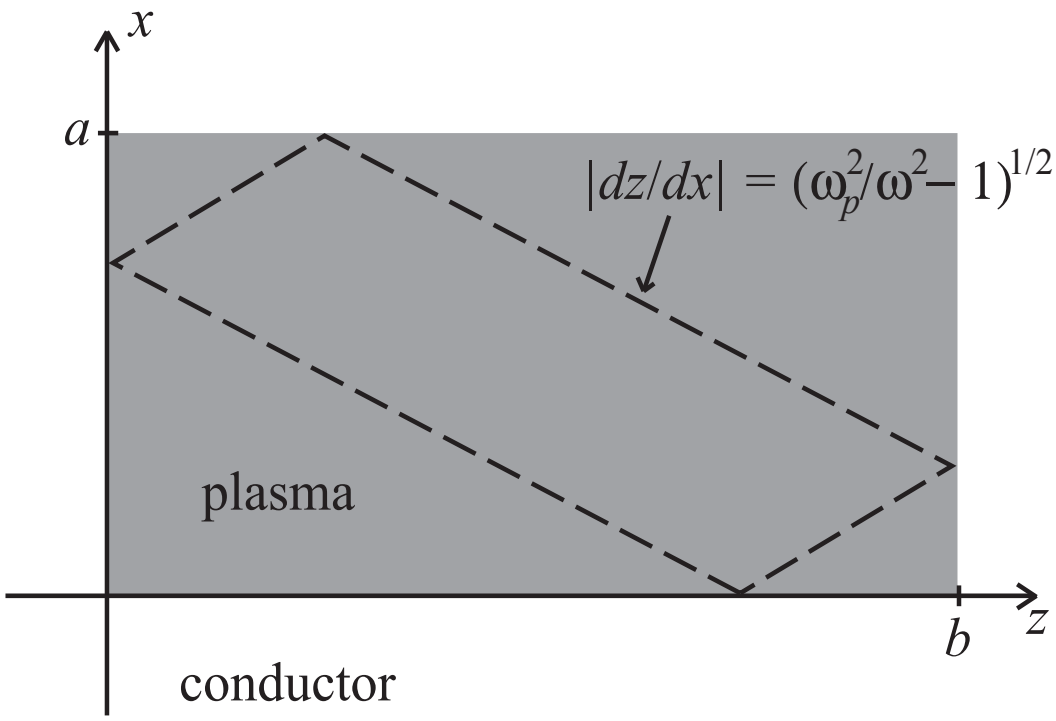

Figure 1.2. An example of a ray-like mode on a magnetized plasma slab of rectangular cross-section, surrounded by a perfect conductor. The mode potential is a sum of four Dirac delta functions, each of which is peaked along one side of the dashed parallelogram. Delta functions corresponding to adjacent sides enter the sum with opposite signs so that the condition of vanishing potential is satisfied along the boundary. There are an infinite number of other ray-like modes with the same frequency as the mode depicted here. The set of ray-like modes is complimentary to the set of modes that are sinusoidal in x and z.

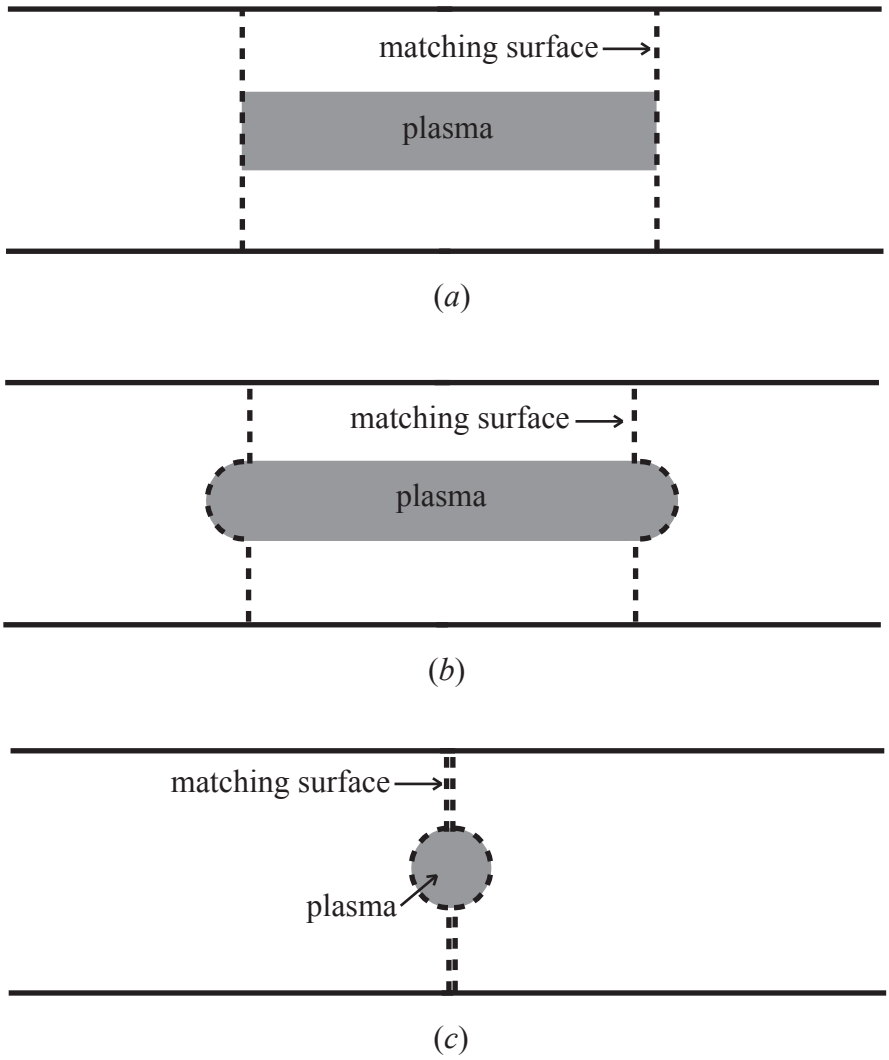

Figure 1.3. Three idealized plasma shapes for which modes of oscillation are calculated: (*a*) a cylinder with flat ends, (*b*) a cylinder with spheroidal ends, and (*c*) a spheroid. In each of the three regions separated by the dashed curves, we express the mode potential as a linear combination of functions that satisfy the mode equation and boundary conditions in that particular region. The numerical task is to choose the coefficients in each linear combination so that the mode potential and the normal derivative of the electric displacement match at the boundary surfaces shown here as dashed curves.

Chapter 2

Properties of the Dougherty Collision Operator

A simplified Fokker-Planck collision operator due to J. P. Dougherty provides a powerful tool for investigation of collisional effects in single-species plasmas, since it captures the essential physics of like-particle collisions yet is simple enough to allow analytic progress [4]. In this chapter, we find a complete set of eigenfunctions of the linearized Dougherty collision operator [5]. Expansion of the distribution function in terms of these eigenfunctions facilitates solution of the kinetic equation. Using the eigenfunctions, we show that in the limit of strong collisionality, the Dougherty operator gives rise to realistic fluid dynamics, including Newton's law of momentum transport and Fourier's law of heat transport, with reasonable formulae for the transport coefficients.

2.1 Background

In the kinetic theory of plasmas, the effect of collisions on the particle distribution function is treated by the Fokker-Planck collision operator of MacDonald, Rosenbluth, and Judd (MRJ) [31]. This operator satisfies the usual properties expected of a good collision operator:

(a) it vanishes for any thermal equilibrium distribution function (any Maxwellian)

(b) it drives the plasma to thermal equilibrium in the long-time limit; that is, the long-time solution of the Boltzmann equation $\partial f/\partial t = C(f,f)$ is a Maxwellian (here f is the distribution for a given particle species and C is the MRJ operator)

(c) it conserves particle number, momentum, and energy.

In addition, the MRJ operator satisfies a property specific to plasmas:

(d) it accurately accounts for the dominance of small-angle scattering; *i.e.*, it contains a velocity-space diffusion term.

However, inversion of the MRJ operator to find the distribution function is not tractable in most cases of interest. Therefore, it is desirable to find an operator that is invertible and yet preserves the important properties listed above.

This *ad hoc* approach to the collision operator as a means to analytic progress is not a new idea. For example, Bhatnagar, Gross, and Krook (BGK) proposed a drastically simplified collision operator in 1957, and in 1958 Lenard and Bernstein (LB) utilized a Fokker-Planck operator with constant diffusion and drag coefficients in order to study analytically the effect of collisions on plasma waves [11, 32]. However, each of these operators neglects at least one of the properties listed above and is incapable of predicting certain phenomena as a result. Specifically, the BGK operator, while conserving the necessary quantities, neglects the dominant role played by small-angle scattering in the collisional relaxation of the distribution function; as a result, in the limit of weak collisionality this operator fails to predict the dramatically enhanced relaxation that occurs over regions of velocity-space in which the distribution varies sharply. Conversely, the LB operator accounts for velocity-space diffusion but does

not conserve momentum or energy; therefore, results obtained from the LB operator cannot match onto those from fluid theory in the limit of strong collisionality.

A generalization of the LB operator, introduced by Dougherty, retains each of the properties (a) through (d). The operator proposed by Dougherty is given by [4]

$$C_D(f,f) = \nu_D \frac{\partial}{\partial \vec{\mathrm{v}}} \cdot \left[\frac{T[f]}{m} \frac{\partial f}{\partial \vec{\mathrm{v}}} + (\vec{\mathrm{v}} - \vec{\mathrm{V}}[f]) f \right] \tag{2.1}$$

where

$$\vec{\mathrm{V}}[f] = \frac{1}{n} \int d\vec{\mathrm{v}} \vec{\mathrm{v}} f \tag{2.2}$$

$$T[f] = \frac{1}{3n} \int d\vec{\mathrm{v}} m (\vec{\mathrm{v}} - \vec{\mathrm{V}})^2 f \tag{2.3}$$

$$n[f] = \int d\vec{\mathrm{v}} f, \tag{2.4}$$

ν_D is a generic collision frequency, and m is the particle mass. Comparison with the MRJ collision operator suggests that the collision parameter ν_D should be of order $\nu_D \sim nq^4 \lambda / (m^{1/2} T^{3/2})$, where λ is the appropriate Coulomb logarithm. Unlike the LB operator, the Dougherty operator conserves all of the desired quantities and therefore matches onto results from fluid theory in the limit of strong collisionality. Note here that strongly collisional does not mean strongly coupled, but rather the weaker condition that the mean-free-path between collisions is smaller than the spatial scale of interest (*e.g.*, mode wavelength).

The advantage of the Dougherty operator over the MRJ operator is that it is analytically tractable. The sacrifice is that the velocity dependence of the Fokker-Planck coefficients is neglected, and therefore results are only qualitatively correct.

If the particle distribution function can be written as $f = f_0 + \delta f$, where δf is a small perturbation and f_0 is the Maxwellian characterized by density n_0, temperature T_0, and zero mean velocity, then one may write

$$\begin{aligned} C_D(f,f) &\cong C_D(f_0,\delta f) + C_D(\delta f, f_0) \\ &\equiv \nu_D \frac{\partial}{\partial \vec{\mathrm{v}}} \cdot \left[\frac{T_0}{m} \frac{\partial \delta f}{\partial \vec{\mathrm{v}}} + \vec{\mathrm{v}} \delta f + \frac{\delta T}{m} \frac{\partial f_0}{\partial \vec{\mathrm{v}}} - \delta \vec{\mathrm{V}} f_0 \right], \end{aligned} \tag{2.5}$$

where

$$\delta T = (3n_0)^{-1} \int d\vec{\mathrm{v}} m(\mathrm{v}^2 - 3T_0/m)\delta f \tag{2.6}$$

$$\delta \vec{\mathrm{V}} = n_0^{-1} \int d\vec{\mathrm{v}} \vec{\mathrm{v}} \, \delta f. \tag{2.7}$$

The first two terms in the square bracket of Eq. (2.5) are the same as in the LB operator, while the remaining terms are responsible for restoring momentum and energy conservation. Dougherty focuses on the inversion of this linearized operator to find δf. Following Chandrasekhar [33], he constructs a Green's function for the linearized kinetic equation

$$\begin{aligned} &\frac{\partial \delta f}{\partial t} + \vec{\mathrm{v}} \cdot \frac{\partial \delta f}{\partial \vec{x}} + \frac{q}{mc} (\vec{\mathrm{v}} \times \vec{B}) \cdot \frac{\partial \delta f}{\partial \vec{\mathrm{v}}} - \nu_D \frac{\partial}{\partial \vec{\mathrm{v}}} \cdot \left[\vec{\mathrm{v}} \delta f + \frac{T_0}{m} \frac{\partial \delta f}{\partial \vec{\mathrm{v}}} \right] \\ &\qquad = \frac{1}{T_0} \delta \vec{E} \cdot \vec{\mathrm{v}} f_0 + \nu_D \left[\frac{m \delta \vec{\mathrm{V}} \cdot \vec{\mathrm{v}}}{T_0} + \frac{\delta T}{T_0} \left(\frac{m\mathrm{v}^2}{T_0} - 3 \right) \right] f_0, \end{aligned} \tag{2.8}$$

treating the right hand side as a source term. Using the Green's function it is possible to obtain an expression for δf in terms of $\delta \vec{\mathrm{V}}$ and δT, and this expression may be substituted in the definitions of these quantities, resulting in two algebraic equations for $\delta \vec{\mathrm{V}}$ and δT. These equations can then be solved and δf determined.

A different method for inverting the linearized Dougherty operator was introduced by DeSouza-Machado *et al* [18]. These authors expand the velocity dependence of δf in an infinite series of orthogonal basis functions (Hermite polynomials), converting the Dougherty operator to an infinite matrix acting on the vector of coefficients in the orthogonal function expansion. The Hermite polynomials diagonalize the LB part of the Dougherty operator [the first two terms in the square bracket of Eq. (2.5)], but not the whole operator.

In contrast, here we expand δf in orthogonal basis functions that diagonalize the whole Dougherty operator. Most of these eigenfunctions are just the Hermite polynomials, but a few are modified by the third and fourth terms in the linearized Dougherty operator. Physically, the modified eigenfunctions (and eigenvalues) reflect the conservation properties of the Dougherty operator. One should note that the eigenfunctions diagonalize only the collision operator, not the streaming and force terms in the Boltzmann equation—these terms couple the eigenfunctions.

Five of the eigenfunctions have eigenvalue zero (corresponding to conservation of particle number, three components of momentum, and energy), and these eigenfunctions are crucial in connecting onto fluid theory. We discuss the relation between these special eigenfunctions and the usual hydrodynamic modes in the limit of strong collisionality, identifying the sound speed, thermal conductivity, and viscosity as predicted by the Dougherty operator.

More formally, the hydrodynamic modes arise because the streaming term in the Boltzmann equation [*i.e.*, $ik\mathrm{v}_z\delta f$ for $\delta f \sim \exp(ikz)$] is not diagonalized by the new eigenfunctions. Although the streaming term may be treated as a small perturbation in

the limit of strong collisionality (hydrodynamic limit), it thoroughly mixes the degenerate eigenfunctions with eigenvalue zero, yielding the hydrodynamic mode eigenfunctions. These hydrodynamic eigenfunctions diagonalize both the collision operator and the streaming term in the important subspace of undamped modes. In second order perturbation theory, the hydrodynamic modes pick up weak damping due to weak coupling to eigenfunctions outside the subspace.

2.2 Eigenfunctions of the Linearized Dougherty Collision Operator

We may put the linearized Dougherty operator in self-adjoint form by writing $\delta f = f_0 \varphi$ and substituting this expression in Eq. (2.5). The result is

$$\begin{aligned} & C_D(f_0, \delta f) + C_D(\delta f, f_0) = \\ & f_0 \nu_D \left[\frac{\partial^2 \varphi}{\partial u^2} - \vec{u} \cdot \frac{\partial \varphi}{\partial \vec{u}} + \frac{\delta T}{T_0}(u^2 - 3) + \frac{\delta \vec{\mathrm{V}}}{\sqrt{T_0 / m}} \cdot \vec{u} \right] \\ & \qquad \equiv f_0 \chi(\varphi), \end{aligned} \tag{2.9}$$

where we have introduced the scaled velocity $\vec{u} \equiv \vec{\mathrm{v}} \big/ \sqrt{T_0 / m}$; the operator χ is self-adjoint with weight function f_0. In order to find the eigenfunctions of this operator, we break it into two parts—a differential operator,

$$\chi_1(\varphi) \equiv \nu_D \left[\frac{\partial^2 \varphi}{\partial u^2} - \vec{u} \cdot \frac{\partial \varphi}{\partial \vec{u}} \right], \tag{2.10}$$

and an integral operator,

$$\chi_2(\varphi) \equiv \nu_D \left[\frac{\delta T}{T_0}(u^2 - 3) + \frac{\delta \vec{\mathrm{V}}}{\sqrt{T_0 / m}} \cdot \vec{u} \right]. \tag{2.11}$$

As mentioned above, the eigenfunctions, $\psi_{n_1 n_2 n_3}$, of χ_1 are the products of modified Hermite polynomials, that is,

$$\psi_{n_1 n_2 n_3} = \frac{He_{n_1}(u_x) He_{n_2}(u_y) He_{n_3}(u_z)}{\sqrt{n_1! n_2! n_3!}}. \tag{2.12}$$

The corresponding eigenvalues are

$$\alpha_{n_1 n_2 n_3} = -\nu_D (n_1 + n_2 + n_3), \tag{2.13}$$

where n_1, n_2, and n_3 are nonnegative integers. The functions $\psi_{n_1 n_2 n_3}$ satisfy the orthogonality relation

$$n_0 \delta_{n_1, m_1} \delta_{n_2, m_2} \delta_{n_3, m_3} = \int d\bar{u} \psi_{n_1 n_2 n_3} f_0 \psi_{m_1 m_2 m_3} \equiv n_0 \left\langle \psi_{n_1 n_2 n_3} \middle| \psi_{m_1 m_2 m_3} \right\rangle. \tag{2.14}$$

We observe that any $\psi_{n_1 n_2 n_3}$ which satisfies $\chi_2(\psi_{n_1 n_2 n_3}) = 0$ is an eigenfunction of the total operator, χ, with eigenvalue $\alpha_{n_1 n_2 n_3}$. We therefore express χ_2 in terms of inner products with the functions $\psi_{n_1 n_2 n_3}$:

$$\begin{aligned} \chi_2(\varphi) = \nu_D \Big[& \frac{1}{6} \left\langle \psi_{200} + \psi_{020} + \psi_{002} \middle| \varphi \right\rangle (\psi_{200} + \psi_{020} + \psi_{002}) \\ & + \left\langle \psi_{100} \middle| \varphi \right\rangle \psi_{100} + \left\langle \psi_{010} \middle| \varphi \right\rangle \psi_{010} + \left\langle \psi_{001} \middle| \varphi \right\rangle \psi_{001} \Big]. \end{aligned} \tag{2.15}$$

Evidently, $\chi_2(\varphi)$ is the projection of φ onto $(\psi_{200} + \psi_{020} + \psi_{002})$, ψ_{100}, ψ_{010}, and ψ_{001}. Therefore, for almost every $\psi_{n_1 n_2 n_3}$, $\chi_2(\psi_{n_1 n_2 n_3}) = 0$, and in each such case, $\psi_{n_1 n_2 n_3}$ is an eigenfunction of χ with eigenvalue $\alpha_{n_1 n_2 n_3}$. Hereafter, we refer to these eigenfunctions and eigenvalues of χ as $\varphi_{n_1 n_2 n_3}$ and $\lambda_{n_1 n_2 n_3}$, respectively. The exceptions, for which the projection in Eq. (2.15) is nonzero, are clearly $\psi_{200}, \psi_{020}, \psi_{002}, \psi_{100}, \psi_{010}$, and ψ_{001}. It is straightforward to find six additional eigenfunctions of the operator χ to replace these exceptions. A sensible choice is

$$\varphi_{100} \equiv u_x,\ \varphi_{010} \equiv u_y,\ \varphi_{001} \equiv u_z,\ \varphi_{200} \equiv \frac{1}{\sqrt{6}}(u^2 - 3), \tag{2.16}$$

with eigenvalues $\lambda_{100} = \lambda_{010} = \lambda_{001} = \lambda_{200} = 0,$ and

$$\varphi_{020} \equiv \frac{1}{\sqrt{3}}\left[u_z^2 - \frac{1}{2}(u_x^2 + u_y^2)\right],\ \varphi_{002} \equiv \frac{1}{2}(u_x^2 - u_y^2), \tag{2.17}$$

with eigenvalues $\lambda_{020} = \lambda_{002} = -2\nu_D$. Defined in this manner, the eigenfunctions $\varphi_{000}, \varphi_{100}, \varphi_{010}, \varphi_{001},$ and $\varphi_{200},$ which span the null-space of χ, correspond to particle number, *x*, *y*, and *z* momentum, and kinetic energy. These eigenfunctions also satisfy the orthogonality relation given by Eq. (2.14).

The completeness of the eigenfunctions found above follows directly from the completeness of the Hermite polyniomials. Except for $\varphi_{200}, \varphi_{020},$ and φ_{002}, the eigenfunctions $\varphi_{n_1n_2n_3}$ are given by $\varphi_{n_1n_2n_3} \equiv \psi_{n_1n_2n_3}$, where the functions $\psi_{n_1n_2n_3}$ are defined by Eq. (2.12). The three exceptions, $\varphi_{200}, \varphi_{020},$ and φ_{002}, are mutually orthogonal, and each can be expressed as a linear combination of the functions ψ_{200}, ψ_{020}, and ψ_{002}. Therefore, the eigenfunctions $\varphi_{n_1n_2n_3}$ span the same space as do the functions $\psi_{n_1n_2n_3}$. Since the set $\{\psi_{n_1n_2n_3}\}$ is known to be complete, it follows that the set $\{\varphi_{n_1n_2n_3}\}$ must be complete as well.

As a simple demonstration of the utility and basic consequences of this complete set of eigenfunctions, we consider the linearized kinetic equation governing the evolution of a small, spatially uniform perturbation in the distribution,

$$\frac{\partial \delta f}{\partial t} = C_D(f_0, \delta f) + C_D(\delta f, f_0). \tag{2.18}$$

The solution can be written down immediately in terms of the eigenfunctions found above:

$$\delta f(\vec{u},t) = f_0(u)\sum_{n_1=0}^{\infty}\sum_{n_2=0}^{\infty}\sum_{n_3=0}^{\infty} a_{n_1n_2n_3}\varphi_{n_1n_2n_3}(\vec{u})\exp[\lambda_{n_1n_2n_3}t], \tag{2.19}$$

where the coefficients $a_{n_1n_2n_3}$ are determined from $\delta f(\vec{u},t=0)$. Note that all of the eigenvalues $\lambda_{n_1n_2n_3}$ are negative except for λ_{000}, λ_{100}, λ_{010}, λ_{001}, and λ_{200}, which are zero. Thus, the initial perturbations in density, fluid velocity, and internal energy—δn, $\delta\vec{\mathrm{V}}$, and δT —are preserved; all other components of the initial perturbation relax at the rate ν_D or faster. In other words, we find that

$$\lim_{t\to\infty} f = \frac{n_0}{(2\pi T_0/m)^{3/2}} e^{-u^2/2}\left[1+\frac{\delta n}{n_0}+\frac{\delta\vec{\mathrm{V}}\cdot\vec{u}}{\sqrt{T_0/m}}+\frac{\delta T(u^2-3)}{T_0}\right]. \tag{2.20}$$

Since $\delta n/n_0$, $\left|\delta\vec{\mathrm{V}}\middle/\sqrt{T_0/m}\right|$, and $\delta T/T_0$ are small in comparison to unity, this time-asymptotic expression is equivalent to a Maxwellian with density $n_0+\delta n$, mean velocity $\delta\vec{\mathrm{V}}$, and temperature $T_0+\delta T$.

In certain circumstances—for example, if the plasma of interest is magnetized—it may be useful to work in cylindrical velocity coordinates, which we define by

$$u_\perp = \sqrt{u_x^2+u_y^2}, \qquad \theta_u = \tan^{-1}(u_y/u_x). \tag{2.21}$$

In these coordinates, the $u_\perp$ dependence of the eigenfunctions of χ may be expressed in terms of the associated Laguerre polynomials, $L_n^m(x)$. Specifically, the functions

$$\varphi^{[1]}_{n_\perp n_z m_1} = u_\perp^{|m_1|} L_{n_r}^{|m_1|}(u_\perp^2/2)\sin(m_1\theta_u) He_{n_z}(u_z),$$
$$\varphi^{[2]}_{n_\perp n_z m_2} = u_\perp^{|m_2|} L_{n_r}^{|m_2|}(u_\perp^2/2)\cos(m_2\theta_u) He_{n_z}(u_z) \tag{2.22}$$

are eigenfuntions of χ with eigenvalues

$$\lambda^{[1]}_{n_r n_z m_1} = -\nu_D\left(n_z + 2n_r + |m_1|\right),$$
$$\lambda^{[2]}_{n_r n_z m_2} = -\nu_D\left(n_z + 2n_r + |m_2|\right), \tag{2.23}$$

provided that $\{n_\perp, n_z, m_2\} \neq \{1,0,0\}$, $\{0,1,0\}$, $\{0,0,1\}$, $\{0,2,0\}$, $\{0,0,2\}$ and that $\{n_\perp, n_z, m_1\} \neq \{0,0,1\}$; here $n_\perp, n_z,$ and m_2 are non-negative integers and m_1 is a positive integer. The remaining eigenfunctions are

$$\phi^{[1]}_{001} = u_\perp \sin\theta_u,$$
$$\phi^{[2]}_{001} = u_\perp \cos\theta_u,$$
$$\phi^{[2]}_{010} = u_z,$$
$$\phi^{[2]}_{100} = u_\perp^2 + u_z^2 - 3, \tag{2.24}$$

having eigenvalues $\lambda^{[1]}_{001} = \lambda^{[2]}_{001} = \lambda^{[2]}_{010} = \lambda^{[2]}_{100} = 0$ and

$$\varphi^{[2]}_{002} = u_\perp^2 \cos(2\theta_u),$$
$$\varphi^{[2]}_{020} = 2u_z^2 - u_\perp^2, \tag{2.25}$$

having eigenvalues $\lambda^{[2]}_{002} = \lambda^{[2]}_{020} = -2\nu_D$.

2.3. The Limit of Strong Collisionality

The validity of the fluid theory in the limit of strong collisionality is based on the existence of hydrodynamic modes that decay slowly compared with the typical collisional relaxation time. The hydrodynamic modes arise as a consequence of the conservation of particle number, momentum, and energy by collisions. Because the

Dougherty operator respects these conservation laws, it naturally gives rise to fluid-like behavior when collisions are strong.

To see that the Dougherty operator gives rise to realistic fluid dynamics, we consider the evolution of a perturbation of the form [34]

$$\delta f(\vec{u},z,t) = f_0(u)\varphi(\vec{u},t)e^{ikz} \tag{2.26}$$

To avoid the complication of collective forces, we imagine a gas of perfectly Debye-shielded particles. The linearized kinetic equation governing the perturbation is then

$$[iku_z\sqrt{T_0/m} - \chi]\varphi = -\frac{\partial\varphi}{\partial t}. \tag{2.27}$$

Solving this equation is equivalent to finding the eigenfunctions of the operator $K \equiv iku_z\sqrt{T_0/m} - \chi$. If collisions are sufficiently strong (*i.e.*, $\nu_D >> k\sqrt{T_0/m}$), then $iku_z\sqrt{T_0/m}$ may be treated as a perturbation to χ in Eq. (2.27). Thus, if $\Phi_{n_1n_2n_3}$ and $\Lambda_{n_1n_2n_3}$ are the eigenfunctions and eigenvalues of *K*, then as a first approximation,

$$\begin{aligned} \Phi_{n_1n_2n_3} &= \varphi_{n_1n_2n_3}, \\ \Lambda_{n_1n_2n_3} &= -\lambda_{n_1n_2n_3}, \end{aligned} \tag{2.28}$$

provided that $\lambda_{n_1n_2n_3}$ is non-degenerate.

However, in the degenerate subspace for which $\lambda_{n_1n_2n_3} = 0$, one must diagonalize the perturbation, $iku_z\sqrt{T_0/m}$, in order to obtain the correct lowest-order approximation to the eigenfunctions of *K*. In this degenerate subspace, in the basis {1, u_x, u_y, u_z, (u^2-3)/$\sqrt{6}$ }, the operator $iku_z\sqrt{T_0/m}$ has the following matrix representation

$$ik u_z \sqrt{T_0/m} = ik\sqrt{T_0/m}\begin{bmatrix} 0 & 0 & 0 & 1 & 0 \\ 0 & 0 & 0 & 0 & 0 \\ 0 & 0 & 0 & 0 & 0 \\ 1 & 0 & 0 & 0 & \sqrt{2/3} \\ 0 & 0 & 0 & \sqrt{2/3} & 0 \end{bmatrix}. \qquad (2.29)$$

The eigenvectors and eigenvalues of this "degenerate block" are

$$\begin{aligned} \Phi^{(0)}_{000} &= \frac{1}{\sqrt{5}}\left[-\sqrt{2} + \frac{1}{\sqrt{2}}(u^2-3)\right],\ \Lambda^{(1)}_{000} = 0; \\ \Phi^{(0)}_{100} &= u_x,\ \Lambda^{(1)}_{100} = 0; \\ \Phi^{(0)}_{010} &= u_y,\ \Lambda^{(1)}_{010} = 0; \\ \Phi^{(0)}_{00\pm1} &= \sqrt{\frac{3}{10}}\left[1 \pm \sqrt{\frac{5}{3}}u_z + \frac{1}{3}(u^2-3)\right],\ \Lambda^{(1)}_{00\pm1} = \pm ik\mathrm{v}_{th}\sqrt{\frac{5}{3}}. \end{aligned} \qquad (2.30)$$

The second order corrections to these eigenvalues are given by the formula

$$\Lambda^{(2)}_{n_1 n_2 n_3} = \sum_{\substack{n_1', n_2', n_3' \\ s.t. \Lambda^{(0)} \neq 0}} \frac{\left|(\Phi^{(0)}_{n_1 n_2 n_3}, ik\mathrm{v}_z \Phi^{(0)}_{n_1' n_2' n_3'})\right|^2}{-\Lambda^{(0)}_{n_1' n_2' n_3'}}\ ; \qquad (2.31)$$

they are $\Lambda^{(2)}_{000} = k^2 T_0 / 3\nu_D m$, $\Lambda^{(2)}_{100} = \Lambda^{(2)}_{010} = k^2 T_0 / 2\nu_D m$, and $\Lambda^{(2)}_{00\pm1} = 4k^2 T_0 / 9\nu_D m$.

Since $\Lambda_{000}, \Lambda_{100}, \Lambda_{010}$, and $\Lambda_{00\pm1}$ are smaller than all other eigenvalues of K by at least a factor of $k\sqrt{T_0/m}\big/\nu_D$, the time-asymptotic behavior of δf is dictated by $\Phi_{000}, \Phi_{100}, \Phi_{010}$, and $\Phi_{00\pm1}$. Specifically, after a sufficiently long time (*i.e.*, $\nu_D t >> 1$), a hydrodynamic phase ensues, during which δf is given by

$$\begin{aligned} \delta f \cong f_0 e^{ikz}[&A_{000}\Phi_{000}e^{-k^2T_0 t/3\nu_D m} + A_{100}\Phi_{100}e^{-k^2T_0 t/2\nu_D m} + A_{100}\Phi_{100}e^{-k^2T_0 t/2\nu_D m} \\ &+ A_{001}\Phi_{001}e^{-4k^2T_0 t/9\nu_D m - ik\sqrt{5T_0/3m}t} + A_{00-1}\Phi_{00-1}e^{-4k^2T_0 t/9\nu_D m + ik\sqrt{5T_0/3m}t}], \end{aligned} \qquad (2.32)$$

where the coefficients $A_{000}, A_{100}, A_{010}$, and $A_{00\pm1}$ are determined from $\varphi(\bar{u}, t=0)$.

The first term in square brackets on the right hand side of Eq. (2.32) is properly identified as a heat conduction mode; the second and third terms represent viscous relaxation; the fourth and fifth terms are counter-propagating, damped sound waves.

The eigenvalues Λ_{000} and Λ_{100} (corresponding to the heat conduction and viscous relaxation modes, respectively) can be compared with the corresponding eigenvalues of the linearized hydrodynamic equations. This comparison yields formulae for the viscosity, η_D, and thermal conductivity, κ_D, corresponding to the Dougherty collision operator:

$$\eta_D = \frac{1}{2} n_0 \frac{T_0}{\nu_D} \tag{2.33}$$

$$\kappa_D = \frac{5}{6} n_0 \frac{T_0}{m\nu_D}. \tag{2.34}$$

These expressions are reasonable approximations to the Braginskii transport coefficients that result from the more accurate MRJ collision operator [35]:

$$\eta = 0.96 n_0 \frac{T_0}{\nu_s} \tag{2.35}$$

$$\kappa = 3.9 n_0 \frac{T_0}{m\nu_s} \tag{2.36}$$

where $\nu_s \equiv 4\pi^{1/2}\lambda q^4 n_0 / (3m^{1/2}T_0^{3/2})$ is the collisional slowing-down rate for a thermal particle.

2.4 Acknowledgements

Chapter 2, in part, is a reprint of the material as it appears in Physics of Plasmas. M. W. Anderson, T. M. O'Neil, *Physics of Plasmas*, **14**, 052103 (2007). The dissertation author was the primary investigator and author of this paper.

Chapter 3

Kinetic Theory of Trivelpiece-Gould Waves with Collisional Velocity Scattering

In this chapter, we use the Dougherty collision operator to investigate the effect of collisional velocity scattering on a plasma wave propagating along a magnetized, single-species plasma column of infinite length [3]. We seek azimuthally symmetric, wave-like solutions of Poisson's equation plus the drift-kinetic equation with Dougherty's collision term and find a dispersion relation for the complex frequency of the wave in terms of the Debye length, the plasma frequency, the collision frequency, and the wavenumbers along and transverse to the magnetic field. For a wave with phase velocity comparable to the thermal velocity, Landau damping is recovered when the collision frequency is sufficiently small. For a wave with phase velocity much greater than the thermal velocity, a simple expression for the complex frequency is obtained, and the damping is dominated by collisions.

3.1 Poisson's Equation

Having in mind a Penning-Malmberg confinement scheme [2], we imagine that the plasma column resides in a coaxial conducting cylinder of radius R and is immersed in an axial magnetic field ($\vec{B} = B\hat{z}$). We take the radial density profile in the absence of the wave to be uniform—that is,

$$n_0(r) = \begin{cases} n_0 & r < a \\ 0 & a < r < R \end{cases} \tag{3.1}$$

where a is the radius of the plasma column. The unperturbed plasma column is symmetric under azimuthal rotation and translation along the magnetic field, and we anticipate azimuthally symmetric eigenmodes of the form

$$\delta\varphi = \delta\hat{\varphi} J_0(k_\perp r) e^{i(k_z z - \omega t)}, \ \delta f = \delta\hat{f} J_0(k_\perp r) e^{i(k_z z - \omega t)} \tag{3.2}$$

inside the plasma (*i.e.*, for $r < a$) and

$$\delta\varphi = \delta\hat{\varphi}[A I_0(k_z r) + B K_0(k_z r)] e^{i(k_z z - \omega t)}, \ \delta f = 0 \tag{3.3}$$

outside the plasma (for $r > a$). Here $J_0(x)$ is a Bessel function of the first kind, $I_0(x)$ and $K_0(x)$ are modified Bessel functions of the first and second kinds, and A and B are constants specified by the requirements that the potential and the electric field be continuous across the radial boundary of the plasma column. The requirement that the potential vanish at the conducting wall imposes on the radial wavenumber, $k_\perp$, the well-known constraint [7, 19]

$$k_z a \frac{I_0'(k_z a) K_0(k_z R) - K_0'(k_z a) I_0(k_z R)}{I_0(k_z a) K_0(k_z R) - K_0(k_z a) I_0(k_z R)} - k_\perp a \frac{J_0'(k_\perp R)}{J_0(k_\perp R)} = 0. \tag{3.4}$$

For each axial wavenumber k_z, this equation admits an infinite sequence of solutions for $k_\perp$, each corresponding to a different radial eigenmode.

Inside the plasma, for a perturbation of the above form, Poisson's equation reduces to

$$-k^2 \delta\hat{\varphi} = 4\pi e \int d\vec{v}\, \delta\hat{f}\,. \tag{3.5}$$

Outside the plasma, the perturbation satisfies Laplace's equation identically.

3.2 The Dougherty Kinetic Equation

In accord with typical experiments on single-species plasmas, we assume that the wavenumbers and frequencies under consideration are sufficiently small that the dynamics may be described using the drift approximation. In other words, we take f to be the distribution of guiding centers with parallel velocity v_z and cyclotron invariant $I_c = mv_\perp^2 / 2B$:

$$f = f(r, z, v_z, v_\perp^2). \tag{3.6}$$

The evolution of this distribution is governed by the drift-kinetic equation

$$\frac{\partial f}{\partial t} + v_z \frac{\partial f}{\partial z} + \frac{c\hat{z} \times \vec{\nabla}\varphi}{B} \cdot \vec{\nabla} f + \frac{e}{m} \frac{\partial \varphi}{\partial z} \frac{\partial f}{\partial v_z} = C(f), \tag{3.7}$$

with collisional effects contained in the term $C(f)$.

The experiments that we have in mind are characterized by the ordering $\lambda_D >> r_c >> b$, where λ_D is the Debye length, r_c is the cyclotron radius, and b is the classical distance of closest approach. This ordering implies two classes of collisions. The first consists of approximately isotropic, velocity-scattering collisions with impact parameters between b and r_c; these collisions are accurately described by a Fokker-Planck collision operator [36, 37]. The second class of collisions, characterized by impact parameters larger than r_c, is highly anisotropic; the cyclotron adiabatic invariant inhibits the exchange of energy between parallel and perpendicular degrees of freedom, so these collisions are effectively 1-D [6]. The long-range collisions

cannot be accounted for by a Fokker-Planck collision operator, so we will ignore them in this chapter and discuss them in the context of fluid theory in Chapter 4.

We account for the short-range collisions using Dougherty's collision operator. In the drift approximation, the Dougherty operator takes the form

$$\begin{aligned} C_D(f) = \nu_D \frac{1}{\mathrm{v}_\perp}\frac{\partial}{\partial \mathrm{v}_\perp}\mathrm{v}_\perp\left[\frac{T[f]}{m}\frac{\partial f}{\partial \mathrm{v}_\perp} + \mathrm{v}_\perp f\right] \\ + \nu_D \frac{\partial}{\partial \mathrm{v}_z}\left[\frac{T[f]}{m}\frac{\partial f}{\partial \mathrm{v}_z} + (\mathrm{v}_z - \mathrm{V}_z[f])f\right], \end{aligned} \tag{3.8}$$

where n, V_z and T are given by the functionals

$$n[f] = \int d\mathrm{v}_z\, d\mathrm{v}_\perp 2\pi \mathrm{v}_\perp f, \tag{3.9}$$

$$\mathrm{V}_z[f] = n^{-1}\int d\mathrm{v}_z\, d\mathrm{v}_\perp 2\pi \mathrm{v}_\perp \mathrm{v}_z f, \tag{3.10}$$

$$T[f] = (3n)^{-1}\int d\mathrm{v}_z\, d\mathrm{v}_\perp 2\pi \mathrm{v}_\perp [\mathrm{v}_\perp^2 + (\mathrm{v}_z - \mathrm{V}_z[f])^2] f\,. \tag{3.11}$$

For a reasonable approximation to the true Fokker-Planck collision operator, the collision parameter ν_D should be of order [37]

$$\nu_D \sim n e^4 m^{-1/2} T^{-3/2} \ln(r_c / b). \tag{3.12}$$

The argument of the Coulomb logarithm is the ratio of the upper and lower bounds on the impact parameters under consideration.

A steady-state solution to Eq. (3.7) is given by

$$f = f_0(r, \mathrm{v}_z, \mathrm{v}_\perp^2) = \frac{n_0(r)}{(2\pi T_0 / m)^{3/2}} e^{-m(\mathrm{v}_z^2 + \mathrm{v}_\perp^2)/2T_0} \tag{3.13}$$

$$\varphi = \varphi_0(r)\,, \tag{3.14}$$

where $\varphi_0(r)$ is determined from $n_0(r)$ via Poisson's equation and $n_0(r)$ is given by Eq. (3.1). We consider a perturbation to this steady state of the form

$$f(r,z,\mathrm{v}_z,\mathrm{v}_\perp^2,t) = f_0(r,\mathrm{v}_z,\mathrm{v}_\perp^2) + \delta f(r,z,\mathrm{v}_z,\mathrm{v}_\perp^2,t), \tag{3.15}$$

$$\varphi(r,z,t) = \varphi_0(r) + \delta\varphi(r,z,t)\,, \tag{3.16}$$

where δf and $\delta\varphi$ are assumed small and have the space and time dependence specified by Eqs. (3.2) and (3.3).

Substituting Eqs. (3.15) and (3.16) into the Dougherty kinetic equation, using Poisson's equation (3.5) to eliminate $\delta\varphi$, and neglecting nonlinear terms, we obtain the linearized Dougherty kinetic equation

$$i\omega\delta\hat{f} = ik_z\mathrm{v}_z\delta\hat{f} - C_D(f_0,\delta\hat{f}) - C(\delta\hat{f},f_0) + \frac{ik_z\mathrm{v}_z}{k^2\lambda_D^2}\frac{f_0}{n_0}\int d\bar{\mathrm{v}}\,\delta\hat{f}, \tag{3.17}$$

where $\lambda_D \equiv [T_0/(4\pi q^2 n_0)]^{1/2}$ is the Debye length in the unperturbed plasma. The linearized Dougherty operator takes a more convenient form when the perturbation is expressed as $\delta\hat{f} = f_0\phi$ and the thermal velocity, $\mathrm{v}_{th} = T_0/m$, and scaled velocity coordinates, $u_z = \mathrm{v}_z/\mathrm{v}_{th}$ and $u_\perp = \mathrm{v}_\perp/\mathrm{v}_{th}$, are introduced:

$$\begin{aligned} C_D(f_0,f_0\phi) + C_D(f_0\phi,f_0) = & \\ & f_0\nu_D\left[\frac{1}{u_\perp}\frac{\partial}{\partial u_\perp}u_\perp\frac{\partial\phi}{\partial u_\perp} - u_\perp\frac{\partial\phi}{\partial u_\perp} + \frac{\partial^2\phi}{\partial u_z^2} - u_z\frac{\partial\phi}{\partial u_z}\right] \\ & + \frac{\delta T}{T_0}\left(u_\perp^2 - 2 + u_z^2 - 1\right) + \frac{\delta\mathrm{V}_z}{\mathrm{v}_{th}}u_z \\ & \equiv \nu_D f_0\chi(\phi), \end{aligned} \tag{3.18}$$

where

$$\delta\mathrm{V}_z = n_0^{-1}\mathrm{v}_{th}^4\int du_z\,du_\perp\,2\pi u_\perp u_z\,\delta f, \tag{3.19}$$

$$\delta T = (3n_0)^{-1} m \mathrm{v}_{th}^5 \int du_z\, du_\perp 2\pi u_\perp [(u_z^2 + u_\perp^2) - 3]\delta f, \tag{3.20}$$

Equation (3.17) constitutes an eigenvalue problem, $\delta\hat{f}$ being the eigenfunction and ω the eigenvalue.

3.3 The Dispersion Equation

From Eq. (3.17), we wish to find a dispersion equation which relates the complex frequency, ω, to the axial and radial wavenumbers and the plasma parameters, including collisionality. To this end, we employ the complete set of orthogonal functions

$$\phi_{mn} \equiv \frac{1}{\sqrt{m!}} He_m(u_z) L_n(u_\perp^2/2), \tag{3.21}$$

where $He_m(x)$ is the m^{th} modified Hermite polynomial, $L_n(x)$ is the n^{th} Laguerre polynomial, and m and n take on nonnegative integer values. These functions satisfy the orthogonality relation

$$(\phi_{n_\perp n_z}, \phi_{m_\perp m_z}) \equiv (2\pi)^{-1/2} \int du_z\, du_\perp u_\perp \phi_{n_\perp n_z} \phi_{m_\perp m_z} e^{-u^2/2} = \delta_{n_\perp m_\perp} \delta_{n_z m_z}. \tag{3.22}$$

We expand the eigenfunction $\delta\hat{f}$ in a series of the form

$$\delta\hat{f}(u_z, u_\perp^2) = f_0 \sum_{m,n=0}^{\infty} a_{mn} \phi_{mn}(u_z, u_\perp^2), \tag{3.23}$$

where the coefficients a_{mn} are constant. Substituting this expression into Eq. (3.17) and exploiting the orthogonality relation (3.22), we obtain an infinite-dimensional matrix equation,

$$\Omega a_{mn} = \sum_{m',n'=0}^{\infty} (\phi_{mn}, u_z \phi_{m'n'}) a_{m'n'} + i\mu \sum_{m',n'=0}^{\infty} (\phi_{mn}, \chi \phi_{m'n'}) a_{mn} + \frac{\delta_{1,m}\delta_{0,n}}{k^2 \lambda_D^2} a_{00}, \tag{3.24}$$

for the coefficients a_{mn} and corresponding eigenvalue Ω; here we have introduced the scaled wave frequency $\Omega \equiv \omega / k_z \mathrm{v}_{th}$ and collision frequency $\mu \equiv \nu_D / k_z \mathrm{v}_{th}$, and the parentheses denote the inner product defined by Eq. (3.22). The first term on the right-hand-side is given by

$$(\phi_{mn}, u_z \phi_{m'n'}) = \delta_{m-1,m'} \delta_{n,n'} \sqrt{m} + \delta_{m,m'-1} \delta_{n,n'} \sqrt{m'}, \tag{3.25}$$

while the second term is simplified by the relations

$$\chi(\phi_{10}) = 0, \tag{3.26}$$

$$\chi(\phi_{20}) = -\frac{4}{3}\phi_{20} - \frac{2\sqrt{2}}{3}\phi_{01}, \tag{3.27}$$

$$\chi(\phi_{01}) = -\frac{2\sqrt{2}}{3}\phi_{20} - \frac{2}{3}\phi_{01}, \tag{3.28}$$

and otherwise

$$\chi(\phi_{mn}) = -(m + 2n). \tag{3.29}$$

In particular, for $m > 2$, Eq. (3.24) reduces to the recursion relation [12]

$$[\Omega + i(2n + m)\mu] a_{mn} = \sqrt{m} a_{m-1,n} + \sqrt{m+1} a_{m+1,n}. \tag{3.30}$$

A necessary condition for the convergence of the series (3.23) is that for a given value of n, the coefficients a_{mn} must approach zero as m approaches infinity. I this condition is satisfied, Eq. (3.30) implies that [12]

$$\frac{a_{m+1,n}}{a_{mn}} \to -\frac{i}{\sqrt{m}\mu} \qquad \text{as} \qquad m \to \infty. \tag{3.31}$$

With this limit in mind, we "truncate" the recursion relation (3.30) at some sufficiently large value of m, $m_{\max}$, by setting

$$[\Omega + i(2n + m_{\max})\mu]a_{m_{\max},n} = \sqrt{m_{\max}}\, a_{m_{\max}-1,n}. \tag{3.32}$$

In addition, we will look for eigenfunctions for which $a_{mn} = 0$ unless $n = 0$ or $n = 1$.

We begin with Eq. (3.32) and iterate the recursion relation backwards for $n = 0$ and $n = 1$. For $n = 0$, for example, Eq. (3.32) is solved for $a_{m_{\max},0}$, yielding

$$a_{m_{\max},0} = \frac{\sqrt{m_{\max}}}{[\Omega + im_{\max}\mu]} a_{m_{\max}-1,0}. \tag{3.33}$$

This expression is then substituted in the preceding equation,

$$[\Omega + i(m_{\max} - 1)\mu]a_{m_{\max}-1,0} = \sqrt{m_{\max} - 1}\, a_{m_{\max}-2,0} + \sqrt{m_{\max}}\, a_{m_{\max},0}\,, \tag{3.34}$$

which is then solved for $a_{m_{\max}-1,0}$, yielding

$$a_{m_{\max}-1,0} = \frac{\sqrt{m_{\max} - 1}}{\Omega + i(m_{\max} - 1)\mu - \dfrac{m_{\max}}{\Omega + im_{\max}\mu}} a_{m_{\max}-2,0}. \tag{3.35}$$

This expression is then substituted in the preceding equation, and so on. By means of these recursive substitutions, all but four of the coefficients a_{mn} can be eliminated. A byproduct of this procedure is the development of continued fractions, the beginnings of which can be seen in Eq. (3.35). The set of equations given by Eq. (3.24) [with the truncation condition (3.32)] is thereby reduced to the four equations

$$-\Omega a_{00} + a_{10} = 0\,, \tag{3.36}$$

$$[1 + (k\lambda_D)^{-2}]a_{00} - \Omega a_{10} + \sqrt{2}a_{20} = 0\,, \tag{3.37}$$

$$3\sqrt{2}a_{10} - 3F_1(\Omega,\mu)a_{20} - 2\sqrt{2}i\mu a_{01} = 0\,, \tag{3.38}$$

$$-2\sqrt{2}i\mu a_{20} - 3F_2(\Omega,\mu)a_{01} = 0\,, \tag{3.39}$$

where $F_1(\Omega,\,\mu)$ and $F_2(\Omega,\,\mu)$ are the continued fractions

$$F_1(\Omega,\,\mu) \equiv \Omega + \frac{4}{3}i\mu - \cfrac{3}{\Omega + 3i\mu - \cfrac{4}{\Omega + 4i\mu - \cdots \cfrac{m_{\max}}{\Omega + m_{\max} i\mu}}}\,, \tag{3.40}$$

$$F_2(\Omega,\,\mu) \equiv \Omega + \frac{2}{3}i\mu - \cfrac{1}{\Omega + 3i\mu - \cfrac{2}{\Omega + 4i\mu - \cdots \cfrac{m_{\max}}{\Omega + (m_{\max}+2) i\mu}}}\,. \tag{3.41}$$

Finally, upon elimination of the coefficients $a_{00}, a_{10}, a_{20},$ and a_{01} from Eqs. (3.36)-(3.39), the following dispersion equation is obtained:

$$(k\lambda_D)^2 = \frac{F_1(\Omega,\,\mu)F_2(\Omega,\,\mu) + 8\mu^2/9}{[F_1(\Omega,\,\mu)F_2(\Omega,\,\mu) + 8\mu^2/9](\Omega^2 - 1) - 2F_2(\Omega,\,\mu)\Omega}\,. \tag{3.42}$$

This result becomes exact in the limit $m_{\max} \to \infty$.

In general, for given values of $k\lambda_D$ and μ, Eq. (3.42) must be solved numerically for the complex frequency Ω; in practice, this requires that the continued fractions $F_1(\Omega,\,\mu)$ and $F_2(\Omega,\,\mu)$ be evaluated approximately by carrying out a sufficiently large number of iterations. The resulting dispersion relation is a polynomial equation, the number of roots of which increases with the number of iterations made in evaluating the continued fractions; each of these roots lies in the lower half of the complex Ω plane (see Fig. 3.1). In other words, there appears to be a countably infinite spectrum of damped eigenmodes, analogous to that found by Ng, Bhattacharjee, and Skiff for the one-dimensional LB kinetic equation [12].

The least damped root of Eq. (3.42) corresponds to the TG wave and approaches the Landau root of the collisionless dispersion relation in the limit $\mu \to 0$. In particular, in this limit, the imaginary part of this root does not approach zero exactly, but instead matches onto the Landau damping coefficient, as shown in Fig. 3.2 for $k\lambda_D = 0.3$. Hereafter, we will focus on this least damped root, which we will refer to simply as the Landau root.

In order to isolate collisional effects from resonant particle effects, we restrict our attention to high-phase-velocity waves [*i.e.*, $\mathrm{Re}(\Omega) >> 1$], for which Landau damping is negligible. In this limit, a suitable approximation to Eq. (3.42) may be obtained by setting $F_1 \to \Omega + 4i\mu/3$ and $F_2 \to \Omega + 2i\mu/3$, since retaining the continued fractions only leads to corrections of higher order in Ω^{-1}. The resulting dispersion equation is

$$(k\lambda_D)^2 = \frac{\Omega^2 + 2i\mu\Omega}{\Omega^4 + 2i\mu\Omega^3 - 3\Omega^2 - 10i\mu\Omega/3}. \tag{3.43}$$

There exists a weakly damped root to this equation when $k\lambda_D << 1$, and this is the Landau root. An approximate expression for this root, valid in both the weakly collisional and strongly collisional limits, can be obtained by solving Eq. (3.43) using perturbation theory. More precisely, we assume that $\mathrm{Re}(\Omega) \sim (k\lambda_D)^{-1}$ (this assumption will be verified after the analysis has been carried out) and take $\mu \sim \mathrm{Re}(\Omega)$; Eq. (3.43) can then be solved order by order in the small parameter $k\lambda_D << 1$. When carried out to second order, this procedure yields the expression

$$\Omega \cong \frac{1}{k\lambda_D}\left[1+\frac{3}{2}(k\lambda_D)^2\left(\frac{1+10i\mu k\lambda_D/9}{1+2i\mu k\lambda_D}\right)\right]. \tag{3.44}$$

In Fig. 3.3, this expression is plotted as a function of μ for $k\lambda_D = 0.05$, and the exact numerical solution of Eq. (3.42) for the Landau root is shown for comparison. With the units restored, Eq. (3.44) becomes

$$\omega = \frac{k_z\omega_p}{k}\left[1+\frac{3}{2}(k\lambda_D)^2\left(\frac{1+10i\alpha/9}{1+2i\alpha}\right)\right], \tag{3.45}$$

where ω_p is the plasma frequency and $\alpha \equiv \nu_D k/(k_z\omega_p)$ is a parameter characterizing the strength of collisionality.

For weak collisionality (*i.e.*, $\alpha << 1$), Eq. (3.45) reduces to

$$\mathrm{Re}(\omega) \cong \frac{k_z\omega_p}{k}\left[1+\frac{3}{2}(k\lambda_D)^2\right], \tag{3.46}$$

$$\mathrm{Im}(\omega) \cong -\frac{4}{3}\nu_D(k\lambda_D)^2. \tag{3.47}$$

Equation (3.46) is the well-known result from collisionless theory for the frequency of a long-wavelength TG wave on a single-species plasma column [19]. Equation (3.47) gives the collisional damping rate. Note that the damping is suppressed by the small factor $(k\lambda_D)^2 << 1$; this suppression is a reminder that the dominant damping mechanism in an electron-ion plasma—electron-ion friction—is not available in the single-species plasma.

Note from Eq. (3.46) that the ordering $k_z/k_\perp << 1$ implies that $\mathrm{Re}(\omega) << \omega_p$. This is the typical wavenumber ordering for plasma wave experiments on a long column, and we assume this ordering here. In fact, this ordering is implicit in our use

of a Fokker-Planck collision operator, since the derivation of such an operator requires the Bogoliubov hypothesis [20], $|\omega| << \omega_p$.

A weakly damped solution to the dispersion equation exists even in the limit of strong collisionality (*i.e.*, $\alpha >> 1$). In this limit, Eq. (3.45) reduces to

$$\mathrm{Re}(\omega) \cong \frac{k_z \omega_p}{k}\left[1 + \frac{5}{6}(k\lambda_D)^2\right], \tag{3.48}$$

$$\mathrm{Im}(\omega) \cong -\frac{1}{3}\left(\frac{\mathrm{v}_{th}^2}{\nu_D}\right)k_z^2. \tag{3.49}$$

Here, we implicitly assume that the plasma is weakly correlated (*i.e.*, $\nu_D << \omega_p$) even though the wave dynamics is strongly collisional, and this is possible since $\mathrm{Re}(\omega) << \omega_p$.

Note that the Bohm-Gross correction to the real part of the frequency—that is, the term $(3/2)(k\lambda_D)^2$ in the bracket of Eq. (3.46)—has been replaced by $(5/6)(k\lambda_D)^2$ in Eq. (3.48). This change, which emerges automatically from kinetic theory, has a simple explanation based on the adiabatic law of compression [21]. The numerical coefficient of the Bohm-Gross term is $(d+2)/(2d)$, where d is the number of degrees of freedom that share the compressive energy. For weak collisionality, there is negligible equipartition, so $d = 1$ and $(d + 2)/(2d) = 3/2$; whereas, for strong collisionality, there is nearly complete equipartition, so $d = 3$ and $(d + 2)/(2d) = 5/6$.

3.4 The Distribution Function

In the limit $\mu << 1,$ we evaluate the sum in Eq. (3.23) to determine the $u_\perp$-integrated eigenfunction, $\delta\tilde{f} \equiv 2\pi \int du_\perp u_\perp \delta\hat{f},$ corresponding to the Landau root for several values of the parameters μ and $k\lambda_D$. In Fig. 3.4, this function is plotted for $\mu = 0.035$ and $k\lambda_D = 0.33.$ (These values were chosen to facilitate comparison with Fig. 2 in [12].) We find that the eigenfunction exhibits the qualitative features of that determined by Ng *et al*. using the LB operator [12]. In the vicinity of the resonance (*i.e*., for $u_z \cong \Omega),$ the eigenfunction deviates significantly from the expression for the collisionless quasi-mode, $u_z e^{-u_z^2/2}[\sqrt{2\pi}(k\lambda_D)^2(\Omega - u_z)]^{-1};$ whereas far from the resonance, the collisionless expression is a good approximation. The width of the "boundary layer" surrounding the resonance increases with collisionality.

In the limit $\mu >> \Omega,$ all of the coefficients in the sum (3.23) are of order μ^{-1} or smaller, with the exceptions of $a_{00}, a_{10}, a_{20},$ and $a_{01};$ in this case, the eigenfunction is given by

$$\delta\hat{f}(u_z, u_\perp^2) = \frac{e^{-(u_z^2+u_\perp^2)/2}}{\sqrt{2\pi}}\left\{1 + \Omega u_z + \frac{1}{2}[\Omega^2 - 1 - (k\lambda_D)^{-2}](u_z^2 + u_\perp^2 - 3)\right\} + O(\mu^{-1}). \tag{3.52}$$

Evidently, as a first approximation, the perturbation to the distribution is completely characterized by the perturbations in particle number, momentum, and energy. In other words, the distribution is simply a Maxwellian with perturbed density, drift

velocity, and temperature, with all other components of the perturbation vanishing as μ^{-1}.

3.5 Comparison with Landau Collision Operator

We have just seen that in the limit of weak collisionality, an eigenmode of the collisional system is nearly identical to the corresponding quasi-mode of the collisionless system, except in the vicinity of the wave-particle resonance. Furthermore, when the phase-velocity of the wave of interest is large compared with the thermal velocity, the fraction of particles in the vicinity of the resonance is exponentially small. Thus, for a high-phase-velocity wave in the weakly collisional limit, we may treat the collision term as a small perturbation to the collisionless drift-kinetic equation. The perturbation theory can be carried out to first order using the more accurate Landau collision operator (which is equivalent to the MRJ operator discussed in Chapter 2), providing an opportunity for comparison with the results obtained using the Dougherty collision operator in this limit.

We proceed by expressing the wave frequency, the distribution function, and the potential as $\omega \cong \omega^{(0)} + \omega^{(1)}$, $\delta f \cong \delta f^{(0)} + \delta f^{(1)}$, and $\delta\varphi \cong \delta\varphi^{(0)} + \delta\varphi^{(1)}$, where the superscripts indicate the size of each term in powers of the collisionality. The zero-order, drift-kinetic/Poisson system of equations is

$$(-i\omega^{(0)} + ik_z \mathrm{v}_z)\delta f^{(0)} + ik_z \mathrm{v}_z \frac{q\delta\varphi^{(0)}}{T} f_0 = 0, \tag{3.53}$$

$$-k^2\delta\varphi^{(0)} = -4\pi q\int d\vec{\mathrm{v}}\delta f^{(0)}, \tag{3.54}$$

from which follows the well-known dispersion equation

$$1+(k\lambda_D)^{-2}\int d\vec{\mathrm{v}}\frac{k_z\mathrm{v}_z}{\omega^{(0)}-k_z\mathrm{v}_z}\frac{f_0}{n_0}=0. \tag{3.55}$$

We ignore the usual subtleties related to the resonance, since, by hypothesis, there are negligibly few resonant particles. To first order in collisionality, the collisional drift-kinetic/Poisson system is

$$\begin{aligned}(-i\omega^{(0)}+ik_z\mathrm{v}_z)\delta f^{(1)}-i\omega^{(1)}\delta f^{(0)}+ik_z\mathrm{v}_z\frac{q\delta\varphi^{(1)}}{T}f_0 = \\ C(f_0,\delta f^{(0)})+C(\delta f^{(0)},f_0),\end{aligned} \tag{3.56}$$

$$-k^2\delta\varphi^{(1)} = -4\pi q\int d\vec{\mathrm{v}}\delta f^{(1)}. \tag{3.57}$$

Substituting the second of these equations into the first, dividing by $(-i\omega^{(0)}+ik_z\mathrm{v}_z)$, and integrating over velocity, we obtain

$$\omega^{(1)}\int d\vec{\mathrm{v}}\frac{\delta f^{(0)}}{\omega^{(0)}-k_z\mathrm{v}_z} = i\int d\vec{\mathrm{v}}(\omega^{(0)}-k_z\mathrm{v}_z)^{-1}[C(f_0,\delta f^{(0)})+C(\delta f^{(0)},f_0)], \tag{3.58}$$

where the first and third terms on the left-hand-side of Eq. (3.56) have cancelled by virtue of the collisionless dispersion equation (3.55). With the collision operator expressed in the Landau form [38], Eq. (3.58) becomes

$$\begin{aligned}&\omega^{(1)}\int d\vec{\mathrm{v}}\frac{f_0\phi}{\omega^{(0)}-k_z\mathrm{v}_z} = i\frac{2\pi q^4\ln\Lambda}{m^2}\times \\ &\times\int d\vec{\mathrm{v}}(\omega^{(0)}-k_z\mathrm{v}_z)^{-1}\frac{\partial}{\partial\vec{\mathrm{v}}}\cdot\int d\vec{\mathrm{v}}'\frac{(\vec{\mathrm{v}}\text{-}\vec{\mathrm{v}}')^2\mathbf{I}-(\vec{\mathrm{v}}\text{-}\vec{\mathrm{v}}')(\vec{\mathrm{v}}\text{-}\vec{\mathrm{v}}')}{\left|\vec{\mathrm{v}}\text{-}\vec{\mathrm{v}}'\right|^3}f_0f_0'\left[\frac{\partial\phi}{\partial\vec{\mathrm{v}}}-\frac{\partial\phi'}{\partial\vec{\mathrm{v}}'}\right],\end{aligned} \tag{3.59}$$

where $\mathbf{I}$ is the unit tensor and we have defined $\phi\equiv k_z\mathrm{v}_z/(\omega^{(0)}-k_z\mathrm{v}_z)$.

To lowest order in $k_z \mathrm{v}_{th}/\omega,$ the integral on the left-hand-side of Eq. (3.59) is given by

$$\int d\vec{\mathrm{v}} \frac{f_0 \varphi}{\omega^{(0)} - k_z \mathrm{v}_z} \cong 2n_0 \frac{k_z^2 \mathrm{v}_{th}^2}{\omega^{(0)3}}. \tag{3.60}$$

It remains to evaluate the integral

$$\int d\vec{\mathrm{v}} (\omega^{(0)} - k_z \mathrm{v}_z)^{-1} \frac{\partial}{\partial \vec{\mathrm{v}}} \cdot \int d\vec{\mathrm{v}}' \frac{(\vec{\mathrm{v}} - \vec{\mathrm{v}}')^2 \mathbf{I} - (\vec{\mathrm{v}} - \vec{\mathrm{v}}')(\vec{\mathrm{v}} - \vec{\mathrm{v}}')}{\left|\vec{\mathrm{v}} - \vec{\mathrm{v}}'\right|^3} f_0 f_0' \left[\frac{\partial \phi}{\partial \vec{\mathrm{v}}} - \frac{\partial \phi'}{\partial \vec{\mathrm{v}}'}\right] \equiv I \tag{3.61}$$

Integrating by parts and expanding the resonant denominators, we obtain

$$\begin{aligned} I &= -\int d\vec{\mathrm{v}}\, d\vec{\mathrm{v}}' \left[\frac{\partial}{\partial \mathrm{v}_z} (\omega^{(0)} - k_z \mathrm{v}_z)^{-1}\right] \frac{(\mathrm{v}_x - \mathrm{v}_x')^2 + (\mathrm{v}_y - \mathrm{v}_y')^2}{\left|\vec{\mathrm{v}} - \vec{\mathrm{v}}'\right|^3} f_0 f' \left[\frac{\partial \phi}{\partial \mathrm{v}_z} - \frac{\partial \phi'}{\partial \mathrm{v}_z}\right] \\ &= -n_0^2 \int d\vec{\mathrm{v}}\, d\vec{\mathrm{v}}' \frac{1}{\omega^{(0)}} \left[\frac{k_z}{\omega^{(0)}} + 2\left(\frac{k_z}{\omega^{(0)}}\right)^2 \mathrm{v}_z + 3\left(\frac{k_z}{\omega^{(0)}}\right)^3 \mathrm{v}_z^2 + \cdots\right] \frac{(\mathrm{v}_x - \mathrm{v}_x')^2 + (\mathrm{v}_y - \mathrm{v}_y')^2}{\left|\vec{\mathrm{v}} - \vec{\mathrm{v}}'\right|^3} \times \\ &\qquad \times \frac{e^{-(\mathrm{v}^2 + \mathrm{v}'^2)/2\mathrm{v}_{th}^2}}{(2\pi)^3 \mathrm{v}_{th}^6} \left[2\left(\frac{k_z}{\omega^{(0)}}\right)^2 (\mathrm{v}_z - \mathrm{v}_z') + 3\left(\frac{k_z}{\omega^{(0)}}\right)^3 (\mathrm{v}_z^2 - \mathrm{v}_z'^2) + \cdots\right]. \end{aligned} \tag{3.62}$$

In terms of center-of-mass and relative coordinates,

$$\vec{\mathrm{v}}_1 = \frac{1}{2}(\vec{\mathrm{v}} + \vec{\mathrm{v}}'); \quad \vec{\mathrm{v}}_2 = \vec{\mathrm{v}} - \vec{\mathrm{v}}', \tag{3.63}$$

the integral takes the form

$$\begin{aligned} I = -n_0^2 \int d\vec{\mathrm{v}}_1\, d\vec{\mathrm{v}}_2 \frac{1}{\omega^{(0)}} &\left[\frac{k_z}{\omega^{(0)}} + 2\left(\frac{k_z}{\omega^{(0)}}\right)^2 \left(\mathrm{v}_{1_z} + \frac{\mathrm{v}_{2_z}}{2}\right) + 3\left(\frac{k_z}{\omega^{(0)}}\right)^3 \left(\mathrm{v}_{1_z} + \frac{\mathrm{v}_{2_z}}{2}\right)^2 + \cdots\right] \times \\ &\times \frac{\mathrm{v}_{2_x}^2 + \mathrm{v}_{2_y}^2}{\mathrm{v}_2^3} \frac{e^{-(2\mathrm{v}_1^2 + \mathrm{v}_2^2/2)/2\mathrm{v}_{th}^2}}{(2\pi)^3 \mathrm{v}_{th}^6} \left[2\left(\frac{k_z}{\omega^{(0)}}\right)^2 \mathrm{v}_{2_z} + 6\left(\frac{k_z}{\omega^{(0)}}\right)^3 \mathrm{v}_{1_z} \mathrm{v}_{2_z} + \cdots\right]. \end{aligned} \tag{3.64}$$

Carrying out the integral over v_1 yields, to lowest order in $k_z \mathrm{v}_{th}/\omega,$

$$I \cong -\frac{n_0^2}{4\pi^{3/2}}\frac{k_z^4}{\omega^{(0)5}}\int d\bar{\mathrm{v}}_2\,\frac{\mathrm{v}_{2_x}^2+\mathrm{v}_{2_y}^2}{\mathrm{v}_2^3}\mathrm{v}_{2_z}^2\,\frac{e^{-\mathrm{v}_2^2/4\mathrm{v}_{th}^2}}{\mathrm{v}_{th}^3}$$
$$= -\frac{16}{15\sqrt{\pi}}i\frac{n_0^2k_z^4\mathrm{v}_{th}}{\omega^{(0)5}}. \tag{3.65}$$

Finally, substitution of Eqs. (3.65) and (3.60) into Eq. (3.59) gives the damping rate

$$\omega^{(1)} \cong -i\frac{16\sqrt{\pi}}{15}\frac{n_0q^4\ln(r_c/b)}{m^2\mathrm{v}_{th}^3}\left(\frac{k_z\mathrm{v}_{th}}{\omega^{(0)}}\right)^2. \tag{3.66}$$

The expression in parentheses is approximately $k_z\mathrm{v}_{th}/\omega \cong k\lambda_D$. Furthermore, the factor outside the parentheses is recognizable as the equiparition rate, $\nu_{\parallel,\perp}$, predicted by the Landau collision operator [39]. Thus, we can rewrite Eq. (3.66) in the more compact form

$$\omega^{(1)} \cong -i\nu_{\parallel,\perp}(k\lambda_D)^2. \tag{3.67}$$

Comparison of Eq. (3.67) with the analogous damping formula (3.47), obtained from the Dougherty operator, suggests that the prefactor $4\nu_D/3$ in Eq. (3.47) must be the equipartition rate predicted by the Dougherty operator. This interpretation can be verified by direct calculation of the Dougherty equipartition rate. Consider the collisional relaxation of the anisotropic Maxwellian velocity distribution

$$f(\mathrm{v}_z,\mathrm{v}_\perp^2) = n_0\frac{e^{-m\mathrm{v}_z^2/(T_0+\delta T_z)}}{\sqrt{2\pi(T_0+\delta T_z)/m}}\frac{e^{-m\mathrm{v}_\perp^2/(T_0+\delta T_\perp)}}{2\pi(T_0+\delta T_\perp)/m}, \tag{3.68}$$

where δT_z and $\delta T_\perp$ are small in comparison with T_0. Expansion about the isotropic Maxwellian distribution

$$f_0 = \frac{n_0e^{-m\mathrm{v}^2/(2T_0)}}{(2\pi T_0/m)^{3/2}} \tag{3.69}$$

to first order in the small quantities yields the linear perturbation

$$\delta f = f_0 \left[\frac{\delta T_{\parallel}(m v_z^2 / T_0 - 1)}{T_0} + \frac{\delta T_{\perp}(m v_{\perp}^2 / T_0 - 2)}{T_0} \right]. \tag{3.70}$$

Substitution of this expression in the linearized Dougherty kinetic equation,

$$\frac{\partial \delta f}{\partial t} = C_D(f_0, \delta f) + C_D(\delta f, f_0), \tag{3.71}$$

multiplication by $m v_z^2 / (2T_0),$ and integration over velocity coordinates yields the equation

$$\frac{d\delta T_{\parallel}}{dt} = \frac{4\nu_D}{3}(\delta T_{\perp} - \delta T_{\parallel}), \tag{3.72}$$

for the evolution of the parallel temperature. In other words, the Dougherty collision model gives the isotropization rate $\nu_{\parallel,\perp}^{(D)} = 4\nu_D / 3,$ as expected. The connection between damping and temperature isotropization in the limit of weak collisionality will be explored further in the next chapter.

3.6 Acknowledgements

Chapter 3, in part, is a reprint of the material as it appears in Physics of Plasmas. M. W. Anderson and T. M. O'Neil, *Physics of Plasmas,* **14**, 112110 (2007). The dissertation author was the primary investigator and author of this paper

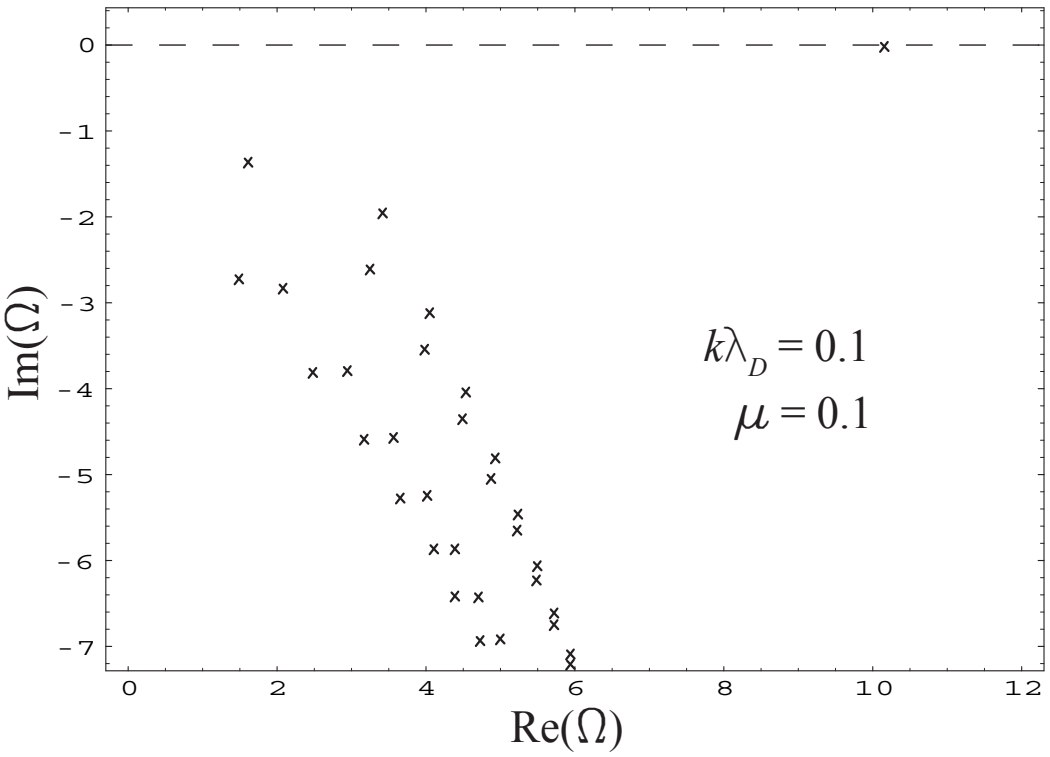

Figure 3.1. Complex eigenvalues of the linearized Dougherty kinetic equation, for $k\lambda_D = 0.1$ and $\mu = 0.1$. The dashed line indicates the real-Ω axis. The eigenvalue with smallest imaginary part gives the complex frequency of the plasma wave (Trivelpiece-Gould wave).

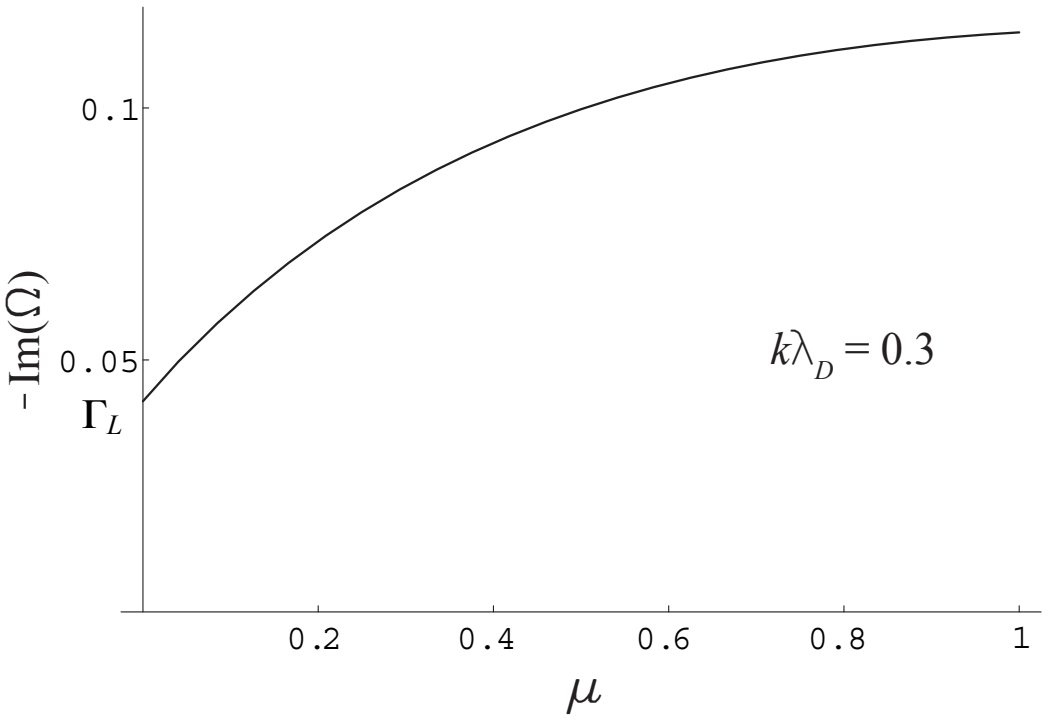

Figure 3.2. Scaled damping rate, $-\mathrm{Im}(\Omega)$, plotted as a function of μ, for $k\lambda_D = 0.3$. The intercept at $\mu = 0$ coincides with the scaled Landau damping rate, Γ_L, of collisionless theory.

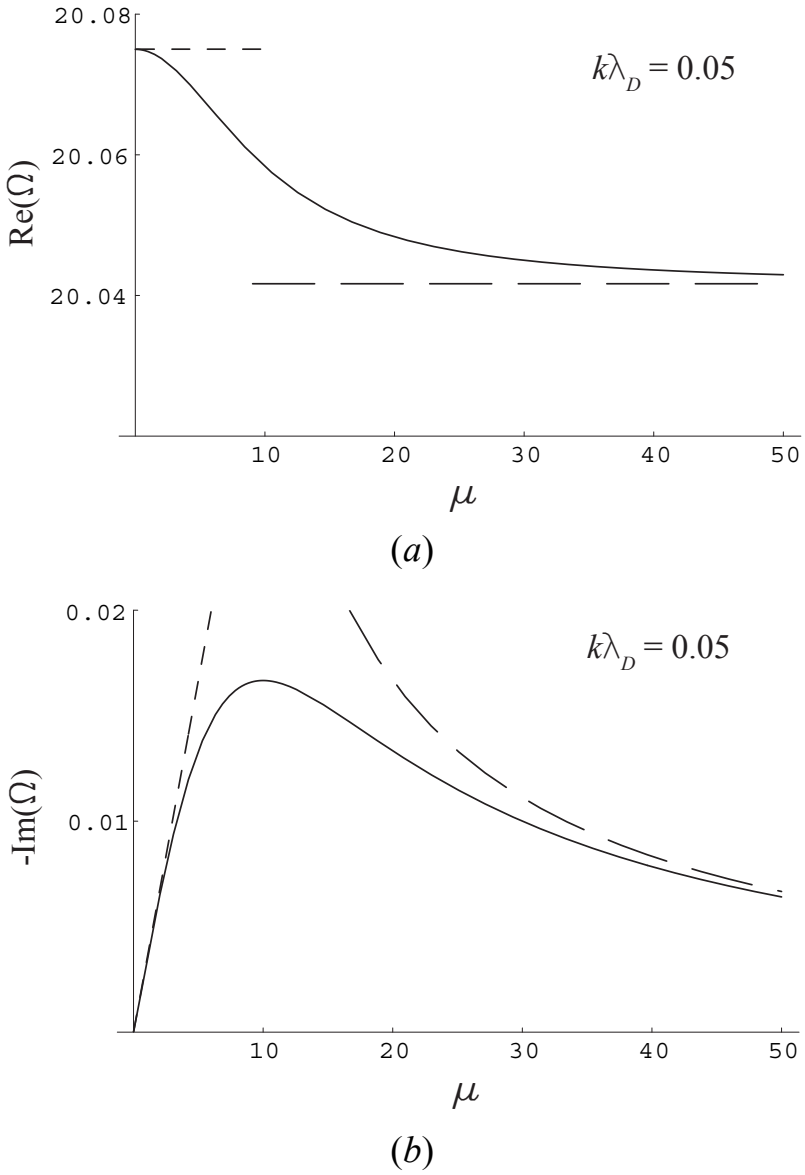

Figure 3.3. Real (*a*) and imaginary (*b*) parts of the analytic approximation (3.45) to the Landau root, plotted (as solid curve) versus μ, for $k\lambda_D = 0.05$. The solid circles represent the exact numerical solution of the dispersion equation (3.42). The short-dashed curves give the asymptotic expressions (3.46) and (3.47), which are valid for $\mu << \Omega$, while the long-dashed curves give the asymptotic forms (3.48) and (3.49), valid for $\mu >> \Omega$.

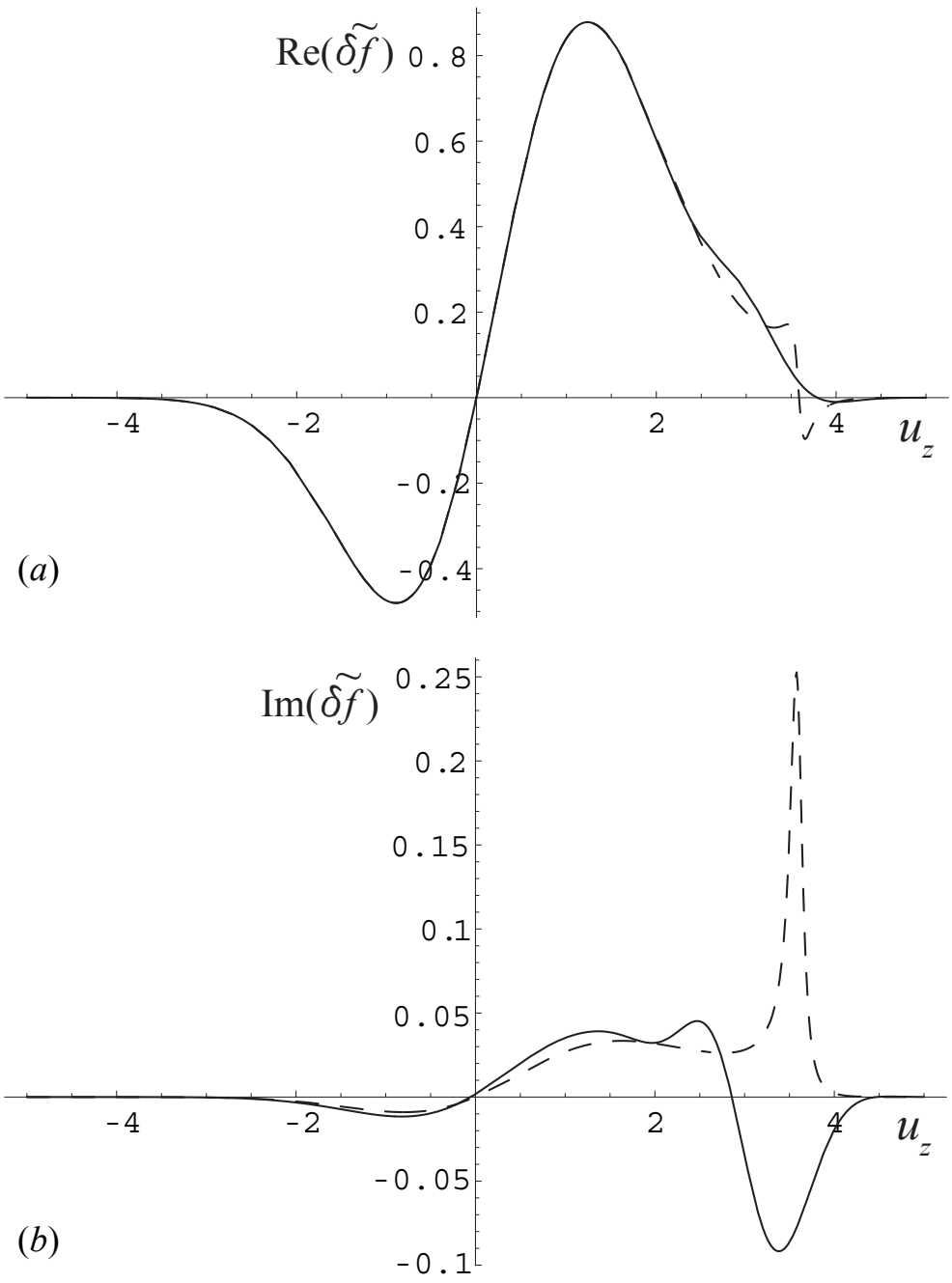

Figure 3.4. Real (*a*) and imaginary (*b*) parts of the $u_\perp$ -integrated eigenfunction, $\delta\tilde{f} \equiv 2\pi \int du_\perp u_\perp \delta\hat{f}$, corresponding to the Landau root, Ω, for $\mu = 0.035$ and $k\lambda_D = 0.33$. The dashed curves give the real and imaginary parts of the expression $u_z \mathrm{Exp}(-u_z^2/2) \times [(2\pi)^{1/2}(k\lambda_D)^2(\Omega - u_z)]^{-1}$.

Chapter 4

Fluid Theory of Trivelpiece-Gould Waves with Collisional Transport and Temperature Isotropization

Fluid theory provides a complementary approach to the kinetic theory presented in Chapter 3. While the kinetic dispersion formula (3.45) captures the effect of short-range collisions for arbitrary collisionality (provided that correlations are weak), it does not account for the effect of long-range collisions. These collisions lie outside the scope of any Fokker-Planck collision operator, but nonetheless dominate the transport of momentum and energy across the magnetic field [6]. Fortunately, this cross-field transport is easily accounted for in the context of fluid theory. In addition, while it is not obvious from the kinetic derivation how collisions cause damp the wave, fluid theory clarifies the damping mechanism underlying the kinetic result.

4.1 Fluid Theory with Collisional Transport

In the limit of strong collisionality, the plasma dynamics is accurately described by fluid equations, provided also that the axial and transverse scalelengths are large compared to the collisional transport step-sizes in these directions. In the fluid description, the effects of finite collisionality are contained in the transport terms.

Again, the analysis is simplest when the unperturbed density and temperature of the plasma column are constant for $r \le a$ and zero for $r > a$. The unperturbed fluid

velocity is then given by $\vec{V}_0 = r\omega_E\hat{\theta}$, where the $\vec{E}\times\vec{B}$ rotation frequency, ω_E, is a constant determined by the unperturbed density, n_0. Assuming that the density, fluid velocity, temperature, and potential perturbations share the parameter dependence

$$\delta n, \delta V_z, \delta T, \delta\varphi \sim J_0(k_\perp r)e^{i(k_z z-\omega t)}, \tag{4.1}$$

the linearized continuity, momentum, and energy equations plus Poisson's equation reduce to

$$-i\omega\delta n + n_0 ik_z\delta V_z = 0, \tag{4.2}$$

$$-i\omega\delta V_z = -ik_z\frac{q}{m}\delta\varphi - \frac{ik_z}{mn_0}T_0\delta n - \frac{ik_z}{m}\delta T - \frac{4}{3}\zeta_\parallel k_z^2\delta V_z - \zeta_\perp k_\perp^2\delta V, \tag{4.3}$$

$$-i\omega\delta T = -\frac{2}{3}T_0 ik_z\delta V_z - \chi_\parallel k_z^2\delta T - \chi_\perp k_\perp^2\delta T, \tag{4.4}$$

$$-k^2\delta\varphi = -4\pi q\delta n. \tag{4.5}$$

Here $\zeta_\parallel$ and $\zeta_\perp$ are the parallel and perpendicular kinematic viscosities and $\chi_\parallel$ and $\chi_\perp$ are the parallel and perpendicular thermal diffusivities. Elimination of the perturbed quantities from these equations yields the dispersion relation

$$\frac{(k\lambda_D)^2+1}{(k\lambda_D)^2(-i\Omega+4\bar{\zeta}_\parallel/3+\bar{\zeta}_\perp)i\Omega} - \frac{2}{3(-i\Omega+4\bar{\zeta}_\parallel/3+\bar{\zeta}_\perp)(-i\Omega+\bar{\chi}_\parallel+\bar{\chi}_\perp)} - 1 = 0, \tag{4.6}$$

where $\Omega = \omega/k_z\mathrm{v}_{th}$ is the scaled wave frequency and $\bar{\zeta}_\parallel = \zeta_\parallel k_z/\mathrm{v}_{th}$, $\bar{\zeta}_\perp = \zeta_\perp k_\perp^2/k_z\mathrm{v}_{th}$, $\bar{\chi}_\parallel = \chi_\parallel k_z/\mathrm{v}_{th}$, and $\bar{\chi}_\perp = \chi_\perp k_\perp^2/k_z\mathrm{v}_{th}$ are the scaled transport rates along and across the magnetic field. The validity of the fluid equations (4.2)-(4.5) requires the ordering $\bar{\zeta}_\parallel, \bar{\zeta}_\perp, \bar{\chi}_\parallel, \bar{\chi}_\perp << \Omega$. Working to first order in the transport rates, we approximate Eq. (4.6) as

$$\Omega^3 = \frac{1}{k^2\lambda_D^2}\Omega + \frac{5}{3}\Omega - i(4\bar{\xi}_\parallel/3 + \nu\bar{\xi}_\perp)\left(\frac{1}{k^2\lambda_D^2}+1\right) - i\frac{2}{3}(4\bar{\xi}_\parallel/3 + \bar{\chi}_\parallel + \bar{\xi}_\perp + \bar{\chi}_\perp). \tag{4.7}$$

For sufficiently long wavelengths (*i.e.*, $k\lambda_D << 1$), the dispersion equation (4.7) can be solved perturbatively for the root corresponding to the TG wave by treating $\bar{\xi}_\parallel, \bar{\xi}_\perp, \bar{\chi}_\parallel, \bar{\chi}_\perp,$ and $k\lambda_D$ on equal footing, and one finds (after restoring the units)

$$\mathrm{Re}(\omega) = \frac{k_z\omega_p}{k}\left[1 + \frac{5}{6}(k\lambda_D)^2\right], \tag{4.8}$$

$$\mathrm{Im}(\omega) = -\left(\frac{2}{3}\xi_\parallel k_z^2 + \frac{1}{2}\xi_\perp k_\perp^2\right). \tag{4.9}$$

The real part of the frequency (4.8) is identical to that obtained by kinetic theory in the limit of strong collisionality, as one would expect. The damping, at this order in the perturbation theory, is due to momentum transport, both along and across the magnetic field. If the contribution from cross-field viscosity is ignored in Eq. (4.9), the kinetic expression (3.49) is recovered by the substitution $\xi_\parallel = \xi_D \equiv \mathrm{v}_{th}^2/(2\nu_D),$ where ξ_D is the kinematic viscosity predicted by the Dougherty operator (see Section 2.3). In other words, the kinetic damping formula (3.49) corresponds to the dissipation of the compressive flow by bulk viscosity.

However, there is no justification for ignoring the contribution to the damping from cross-field viscosity. Typical experiments on single-species plasmas are characterized by the ordering $r_c << \lambda_D,$ where r_c is the cyclotron radius, and in this regime, the cross-field shear viscosity is roughly [6]

$$\zeta_{\perp} \cong \nu_c \lambda_D^2, \tag{4.10}$$

where $\nu_c \equiv nq^4 / (m^{1/2} T^{3/2})$. Comparison of the two terms in the expression (4.9) using the estimate (4.10) indicates that transport of axial momentum across the magnetic field is the dominant damping mechanism in the limit of strong collisionality. For sufficiently large transverse wavenumbers, [*i.e.*, $k_{\perp}\lambda_D \sim (\omega_p / \nu_c)(k_z \lambda_D)^{1/3}$], the wave is heavily damped by this mechanism. The estimate (4.10) is based on collisions between particles on different field lines—that is, collisions with impact parameter ρ satisfying $r_c << \rho < \lambda_D$. These collisions can only be described by a nonlocal collision operator and thus lie outside the scope of the Dougherty operator or any other Fokker-Planck operator.

The contribution to the damping rate due to heat conduction appears at higher order in $k\lambda_D$. This discrepancy stands in contrast with the roughly equal contributions from heat conduction and viscosity to the damping of a sound wave in a neutral fluid.

4.2 Fluid Theory with Temperature Isotropization

In the limit of weak collisionality, a fluid model can still be pursued if the phase velocity of the wave is much larger than the thermal velocity. In particular, the ordering $\mathrm{Re}(\omega)/k_z >> \mathrm{v}_{th}$ implies that the particles comprising a given fluid element require many wave periods to disperse and also that the number of resonant particles is exponentially small. However, this fluid model must allow for two distinct temperatures, $T_{\parallel}$ and $T_{\perp}$, corresponding to the parallel and cyclotron degrees of

freedom, since the timescale for exchange of energy between these degrees of freedom is longer than the wave timescale. We assume that the collisional relaxation of the two temperatures is governed by the equation [22]

$$\frac{dT_{\parallel}}{dt} = \nu_{\parallel,\perp}(T_{\perp} - T_{\parallel}), \tag{4.11}$$

which defines the equipartition rate, $\nu_{\parallel,\perp}$. We also assume that the change in internal energy of a fluid element is equal to the work done on it by its surroundings:

$$\frac{d}{dt}\left(\frac{1}{2}T_{\parallel} + T_{\perp}\right) = -\frac{T_{\parallel}}{n}\frac{dn}{dt}. \tag{4.12}$$

In other words, we neglect heat flux. This approximation seems reasonable in the limit of large phase-velocity, where distance traveled by a thermal particle along the magnetic field during a wave period is small compared to the parallel wavenumber. By the same reasoning, we neglect viscous fluxes and assume that the evolution of the fluid velocity is given by Euler's equation of motion:

$$mn\frac{dV_z}{dt} = -\frac{\partial(nT_{\parallel})}{\partial z} - qn\frac{\partial \varphi}{\partial z} \tag{4.13}$$

Finally, the density evolves according to the continuity equation and determines the potential through Poisson's equation.

Once again, we consider perturbations of the form

$$\delta n, \delta V_z, \delta T_{\parallel}, \delta T_{\perp}, \delta\varphi \sim J_0(k_{\perp} r)e^{i(k_z z - \omega t)}. \tag{4.14}$$

Substitution into the fluid equations and linearization about the unperturbed state yields

$$-i\omega\delta n + n_0 i k_z \delta V_z = 0, \tag{4.15}$$

$$-i\omega\delta V_z = -ik_z\frac{q}{m}\delta\varphi - \frac{ik_z}{mn_0}T_0\delta n - \frac{ik_z}{m}\delta T_\parallel, \tag{4.16}$$

$$-i\omega\left(\frac{1}{2}\delta T_\parallel + \delta T_\perp\right) = -i\omega\frac{T_0}{n_0}\delta n \tag{4.17}$$

$$-i\omega\delta T_\parallel = \nu_{\parallel,\perp}(\delta T_\perp - \delta T_\parallel) \tag{4.18}$$

$$-k^2\delta\varphi = -4\pi q\delta n. \tag{4.19}$$

Eliminating the perturbed quantities, we obtain the dispersion equation

$$\omega^2 = \frac{k_z^2\omega_p^2}{k^2}\left[1+\frac{3}{2}(k\lambda_D)^2\frac{1+5i\nu_{\parallel,\perp}/(6\omega)}{1+3i\nu_{\parallel,\perp}/(2\omega)}\right]. \tag{4.20}$$

A solution with phase-velocity $\mathrm{Re}(\omega)/k_z >> \mathrm{v}_{th}$ exists only for wavenumbers such that $k\lambda_D << 1$. To lowest order in $\nu_{\parallel,\perp}/\omega,$ this solution is given by

$$\mathrm{Re}(\omega) = \frac{k_z\omega_p}{k}\left[1+\frac{3}{2}(k\lambda_D)^2\right], \tag{4.21}$$

$$\mathrm{Im}(\omega) = -\nu_{\parallel,\perp}(k\lambda_D)^2 \tag{4.22}$$

Equation (4.21) is the familiar formula for the frequency of a TG wave, with the Bohm-Gross correction. The kinetic damping formula (3.47) for weak collisionality is recovered from Eq. (4.22) by the substitution $\nu_{\parallel,\perp} = \nu_{\parallel,\perp}^{(D)} \equiv 4\nu_D/3,$ where $\nu_{\parallel,\perp}^{(D)}$ is the isotropization rate predicted by Dougherty's collision operator.

While the kinetic derivation of the damping formula (3.47) obscures the underlying damping mechanism, the two-temperature fluid model used here suggests a physical interpretation of the kinetic result. Consider one complete compression-decompression cycle of a fluid element in the presence of the wave, beginning when

the density of the fluid element is a minimum; the situation is depicted schematically in Fig. 4.1. The time evolution of the parallel temperature is determined by a competition between two factors; compression (or decompression) tends to increase (or decrease) the parallel temperature, but the parallel temperature is also weakly driven towards the perpendicular temperature by collisions. Most of the time, the latter is a relatively small effect, since collisions are weak, so the parallel temperature oscillates nearly in phase with the density. However, when the time rate of change of the density approaches zero, collisional relaxation momentarily dominates, with the result that the parallel temperature oscillation precedes the density oscillation slightly (by a time difference of order $\nu_{\parallel,\perp}/\omega^2$). Consequently, the parallel pressure is greater (on average) during compression than during decompression, so positive net work is done on the fluid element at the expense of the wave energy.

The form of the damping formula (4.22) is actually somewhat misleading; the quantity $k\lambda_D$ appearing in the parentheses is just the ratio of the thermal velocity to the phase velocity. Thus, Eq. (4.22) can be rewritten as

$$\mathrm{Im}(\omega) \cong -\nu_{\parallel,\perp}\left(\frac{\mathrm{v}_{th}^2}{\omega^2}\right)k_z^2, \tag{4.23}$$

where the quantity $2\nu_{\parallel,\perp}(\mathrm{v}_{th}^2/\omega^2)$ is the effective bulk viscosity for frequencies $\omega >> k_z v_{th}, \nu_{\parallel,\perp}$.

For simplicity, we have not included long-range collisions in the two-temperature fluid model. These collisions have little effect on temperature relaxation, since a conserved cyclotron adiabatic invariant prevents such collisions from

transferring energy between perpendicular and parallel degrees of freedom. However, as in the limit of strong collisionality, these long-range collisions contribute to the wave damping by transporting momentum across the magnetic field. The nature of this transport is the same regardless of the strength of collisionality, so the second term in the damping formula (4.9)—with cross-field viscosity again given by Eq. (4.10)—still gives a reasonable estimate of this contribution even when collisions are weak.

4.3 Acknowledgements

Chapter 4, in part, is a reprint of the material as it appears in Physics of Plasmas. M. W. Anderson and T. M. O'Neil, *Physics of Plasmas*, **14**, 112110 (2007). The dissertation author was the primary investigator and author of this paper.

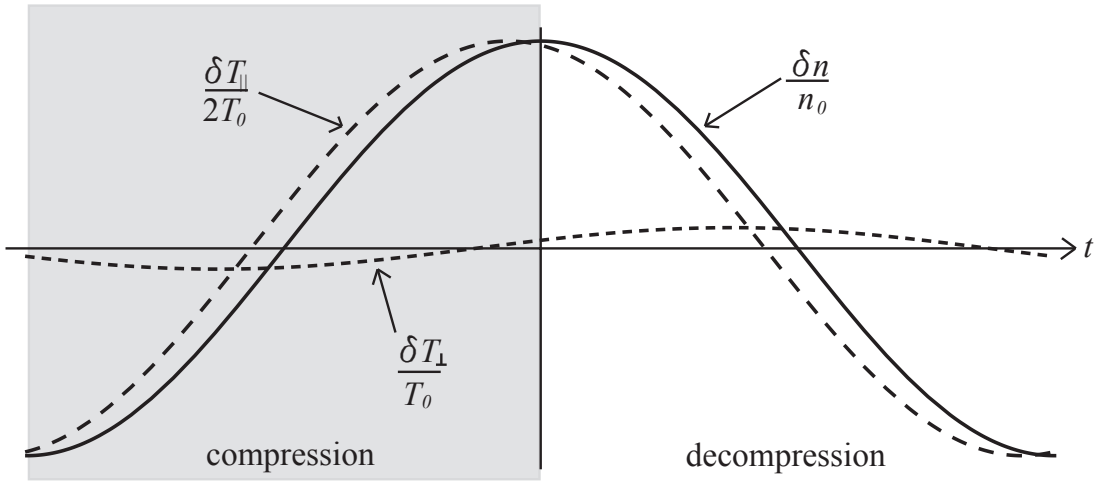

Figure 4.1 Schematic plot of the time evolution of the density perturbation and parallel and perpendicular temperature perturbations at a fixed location in space over one wave period, in the limit of weak collisionality. Due to the weak collisional temperature relaxation, the oscillation in parallel temperature leads the density oscillation by a time difference of order $\nu_{\parallel,\perp}/\omega^2$. Consequently, compression occurs at a higher pressure than does the decompression, leading to a net heating at the expense of the wave energy.

Chapter 5

Standing Plasma Waves on a Cold, Finite-Length Plasma Column

In this chapter, the effects of finite plasma length are considered. We calculate azimuthally symmetric modes of oscillation for a cold, finite-length plasma column. Similar mode calculations have been carried out in past work, but here a novel finding is presented: each mode is a mixture of multiple degenerate standing waves, often exhibiting sharp features along resonance cones corresponding to the frequency of the mode. The observed mixing is a low-temperature phenomenon, requiring that the cold-fluid dispersion relation be valid even for wavelengths much smaller than the dimensions of the plasma. In this regime, Landau damping is exponentially small, so the modes are damped by viscosity. Perturbation theory yields a formal expression for the viscous damping rate when the damping is sufficiently weak.

5.1 Cold-Fluid Equations of Motion

As an approximation to the Penning-Malmberg trap configuration shown in Fig. 1.1, we assume that mode potential satisfies the boundary conditions $\delta\varphi = 0$ at $r = R$ and at $z \to \pm\infty$, where R is the radius of the conducting wall of the trap. For azimuthally symmetric modes, Poisson's equation takes the form

$$\frac{1}{r}\frac{\partial}{\partial r}r\frac{\partial \delta\varphi}{\partial r}+\frac{\partial^2 \delta\varphi}{\partial z^2}=-4\pi q\delta n\,, \tag{5.1}$$

where $\delta\varphi$ is the mode potential, δn is the corresponding density perturbation, and q is the charge of a single particle.

In accord with the experiments that we have in mind, we assume that the axial magnetic field in the trap is sufficiently large that the drift approximation is justified. In cold-fluid theory, small azimuthally symmetric perturbations then evolve in time following the linearized continuity and momentum equations,

$$\frac{\partial \delta n}{\partial t}+\frac{\partial}{\partial z}(n_0\delta V_z)=0 \tag{5.2}$$

$$mn_0\frac{\partial \delta V_z}{\partial t}=-qn_0\frac{\partial \delta\varphi}{\partial z} \tag{5.3}$$

where δV_z is the perturbed fluid velocity associated with the mode and n_0 is the unperturbed density.

Seeking normal-mode solutions to Eqs. (5.2)-(5.3), we assume that the perturbation oscillates with frequency ω,

$$\begin{Bmatrix}\delta n(r,z,t)\\ \delta V_z(r,z,t)\\ \delta\varphi(r,z,t)\end{Bmatrix}=\mathrm{Re}\left[e^{-i\omega t}\times\begin{Bmatrix}\delta n_\omega(r,z)\\ \delta V_{z,\omega}(r,z)\\ \delta\varphi_\omega(r,z)\end{Bmatrix}\right] \tag{5.4}$$

and substitute, obtaining

$$\frac{1}{r}\frac{\partial}{\partial r}r\frac{\partial \delta\varphi_\omega}{\partial r}+\frac{\partial^2 \delta\varphi_\omega}{\partial z^2}=-4\pi q\delta n_\omega \tag{5.5}$$

$$-i\omega\delta n_\omega+\frac{\partial}{\partial z}(n_0\delta V_{z,\omega})=0 \tag{5.6}$$

$$-i\omega m n_0 \delta V_{z,\omega} = -q n_0 \frac{\partial \delta\varphi_\omega}{\partial z} \tag{5.7}$$

Equations (5.5)-(5.7) can be combined to give

$$\frac{1}{r}\frac{\partial}{\partial r} r \frac{\partial \delta\varphi_\omega}{\partial r} + \frac{\partial}{\partial z}\left[1 - \frac{\omega_p^2(r,z)}{\omega^2}\right]\frac{\partial \delta\varphi_\omega}{\partial z} = 0, \tag{5.8}$$

a partial differential equation for the mode potential. Equation (5.8) represents a generalized eigenvalue problem, since typically both $\delta\varphi_\omega$ and ω are unknown.

Multiplication of Eq. (5.8) by $\delta\varphi_\omega$ and integration over the interior of the trap gives a formal expression for the mode frequency in terms of the mode potential [8],

$$\omega^2 = \frac{\int r\,dr\,dz \omega_p^2(r,z)(\partial \delta\varphi_\omega / \partial z)^2}{\int r\,dr\,dz[(\partial \delta\varphi_\omega / \partial z)^2 + (\partial \delta\varphi_\omega / \partial r)^2]}, \tag{5.9}$$

where integration by parts has been employed . It follows from this formula that the allowed mode frequencies are real and bounded by the plasma frequency; that is, $0 \le \omega^2 \le \omega_p^2$.

Alternatively, one can derive an integral equation [40] for the *z*-component of the mode electric field, $\delta E_{z,\omega} = -\partial \delta\varphi_\omega / \partial z,$ by inverting Poisson's equation with the Green's function, $G(r,z\,|\,r',z'),$ defined by the conditions

$$\frac{1}{r}\frac{\partial}{\partial r} r \frac{\partial G}{\partial r} + \frac{\partial^2 G}{\partial z^2} = \frac{\delta(r-r')\delta(z-z')}{r} \tag{5.10}$$

$$G\big|_{r=R} = G\big|_{|z-z'|\to\infty} = 0. \tag{5.11}$$

In terms of the Green's function, Eq. (5.1) can be recast as

$$\delta\varphi_\omega(r,z) = -4\pi q \int r'\,dr'\,dz'\,\delta n_\omega(r',z') G(r,z\,|\,r',z'). \tag{5.12}$$

Equations (5.6) and (5.7) give the perturbed density in terms of the electric field:

$$4\pi q\delta n_\omega = -\frac{\partial}{\partial z}\left[\frac{\omega_p^2(r,z)}{\omega^2}\delta E_{z,\omega}\right]. \tag{5.13}$$

Inserting this expression in Eq. (5.12), integrating by parts, and taking the partial derivative with respect to z, one obtains the integral equation

$$-\omega^2\delta E_{z,\omega}(r,z) = \int r'\,dr'\,dz'\omega_p^2(r',z')\frac{\partial G}{\partial z\partial z'}\delta E_{z,\omega}(r',z'). \tag{5.14}$$

Unlike Eq. (5.8), Eq. (5.14) constitutes a linear eigenvalue problem, $-\omega^2$ being the eigenvalue and $\delta E_{z,\omega}$, the eigenfunction. Furthermore, the integral operator on the right-hand-side is self-adjoint with respect to the inner product $(f_1, f_2) \equiv \int r\,dr\,dz\omega_p^2(r,z)f_1 f_2$. It follows that all mode frequencies are real and that for any two modes with distinct frequencies ω and ω', the axial electric fields are orthogonal inside the plasma:

$$\int r\,dr\,dz\omega_p^2(r,z)\delta E_{z,\omega}(r,z)\delta E_{z,\omega'}(r,z) = 0 \qquad (\omega \neq \omega'). \tag{5.15}$$

We will take Eq. (5.8)—not Eq. (5.14)—as our starting point for the mode calculations in the remainder of this chapter. However, it should be emphasized that $\delta E_{z,\omega}$—not $\delta\varphi_\omega$—is the true eigenfunction. For a mode that consists of many component waves, this distinction is important, since it is easy to underestimate the degree of the mixing when viewing a plot of the mode potential (see Figs. 5.2 and 5.4). For example, a wave with axial wavenumber k_z which appears with amplitude A in the z-component of the mode electric field will appear with amplitude A/k_z in the mode potential,

since $\delta E_{z,\omega} = -\partial \delta\varphi_\omega / \partial z$. In this sense, large axial wavenumbers are suppressed relative to smaller wavenumbers in the mode potential. In contrast, the density gives an exaggerated impression of the mixing; a wave which appears with amplitude A in the z-component of the mode electric field will appear with amplitude $(k_\perp^2 + k_z^2)A / k_z$ in the mode density.

5.2 Trivelpiece-Gould Waves

Before considering modes of a finite-length plasma cylinder, we present the solutions of Eq. (5.8) obtained by Trivelpiece and Gould for the case of an infinitely long cylinder [1]. In this case, Eq. (5.8) simplifies to

$$\frac{1}{r}\frac{\partial}{\partial r} r \frac{\partial \delta\varphi_\omega}{\partial r} + \left[1 - \frac{\omega_p^2(r)}{\omega^2}\right]\frac{\partial^2 \delta\varphi_\omega}{\partial z^2} = 0, \tag{5.16}$$

which is separable. Specifically, for any real ω, there exist an infinite number of degenerate solutions of the form

$$\delta\varphi_\omega(r,z) = \psi_m^{TG}(\omega;r) e^{\pm i k_m z}. \tag{5.17}$$

Substitution into Eq. (5.16) yields an ODE for the radial dependence, $\psi_m^{TG}(\omega;r)$,

$$\frac{1}{r}\frac{d}{dr} r \frac{d\psi_m^{TG}(\omega;r)}{dr} - k_m^2\left[1 - \frac{\omega_p^2(r)}{\omega^2}\right]\psi_m^{TG}(\omega;r) = 0. \tag{5.18}$$

In thermal equilibrium, the radial plasma density profile, $n_0(r)$, is nearly constant out to some radius and there abruptly falls off on the scale of the Debye length. Following

Trivelpiece and Gould, we take an unperturbed density profile that is constant out to some radius, a, and zero outside this radius,

$$n_0(r) = n_0 H(r-a), \tag{5.19}$$

where $H(x)$ is the Heaviside step function. This choice corresponds to an equilibrium density profile in the limit of zero temperature. Insistence on a finite-temperature equilibrium density profile in place of the approximation (5.19) necessitates numerical solution of Eq. (5.18), but the qualitative behavior of these solutions (*e.g.*, oscillatory out to some radius; monotonically decreasing outside this radius) is the same.

With the assumption of a step-function density profile, Eq. (5.18) becomes a Bessel equation in the domain $r < a$ and a modified Bessel equation in the domain $a < r < R$. Making use of the boundary condition $\delta\varphi = 0$ at $r = R$ and requiring that $\delta\varphi$ be continuous at $r = a$, one finds solutions of the form

$$\psi_m^{TG}(\omega; r) \sim \begin{cases} \dfrac{J_0(k_m r\sqrt{\omega_p^2/\omega^2 - 1})}{J_0(k_m a\sqrt{\omega_p^2/\omega^2 - 1})} & r \le a \\ \dfrac{I_0(k_m r)K_0(k_m R) - I_0(k_m R)K_0(k_m r)}{I_0(k_m a)K_0(k_m R) - I_0(k_m R)K_0(k_m a)} & a < r \le R. \end{cases} \tag{5.20}$$

The wavenumber $k_m = k_m(\omega)$ is given by the m^{th} nonnegative solution to the equation

$$\sqrt{\omega_p^2/\omega^2 - 1}\,\frac{J_1(ka\sqrt{\omega_p^2/\omega^2 - 1})}{J_0(ka\sqrt{\omega_p^2/\omega^2 - 1})} + \frac{I_0'(ka)K_0(kR) - I_0(kR)K_0'(ka)}{I_0(ka)K_0(kR) - I_0(kR)K_0(ka)} = 0, \tag{5.21}$$

which comes from the requirement that $\partial\delta\varphi/\partial r$ be continuous at $r = a$. These are the azimuthally symmetric Trivelpiece-Gould waves. By defining the transverse wavenumber $k_{\perp,m} \equiv k_m(\omega_p^2/\omega^2 - 1)^{1/2}$, one recovers the dispersion equation (1.11).

In addition to the Trivelpiece-Gould waves, there exists another class of solutions to Eq. (5.16) of the form [7]

$$\delta\varphi_\omega(r,z) = \psi_m^A(\omega;r)e^{\pm\kappa_m z}. \tag{5.22}$$

For these solutions, the radial dependence is given by

$$\psi_m^A(\omega;r) \sim \begin{cases} \dfrac{I_0(\kappa_m r\sqrt{\omega_p^2/\omega^2-1})}{I_0(\kappa_m a\sqrt{\omega_p^2/\omega^2-1})} & r \le a \\ \dfrac{J_0(\kappa_m r)N_0(\kappa_m R)-J_0(\kappa_m R)N_0(\kappa_m r)}{J_0(\kappa_m a)N_0(\kappa_m R)-J_0(\kappa_m R)N_0(\kappa_m a)} & a < r \le R, \end{cases} \tag{5.23}$$

where κ_m is the m^{th} nonnegative solution to the equation

$$\sqrt{\omega_p^2/\omega^2-1}\,\frac{I_1(\kappa a\sqrt{\omega_p^2/\omega^2-1})}{I_0(\kappa a\sqrt{\omega_p^2/\omega^2-1})} + \frac{J_0'(\kappa a)N_0(\kappa R)-J_0(\kappa R)N_0'(\kappa a)}{J_0(\kappa a)N_0(\kappa R)-J_0(\kappa R)N_0(\kappa a)} = 0. \tag{5.24}$$

We will refer to these solutions as "annular solutions", since they are localized in the annular vacuum region $a < r < R$. Because the annular solutions become exponentially large as $z \to \pm\infty$, they are typically ignored in the theory of the infinitely long cylinder; however, we will need these solutions when we solve for modes of a finite-length plasma cylinder.

The functions $\psi_m^{TG}(\omega;r)$ and $\psi_m^A(\omega;r)$ are orthogonal on the interval $0 < r < R$ with weight function $\varepsilon(\omega,r) \equiv 1-\omega_p^2(r)/\omega^2$; we choose the normalization so that [7]

$$\int_0^R r\,dr\varepsilon(\omega,r)\psi_m^{TG}(\omega;r)\psi_{m'}^{TG}(\omega;r) = -\frac{R^2}{2}\delta_{mm'} \tag{5.25}$$

and

$$\int_0^R r\,dr\varepsilon(\omega,r)\psi_m^A(\omega;r)\psi_m^A(\omega;r)=\frac{R^2}{2}\delta_{mm'}\,. \tag{5.26}$$

The difference in sign ensures that both $\psi_m^{TG}(\omega;r)$ and $\psi_m^A(\omega;r)$ are real-valued functions. Several of the functions $\psi_m^{TG}(\omega;r)$ and $\psi_m^A(\omega;r)$ are plotted in Fig. 5.1 for $R=1,\ a=1/2,$ and $\omega/\omega_p=1/10.$

5.3 Modes of a Plasma Column with Flat Ends

We now search for modes of a finite-length plasma cylinder. Jennings *et al* approached this problem by discretizing Eq. (5.8), while Rasband *et al* employed a finite-element method [8, 9]. Following Prasad and O'Neil [7], we choose to represent each mode as a linear combination of the TG and annular solutions discussed in the previous section. This approach manifests the mixing of degenerate waves.

In this section, we focus on a well-known model which takes the unperturbed plasma density to be constant inside a right-circular cylinder of radius a and length L and zero outside this cylinder [Fig. 1.3(*a*)]:

$$n_0(r,z)=n_0H(r-a)H(|z|-L/2)\,. \tag{5.27}$$

In this case, although the Trivelpiece-Gould and annular solutions are no longer global solutions to Eq. (5.8), they still satisfy this equation in the region $|z|<L/2$. We assume that the mode potential in this region can be expressed as a linear combination of these solutions,

$$\delta\varphi_\omega(r,z)=\sum_{m=1}^{\infty}B_m\psi_m^{TG}(\omega;r)\frac{\sin(k_m z)}{\sin(k_m L/2)}+\sum_{m=1}^{\infty}C_m\psi_m^{A}(\omega;r)\frac{\sinh(\kappa_m z)}{\sinh(\kappa_m L/2)}. \qquad (5.28)$$

For $|z|>L/2$, Eq. (5.8) reduces to Laplace's equation, and thus, in this region, the mode potential can be expressed as a linear combination of vacuum solutions,

$$\delta\varphi_\omega(r,z)=\mathrm{sign}(z)\sum_{n=1}^{\infty}A_n J_0(\chi_{0n}r/R)e^{-\chi_{0n}(z-L/2)/R}. \qquad (5.29)$$

Here we have assumed that the mode potential is odd in z; the generalization to even modes is straightforward.

For the sake of numerical tractability, we must approximate Eqs. (5.28) and (5.29) by the partial series

$$\delta\varphi_\omega(r,z)=\sum_{m=1}^{N/2}B_m\psi_m^{TG}(\omega;r)\frac{\sin(k_m z)}{\sin(k_m L/2)}+\sum_{m=1}^{N/2}C_m\psi_m^{A}(\omega;r)\frac{\sinh(\kappa_m z)}{\sinh(\kappa_m L/2)} \qquad (5.30)$$

and

$$\delta\varphi_\omega(r,z)=\mathrm{sign}(z)\times\sum_{m=1}^{N}A_m J_0(\chi_{0m}r/R)e^{-\chi_{0m}(z-L/2)/R}, \qquad (5.31)$$

where N is some finite number of basis functions presumed to be sufficient to represent the mode to the desired degree of accuracy.

Note that the set of basis functions used here is not complete in the usual sense; we have only assumed that it is sufficient to represent a global solution to the mode equation with frequency ω. Expressing the global solution as a linear combination of local solutions in distinct domains has the advantage that convergence is much faster than would be the case if a more conventional basis were employed—for example, if the Fourier expansion $\delta\varphi_\omega=\Sigma_{m,n}A_{mn}J_0(\chi_{0m}r/R)\sin[(2n-1)z/L]$ were used in place

of Eq. (5.28). Suppose that, in order to achieve some prescribed level of resolution of the mode, N^2 basis functions from the more standard basis are required; the same resolution can be achieved with just N basis functions of the type used here.

Taken together, the series (5.30) and (5.31) satisfy Eq. (5.8) everywhere inside the trap; all that remains is to find a set of coefficients, A_m, B_m, and C_m, and a frequency, ω, such that the resulting mode potential satisfies the required matching conditions at the boundary, $z = \pm L/2$. One such condition is that $\delta\varphi$ be continuous at $z = \pm L/2$. Exploiting the orthogonality of the Bessel functions, we write this condition as

$$\frac{R^2}{2} J_1^2(\chi_{0n}) A_n = \sum_{m=1}^{N/2} B_m \int_0^R r\, dr J_0(\chi_{0n} r/R) \psi_m^{TG}(\omega; r) + \sum_{m=1}^{N/2} C_m \int_0^R r\, dr J_0(\chi_{0n} r/R) \psi_m^{A}(\omega; r). \tag{5.32}$$

The other matching condition is that the z-component of the electric displacement, $\delta D_z = [\omega_p^2(r,z)/\omega^2 - 1]\partial\delta\varphi/\partial z$, be continuous at $z = \pm L/2$. Using the orthogonality relations (5.25) and (5.26), we write this condition as

$$\frac{R^2}{2} k_m \cot(k_m L/2) B_m = \sum_{n=1}^{N} A_n (\chi_{0n}/R) \int_0^R r\, dr J_0(\chi_{0n} r/R) \psi_m^{TG}(\omega; r) \tag{5.33}$$

and

$$-\frac{R^2}{2} \kappa_m \coth(\kappa_m L/2) C_m = \sum_{n=1}^{N} A_n (\chi_{0n}/R) \int_0^R r\, dr J_0(\chi_{0n} r/R) \psi_m^{A}(\omega; r). \tag{5.34}$$

Elimination of A_n in Eqs. (5.33) and (5.34) using Eq. (5.32) yields two sets of coupled equations for the amplitudes of the Trivelpiece-Gould and vacuum components, B_m and C_m:

$$k_m \cot(k_m L/2) B_m - \sum_{m'=1}^{N/2} B_{m'} \sum_{n=1}^{N} \frac{\chi_{0n}}{R} \frac{\int_0^R r\,dr J_0(\chi_{0n} r/R)\psi_{m'}^{TG}(\omega;r)}{R^2 J_1(\chi_{0n})/2} \frac{\int_0^R r\,dr J_0(\chi_{0n} r/R)\psi_{m}^{TG}(\omega;r)}{R^2 J_1(\chi_{0n})/2} - \sum_{m'=1}^{N/2} C_{m'} \sum_{n=1}^{N} \frac{\chi_{0n}}{R} \frac{\int_0^R r\,dr J_0(\chi_{0n} r/R)\psi_{m'}^{A}(\omega;r)}{R^2 J_1(\chi_{0n})/2} \frac{\int_0^R r\,dr J_0(\chi_{0n} r/R)\psi_{m}^{TG}(\omega;r)}{R^2 J_1(\chi_{0n})/2} = 0 \tag{5.35}$$

and

$$\kappa_m \coth(\kappa_m L/2) C_m + \sum_{m'=1}^{N/2} B_{m'} \sum_{n=1}^{N} \frac{\chi_{0n}}{R} \frac{\int_0^R r\,dr J_0(\chi_{0n} r/R)\psi_{m'}^{TG}(\omega;r)}{R^2 J_1(\chi_{0n})/2} \frac{\int_0^R r\,dr J_0(\chi_{0n} r/R)\psi_{m}^{A}(\omega;r)}{R^2 J_1(\chi_{0n})/2} + \sum_{m'=1}^{N/2} C_{m'} \sum_{n=1}^{N} \frac{\chi_{0n}}{R} \frac{\int_0^R r\,dr J_0(\chi_{0n} r/R)\psi_{m'}^{A}(\omega;r)}{R^2 J_1(\chi_{0n})/2} \frac{\int_0^R r\,dr J_0(\chi_{0n} r/R)\psi_{m}^{A}(\omega;r)}{R^2 J_1(\chi_{0n})/2} = 0. \tag{5.36}$$

Equations (5.35) and (5.36) specify N equations for N unknowns, which can be expressed in matrix notation as

$$\sum_{m'=1}^{N} M_{mm'}(\omega) x_{m'} = 0 \quad [\text{or } M(\omega)\vec{x} = 0], \tag{5.37}$$

where $\vec{x} \equiv (B_1, B_2, ..., B_{N/2}, C_1, C_2, ..., C_{N/2})$ and $M(\omega)$ is a symmetric matrix with elements

$$M_{mm'}(\omega) = k_m \cot(k_m L/2)\delta_{mm'} - \sum_{n=1}^{N} \frac{\chi_{0n}}{R} \frac{\int_0^R r\,dr J_0(\chi_{0n} r/R)\psi_{m'}^{TG}(\omega;r)}{R^2 J_1(\chi_{0n})/2} \frac{\int_0^R r\,dr J_0(\chi_{0n} r/R)\psi_{m}^{TG}(\omega;r)}{R^2 J_1(\chi_{0n})/2} \quad (5.38)$$

for $m \le N/2$ and $m' \le N/2$,

$$M_{mm'}(\omega) = \kappa_m \coth(\kappa_m L/2)\delta_{mm'} - \sum_{n=1}^{N} \frac{\chi_{0n}}{R} \frac{\int_0^R r\,dr J_0(\chi_{0n} r/R)\psi_{m'}^{A}(\omega;r)}{R^2 J_1(\chi_{0n})/2} \frac{\int_0^R r\,dr J_0(\chi_{0n} r/R)\psi_{m}^{A}(\omega;r)}{R^2 J_1(\chi_{0n})/2} \quad (5.39)$$

for $N/2 < m \le N$ and $N/2 < m' \le N$, and

$$M_{mm'}(\omega) = -\sum_{n=1}^{N} \frac{\chi_{0n}}{R} \frac{\int_0^R r\,dr J_0(\chi_{0n} r/R)\psi_{m'}^{A}(\omega;r)}{R^2 J_1(\chi_{0n})/2} \frac{\int_0^R r\,dr J_0(\chi_{0n} r/R)\psi_{m}^{TG}(\omega;r)}{R^2 J_1(\chi_{0n})/2} \quad (5.40)$$

for $m \le N/2$ and $N/2 < m' \le N$. Equation (5.37) constitutes a generalized eigenvalue problem; each matrix element depends on the unknown mode frequency, ω, through the functions $\psi_m^{TG}(\omega;r)$ and $\psi_m^{A}(\omega;r)$ and the wavenumbers $k_m = k_m(\omega)$ and $\kappa_m = \kappa_m(\omega)$.

In order to better understand the matrix equation (5.37), it is instructive to consider the simple case in which the plasma extends to the trap wall—that is, $a = R$. In this case, there are no annular solutions, so the matrix M is given entirely by Eq. (5.38). Furthermore, the TG solutions have the same radial dependence as the vacuum solutions—

$$\psi_m^{TG}(\omega;r) = \frac{k_m^2(\omega)}{(\chi_{0m}/R)^2} \frac{J_0(\chi_{0m} r/R)}{J_1(\chi_{0m})} \quad (5.41)$$

[the normalization follows from Eq. (5.25)]. Consequently, the second term on the right-hand side of Eq. (5.38) is zero unless $m = m'$, implying that a given TG wave reflects entirely back into itself at $z = \pm L/2$. In other words, the matrix *M* is diagonal, and Eq. (5.37) takes the simple form

$$[k_m \cot(k_m L/2) - k_m^2 R/\chi_{0m}]B_m = 0. \tag{5.42}$$

Thus, when the plasma extends to the trap wall, the modes are just standing TG waves with radial dependence given by Eq. (5.41) and axial wavenumber quantized according to the condition that the diagonal matrix element equal zero,

$$\cot(k_m L/2) - k_m R/\chi_{0m} = 0. \tag{5.43}$$

For a long plasma, it follows that for radial modenumber *m*, the allowed axial wavenumbers are given by $k_{mn} = (2n-1)\pi/L - \delta k_{mn}$, where *n* is an integer and δk_{mn} is a correction of order R/L^2. Inserting this expression in Eq. (5.43) and expanding the cotangent term, one finds that to first order in R/L^2, $\delta k_{mn} \cong (2n-1)2\pi R/(\chi_{0m} L^2)$.

When the plasma does not extend to the trap wall, the radial dependence of the TG waves no longer matches that of the vacuum solutions. Consequently, at $z = \pm L/2$, an incident TG wave reflects partially back into itself and partially into other TG waves. It follows that each mode must be a mixture of multiple component waves. From a cursory analysis of the matrix *M*, one can guess which waves should appear prominently in the admixture for a mode with frequency ω. According to the normalization condition (5.25), the second term on the right-hand side of Eq. (5.38)—and thus any off-diagonal matrix element—is of order R/L^2 or smaller [7]. In

contrast, the first term on the right-hand side of Eq. (5.38), which appears only on the diagonal of the matrix, can be any size, diverging as $k_m(\omega)L/2$ approaches any multiple of π, and vanishing as $k_m(\omega)L/2$ approaches any odd multiple of $\pi/2$. If the wavenumber $k_m(\omega)$ is such that $\left|k_m \cot(k_m L/2)\right| >> R/L^2$, the m^{th} diagonal element will be large, and one can see that the amplitude of the m^{th} wave must then be small in order for Eq. (5.37) to be satisfied. Conversely, the amplitude of the m^{th} wave may be large only if the m^{th} diagonal element is small compared to R/L^2; as in the previous example, this occurs for wavenumbers $k_m(\omega) = (2n-1)\pi/L - \delta k_m(\omega)$, where *n* is an integer and $\delta k_m(\omega)$ is a correction of order R/L^2. For a given mode frequency, there can be many such waves, and these waves will give the dominant contribution to the admixture for that mode.

The heuristic argument outlined in the preceding paragraph is a revised version of an argument introduced by Prasad and O'Neil [7]. These authors derived a generalized version of Eq. (5.37) for a mode with azimuthal dependence and carried out a perturbative solution based on the smallness of the off-diagonal matrix elements. However, a tacit assumption underlying the perturbation theory is that only one of the diagonal elements of the matrix is small compared to the off-diagonal elements in its row, and this assumption is unjustified.

We proceed by evaluating the matrix $M(\omega)$ on a grid in ω-space and calculating the determinant at each point on this grid. We search for values of ω for which $\mathrm{Det}[M(\omega)] = 0$; at these values the null-vector, $\vec{x}$, gives a solution to Eq.

(5.37). As expected, the contribution to each solution is greatest from wavenumbers $k_m(\omega) \cong (2n-1)\pi / L$. However, as the number of basis functions, N, is increased, increasingly short-wavelength waves enter the admixture for each solution with significant amplitude, and this trend continues to the limit of our computational capability. The lack of convergence should not be surprising. The off-diagonal matrix elements fall off only as m^{-1} and so are non-negligible even for large m; thus, for arbitrarily large m, the m^{th} diagonal matrix element can still be smaller than the off-diagonal elements in the m^{th} row, provided that the wavenumber k_m is close enough to $(2n-1)\pi / L$, where n is an integer.

An exemplary solution is plotted in Fig. 5.2—with various numbers of basis functions retained—as an illustration of the appearance of increasingly large wavenumbers in each solution. In Fig. 5.2(*a*), only four TG waves are retained, and the dominant term in the admixture comes from the first TG wave, which has wavenumber $k_1(\omega) \cong 3\pi / L - 6.94(R / L^2)$, where ω is the frequency of the solution. In Fig. 5.2(*b*), eight waves are retained, and now the seventh wave, which has wavelength $k_7(\omega) \cong 39\pi / L - 2.45(R / L^2)$, enters the admixture with amplitude comparable to that of the first wave. With more waves retained, the solution incurs significant contributions from even shorter wavelengths.

5.4 Modes of a Plasma Column with Spheroidal End-shape

There is reason to suspect that the appearance of increasingly short wavelengths in each of the solutions obtained in the previous section stems from the crude representation of the plasma shape as a cylinder with perfectly flat ends. The mode structure is determined by the coupling between TG waves reflecting at the ends of the plasma cylinder, and this coupling must be affected by the end-shape. In this section, we generalize the method of Section 5.3 and look for modes of a plasma cylinder with a spheroidal end-shape. In this case, the plasma boundary is given by $r = a$ for $|z| < L/2$ and by $[(z - L/2)/(2\Delta L_0)]^2 + (r/a)^2 = 1$ for $|z| > L/2$.

Following the procedure of Section 5.3, we divide the space inside the trap into regions with distinct solution sets, as depicted in Fig. 1.3(*b*). The surface that separates these regions is given by $z = [L + \Delta L(r)]/2,$ where

$$\Delta L(r) = \begin{cases} 2\Delta L_0 \sqrt{1-(r/a)^2} & r < a \\ 0 & a < r < R \end{cases} \tag{5.44}$$

is the deviation from the flat matching surface taken in Section 5.3. We express the mode potential as the series (5.30) and (5.31) in the appropriate domains. Again, the matching conditions on $\delta\varphi$ and $\delta\vec{D} = [\omega_p^2(r,z)/\omega^2 - 1](\partial\delta\varphi/\partial z)\hat{z} - (\partial\delta\varphi/\partial r)\hat{r}$ yield coupled equations for the coefficients B_n and C_n. The continuity of $\delta\varphi$ gives

$$\begin{aligned} \sum_{n=1}^{N} A_n J_0(\chi_{0n} r/R) e^{-\chi_{0n}\Delta L(r)/(2R)} = &\sum_{m=1}^{N/2} B_m \psi_m^{TG}(\omega;r) \frac{\sin\{k_m(\omega)[L+\Delta L(r)]/2\}}{\sin\{k_m(\omega)L/2\}} \\ &+ \sum_{m=1}^{N/2} C_m \psi_m^{A}(\omega;r) \frac{\sinh\{\kappa_m(\omega)[L+\Delta L(r)]/2\}}{\sinh\{\kappa_m(\omega)L/2\}}, \end{aligned} \tag{5.45}$$

while the continuity of $\delta\bar{D}\cdot\hat{n}$ gives

$$\begin{aligned}
&\sum_{n=1}^{N} A_n(\chi_{0n}/R)e^{-\chi_{0n}\Delta L(r)/(2R)}[n_z(r)J_0(\chi_{0n}r/R)+n_r(r)J_1(\chi_{0n}r/R)] = \\
&\quad -\sum_{m=1}^{N/2} B_m\left[n_r(r)\frac{d\psi_m^{TG}(\omega;r)}{dr}\frac{\sin\{k_m(\omega)[L+\Delta L(r)]/2\}}{\sin\{k_m(\omega)L/2\}}\right. \\
&\qquad \left. +n_z(r)\varepsilon(\omega,r)k_m(\omega)\psi_m^{TG}(\omega;r)\frac{\cos\{k_m(\omega)[L+\Delta L(r)]/2\}}{\sin\{k_m(\omega)L/2\}}\right] \\
&\qquad -\sum_{m=1}^{N/2} C_m\left[n_r(r)\frac{d\psi_m^{A}(\omega;r)}{dr}\frac{\sinh\{\kappa_m(\omega)[L+\Delta L(r)]/2\}}{\sinh\{\kappa_m(\omega)L/2\}}\right. \\
&\qquad\quad \left. +n_z(r)\varepsilon(\omega,r)\kappa_m(\omega)\psi_m^{A}(\omega;r)\frac{\cosh\{\kappa_m(\omega)[L+\Delta L(r)]/2\}}{\sinh\{\kappa_m(\omega)L/2\}}\right],
\end{aligned} \tag{5.46}$$

where $n_r(r)$ and $n_z(r)$ are the radial and axial components of the unit vector $\hat{n}$ that is normal to the matching surface.

The analysis of Section 5.3 relies on the orthogonality properties of the Bessel functions and the functions $\psi_m^{TG}(\omega;r)$ and $\psi_m^{A}(\omega;r)$; however, this approach fails here because the curvature of the plasma boundary introduces additional *r*-dependence. Instead, we discretize the radial coordinate, taking *P* points, $\{r_1, r_2, \ldots, r_P\}$, and evaluate Eqs. (5.45) and (5.46) on this grid, obtaining two sets of coupled equations,

$$\begin{aligned}
&\sum_{n=1}^{N} A_n J_0(\chi_{0n}r_p/R)e^{-\chi_{0n}\Delta L(r_p)/(2R)} = \\
&\qquad \sum_{m=1}^{N/2} B_m\psi_m^{TG}(\omega;r_p)\frac{\sin\{k_m(\omega)[L+\Delta L(r_p)]/2\}}{\sin\{k_m(\omega)L/2\}} \\
&\qquad\quad +\sum_{m=1}^{N/2} C_m\psi_m^{A}(\omega;r_p)\frac{\sinh\{\kappa_m(\omega)[L+\Delta L(r_p)]/2\}}{\sinh\{\kappa_m(\omega)L/2\}},
\end{aligned} \tag{5.47}$$

and

$$\sum_{n=1}^{N} A_n(\chi_{0n}/R)e^{-\chi_{0n}\Delta L(r_p)/(2R)}[n_z(r_p)J_0(\chi_{0n}r_p/R)+n_r(r_p)J_1(\chi_{0n}r_p/R)] =$$

$$-\sum_{m=1}^{N/2} B_m\left[n_r(r_p)\left.\frac{d\psi_m^{TG}(\omega;r)}{dr}\right|_{r=r_p}\frac{\sin\{k_m(\omega)[L+\Delta L(r_p)]/2\}}{\sin\{k_m(\omega)L/2\}}\right.$$

$$\left.+n_z(r_p)\varepsilon(\omega,r_p)k_m(\omega)\psi_m^{TG}(\omega;r_p)\frac{\cos\{k_m(\omega)[L+\Delta L(r_p)]/2\}}{\sin\{k_m(\omega)L/2\}}\right] \qquad (5.48)$$

$$-\sum_{m=1}^{N/2} C_m\left[n_r(r_p)\left.\frac{d\psi_m^{A}(\omega;r)}{dr}\right|_{r=r_p}\frac{\sinh\{\kappa_m(\omega)[L+\Delta L(r_p)]/2\}}{\sinh\{\kappa_m(\omega)L/2\}}\right.$$

$$\left.+n_z(r_p)\varepsilon(\omega,r_p)\kappa_m(\omega)\psi_m^{A}(\omega;r_p)\frac{\cosh\{\kappa_m(\omega)[L+\Delta L(r_p)]/2\}}{\sinh\{\kappa_m(\omega)L/2\}}\right].$$

Equations (5.47) and (5.48) comprise a system of $2P$ equations for $2N$ unknowns and can be expressed as a single matrix equation,

$$\sum_{n=1}^{2N} M'_{pn}(\omega)x'_n = 0 \quad [\text{or } M'(\omega)\vec{x}' = 0], \qquad (5.49)$$

where $\vec{x}' \equiv (A_1, A_2, ..., A_N, B_1, B_2, ..., B_{N/2}, C_1, C_2, ...C_{N/2})$ and $M'(\omega)$ is a $2P \times 2N$ matrix; the primes are a reminder that the matrix M' and the vector $\vec{x}'$ are distinct from M and $\vec{x}$ as defined in Section 5.3.

In order for every basis function to be well-resolved on the radial grid, we take $P >> N,$ and thus Eq. (5.49) becomes an over-determined system of equations that cannot be satisfied exactly. Thus, we seek a nonzero vector $\vec{x}'$ and frequency ω which minimize the mean squared mismatch at the boundary, $\Delta(\omega, \vec{x}')$, defined as

$$\Delta(\omega, \vec{x}') \equiv \frac{1}{P}[M'(\omega)\vec{x}']^2. \qquad (5.50)$$

We exclude the trivial solution, $\vec{x}' = 0,$ by imposing a normalization constraint. We observe that a variety of different normalization constraints lead to the same solutions. A simple choice is the following:

$$[S(\omega)\vec{x}']^2 = 1, \tag{5.51}$$

where

$$S_{nn'}(\omega) = \frac{k_n(\omega)\delta_{nn'}}{\sin[k_n(\omega)L/2]} \tag{5.52}$$

for $n \le N/2$ and $S_{nn'} = 0$ otherwise. This constraint simply requires that the squared amplitudes of all Trivelpiece-Gould components making up the mode electric field sum to one.

For fixed $\omega,$ the minima of $\Delta(\omega, \vec{x}')$ under this normalization constraint are given by the condition

$$\delta\Big([M'(\omega)\vec{x}']^2 - \lambda\{[S(\omega)\vec{x}']^2 - 1\}\Big) = 1, \tag{5.53}$$

where λ is a Lagrange multiplier and the variation is taken with respect to $\vec{x}'$. Carrying out the variation yields

$$[M'(\omega)]^T M'(\omega)\vec{x}' = \lambda[S(\omega)]^T S(\omega)\vec{x}', \tag{5.54}$$

where the superscript *T* denotes the transpose. In other words, for fixed $\omega,$ the local minima of $\Delta(\omega, \vec{x}')$ are given by the "generalized eigenvectors" of the matrix $[M'(\omega)]^T M'(\omega)$ with respect to the matrix $[S(\omega)]^T S(\omega)$. The global minimum (on the surface of constraint) is given by the eigenvector with the smallest eigenvalue; all

eigenvalues are positive since both $[M'(\omega)]^T M'(\omega)$ and $[S(\omega)]^T S(\omega)$ are positive-definite.

To find a mode frequency, we therefore evaluate the matrices $[M'(\omega)]^T M'(\omega)$ and $[S(\omega)]^T S(\omega)$ on a grid in ω and determine the smallest eigenvalue, $\lambda_{\min}(\omega)$, at each grid point. For $N >> 1$, the function $\lambda_{\min}(\omega)$ typically has many local minima. As *N* and *P* are increased, some of these minima approach zero (as does the corresponding mismatch), and the value of ω where such a minimum occurs gives the frequency of a mode. The mode potential is given by the eigenvector, $\vec{x}'$, corresponding to $\lambda_{\min}(\omega)$ at the mode frequency. The procedure is illustrated in Fig. 5.3.

In practice, when only a few terms are retained in the series (5.30) and (5.31) and the corresponding function $\lambda_{\min}(\omega)$ is plotted, one observes relatively few local minima, and the location of each minimum gives a rough indication of the frequency of a mode comprised mostly of long-wavelength waves [Fig. 5.3(*a*)]. Using this information, one can then keep many more terms in the series and plot the corresponding function $\lambda_{\min}(\omega)$ over a much smaller frequency interval about one of these minima [Fig. 5.3(*b*)]. Of course, this strategy only works for the relatively smooth modes comprised mostly of long-wavelength waves, but these are typically the most relevant modes in an experiment. Figure 5.4 illustrates the matching of the potential and electric displacement at the sample points along the matching surface for an exemplary solution.

Several solutions are plotted in Fig. 5.5. We observe that strong mixing occurs only amongst waves with axial wavelengths larger than the variation in plasma length, ΔL_0, and in particular for wavenumbers $k_m \cong (2n-1)\pi / L$, where *n* is an integer. For example, Fig. 5.5(*a*) shows a mode that is mostly a mixture of the $m = 1$ and $m = 2$ waves having wavenumbers $k_1 \cong \pi / L$ and $k_2 \cong 3\pi / L$. [Recall that the wavenumbers $k_m = k_m(\omega)$ of the component waves are determined by Eq. (5.21) and the frequency of the mode, ω.] Waves with shorter axial wavelengths are less strongly mixed but tend to add constructively to create fine-scale cone-like structures in the mode along resonance cones with slope $dz / dr = \pm(\omega_p^2 / \omega^2 - 1)^{1/2}$. The modes shown in Figs. 5.5(*b*)-(*e*) exhibit these cone-like features.

It should be noted that Jennings *et al* also find solutions to the mode equation that do not resemble any single Trivelpiece-Gould wave [8]. In addition, the authors note that according to Eq. (5.9), very different waveforms can have similar frequencies. However, Jennings *et al* conclude that the more complicated solutions are not real modes, but the result of miscalculation by the numerical algorithm. Presumably, this work was motivated by experiments involving warm plasmas, in which Landau damping rates consistent with the single-wave approximation had been observed, so the complicated solutions were not investigated further.

By choosing $\Delta L_0 << L$ and $a << R$, we approach the limit where Dubin's theory for modes of a spheroidal plasma should apply. An example of a solution obtained in this limit is depicted in Fig. 5.6(*a*); Figure 5.6(*b*) depicts the corresponding Dubin mode Dubin mode for comparison. It should be mentioned that the

convergence of the solutions for spheroidal plasmas is slower than for long, cylindrical plasmas; that is, for a given number of basis functions, the mismatch at the sample points $\{r_1, r_2, \ldots, r_P\}$ tends to be larger. While Fig. 5.6(*a*) represents the limit of our computational capabilities, we expect that if many more basis functions could be retained, the mismatch would tend to zero without significant change in the appearance of the mode potential. However, the high-*k* features in the electric field plotted in Fig. 5.6(*a*) may be artifacts of the incomplete convergence.

5.5 Viscous Damping

In the low-temperature regime that we have in mind, the phase velocity of any given component comprising a mode is small in comparison to the thermal velocity, so Landau damping is negligible. Instead, as we have seen in Chapter 4, these modes are damped by viscous processes.

Here we calculate an expression for this viscous damping rate, assuming that the damping is weak, so that perturbation theory can be used. With viscosity included, the momentum equation (5.7) takes the form

$$-i\omega m n_0 \delta V_{z,\omega} = -q n_0 \frac{\partial \delta \varphi_\omega}{\partial z} + \frac{1}{r}\frac{\partial}{\partial r}\left(r m n_0 \zeta_\perp \frac{\partial \delta V_{z,\omega}}{\partial r} \right) + \frac{4}{3}\frac{\partial}{\partial z}\left(m n_0 \zeta_\parallel \frac{\partial \delta V_{z,\omega}}{\partial z} \right), \quad (5.55)$$

where $\zeta_\perp$ is the cross-field kinematic viscosity and $\zeta_\parallel$ is the parallel kinematic viscosity. Poisson's equation (5.5) and the continuity equation (5.6) remain unchanged. We define the parameters $\alpha_\parallel \equiv \zeta_z / (\omega L_\parallel^2)$ and $\alpha_\perp \equiv \zeta_\perp / (\omega L_\perp^2)$, where $L_\parallel$

and $L_\perp$ are the axial and transverse scale-lengths of the mode. For a weakly damped mode, these are small parameters. We thus expand the mode and its frequency as perturbation series, keeping only terms of zero- and first-order in $\alpha_\parallel$ and $\alpha_\perp$:

$\delta n_\omega \cong \delta n_\omega^{(0)} + \delta n_\omega^{(1)}$; $\delta V_{z,\omega} \cong \delta V_{z,\omega}^{(0)} + \delta V_{z,\omega}^{(1)}$; $\delta\varphi_\omega \cong \delta\varphi_\omega^{(0)} + \delta\varphi_\omega^{(1)}$; and $\omega \cong \omega^{(0)} - i\gamma^{(1)}$.

Together, $\delta n_\omega^{(0)}, \delta V_{z,\omega}^{(0)}$, and $\delta\varphi_\omega^{(0)}$ satisfy the inviscid fluid equations for a mode with frequency $\omega^{(0)}$. To first order, the viscous momentum equation (5.55) can be rewritten as

$$\begin{aligned} -i\omega m n_0 (\delta V_\omega^{(0)} + \delta V_\omega^{(1)}) = -q n_0 \frac{\partial}{\partial z}(\delta\varphi_\omega^{(0)} + \delta\varphi_\omega^{(1)}) \\ + \frac{1}{r}\frac{\partial}{\partial r}\left[r n_0 \zeta_\perp \frac{\partial}{\partial r}\left(\frac{q}{i\omega}\frac{\partial \delta\varphi_\omega^{(0)}}{\partial z}\right)\right] + \frac{4}{3}\frac{\partial}{\partial z}\left[n_0 \zeta_\parallel \frac{\partial}{\partial z}\left(\frac{q}{i\omega}\frac{\partial \delta\varphi_\omega^{(0)}}{\partial z}\right)\right]. \end{aligned} \tag{5.56}$$

Insertion of this expression into the continuity equation (5.6) gives δn_ω in terms of $\delta\varphi_\omega$. Poisson's equation then becomes

$$\begin{aligned} \frac{1}{r}\frac{\partial}{\partial r} r \frac{\partial \delta\varphi_\omega^{(1)}}{\partial r} + \frac{\partial^2 \delta\varphi_\omega^{(1)}}{\partial z^2} = \frac{\partial}{\partial z}\left(\frac{\omega_p^2}{\omega^{(0)2}}\frac{\partial \delta\varphi_\omega^{(1)}}{\partial z}\right) + \frac{\partial}{\partial z}\left(\frac{2\omega_p^2 i\gamma^{(1)}}{\omega^{(0)3}}\frac{\partial \delta\varphi_\omega^{(0)}}{\partial z}\right) \\ + \frac{\partial}{\partial z}\left\{ \frac{1}{r}\frac{\partial}{\partial r}\left[r \frac{i\omega_p^2 \zeta_\perp}{\omega^{(0)3}}\frac{\partial}{\partial r}\left(\frac{\partial \delta\varphi_\omega^{(0)}}{\partial z}\right)\right]\right\} + \frac{4}{3}\frac{\partial^2}{\partial z^2}\left(\frac{i\omega_p^2 \zeta_\parallel}{\omega^{(0)3}}\frac{\partial^2 \delta\varphi_\omega^{(0)}}{\partial z^2}\right). \end{aligned} \tag{5.57}$$

Here we have used the fact that $\delta\varphi_\omega^{(0)}$ and $\omega^{(0)}$ together satisfy the inviscid mode equation (5.8), which implies that the zero-order terms cancel. Multiplying Eq. (5.57) by $\delta\varphi_\omega^{(0)}$, integrating over the entire domain of the trap, and integrating each term by parts twice eliminates the terms involving $\delta\varphi_\omega^{(1)}$ [by virtue of Eq. (5.8)], and we are

left with an expression for the first-order viscous correction to the frequency in terms of the inviscid approximation to the mode:

$$\gamma^{(1)} = \frac{\int r\,dr\,dz\omega_p^2(r,z)\left[(2\zeta_{\parallel}/3)(\partial\delta E_{z,\omega}^{(0)}/\partial z)^2 + (\zeta_{\perp}/2)(\partial\delta E_{z,\omega}^{(0)}/\partial r)^2\right]}{\int r\,dr\,dz\omega_p^2(r,z)\delta E_{z,\omega}^{(0)2}}, \qquad (5.58)$$

where $\delta E_{z,\omega}^{(0)} = -\partial\delta\varphi_{\omega}^{(0)}/\partial z$. This expression is purely real and nonnegative and gives the viscous damping rate of the mode.

Due to the mixing of degenerate waves, the axial and transverse scale-lengths, $L_{\parallel}$ and $L_{\perp}$, of even the least-damped modes can be much smaller than the corresponding dimensions of the plasma. As a result, the damping of these modes is significantly greater than one would predict based on the single-wave approximation [7-9], which takes the mode potential inside the plasma to be given by a single Trivelpiece-Gould wave with wavenumber $k_m = m\pi/L[1-O(R/L)]$. For example, according to Eq. (5.58), the mode displayed in Fig. 5.4(*c*) damps at the rate $\gamma = (27.0\zeta_{\perp} + 0.325\zeta_{\parallel})/R^2$. By comparison, if this mode is approximated by its largest-amplitude Trivelpiece-Gould component (*m* =1, in this case), the smaller rate $\gamma = (2.94\zeta_{\perp} + 0.0930\zeta_{\parallel})/R^2$ is obtained.

5.6 Acknowledgements

Some of the material in this chapter is in preparation for publication. The dissertation author is the primary investigator and author of this material.

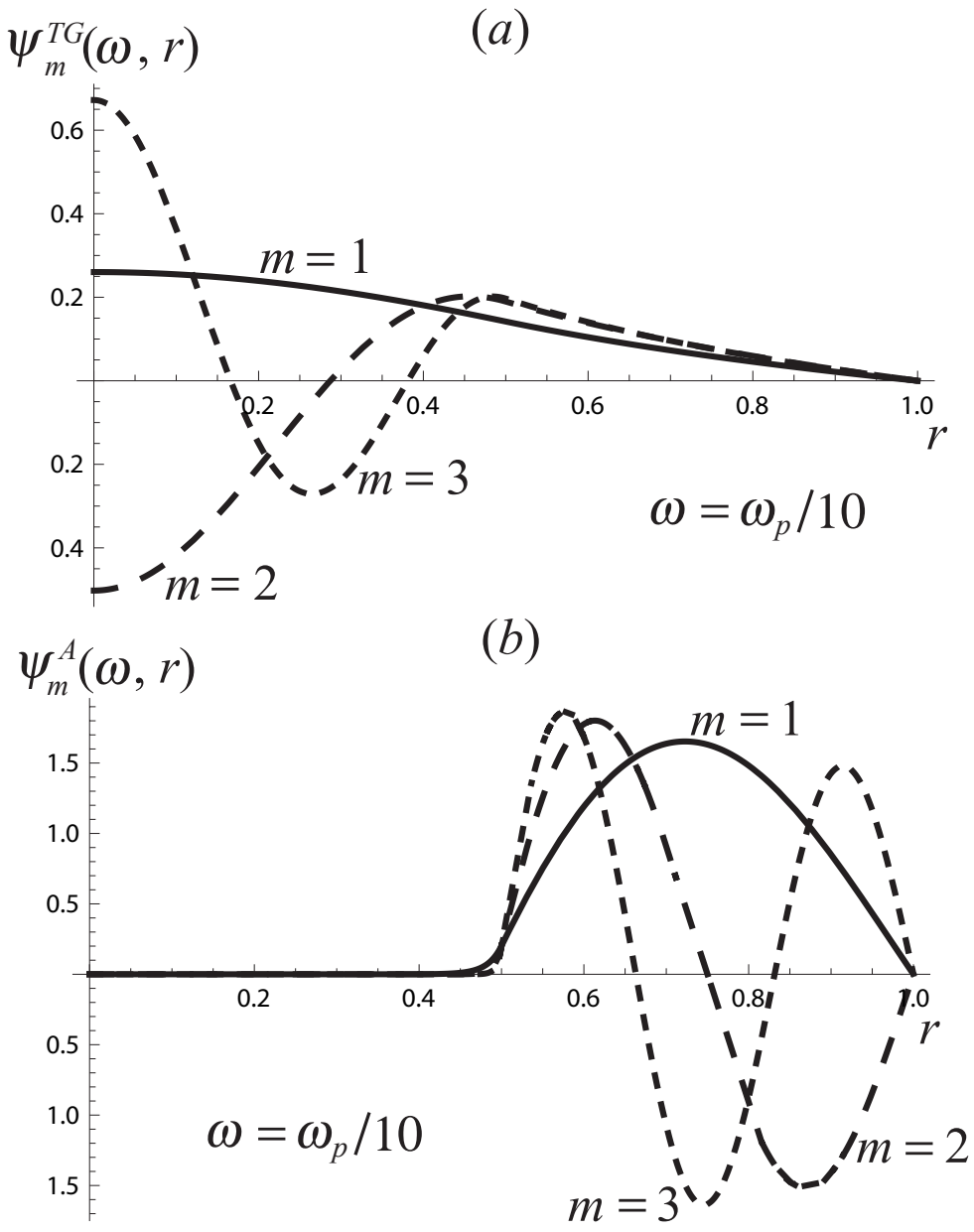

Figure 5.1. Several of the functions $\psi_m^{TG}(\omega;r)$ and $\psi_m^{A}(\omega;r)$ plotted for the parameter values $\omega/\omega_p = 0.1$, $a = 0.5$, and $R = 1$. These functions give the radial dependence of the Trivelpiece-Gould and annular solutions on an infinitely long plasma cylinder.

Figure. 5.2. The axial electric field, $\delta E_{z,\omega}$, and potential, $\delta\varphi_{\omega}$, corresponding to a solution of the matrix equation (5.37) obtained by retaining (*a*) 8 terms and (*b*) 16 terms in the series (5.30) and (5.31). The plasma has length $L = 14.0$ and radius $a = 0.5$, and the trap has radius $R = 1$. As the number of basis functions is increased, the solution involves increasingly large wavenumbers.

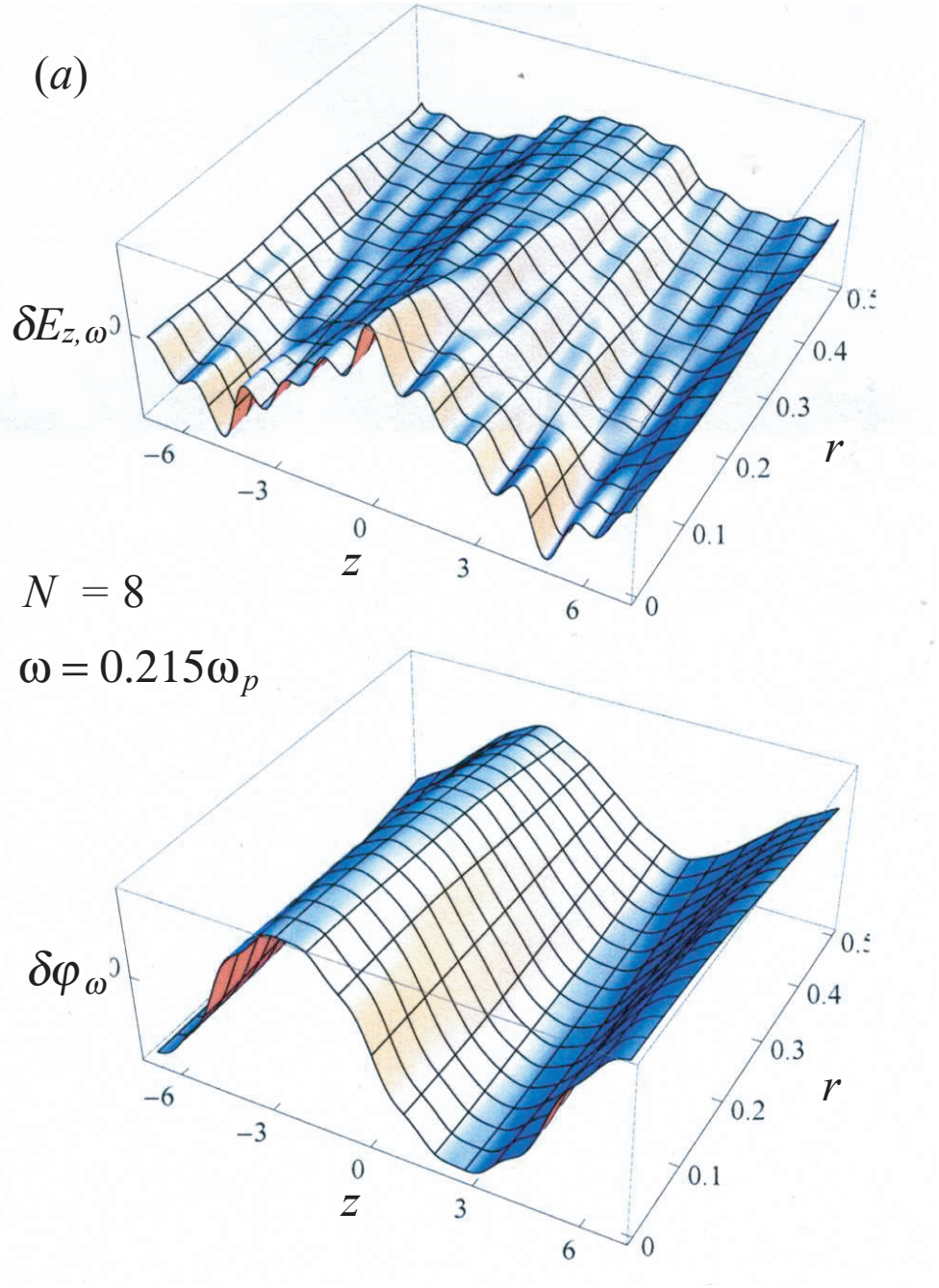
(a)
$\delta E_{z,\omega}$
−6
−3
0
3
6
z
0
0.1
0.2
0.3
0.4
r
$N = 8$
$\omega = 0.215\omega_p$
$\delta\varphi_\omega$
−6
−3
0
3
6
z
0
0.1
0.2
0.3
0.4
r

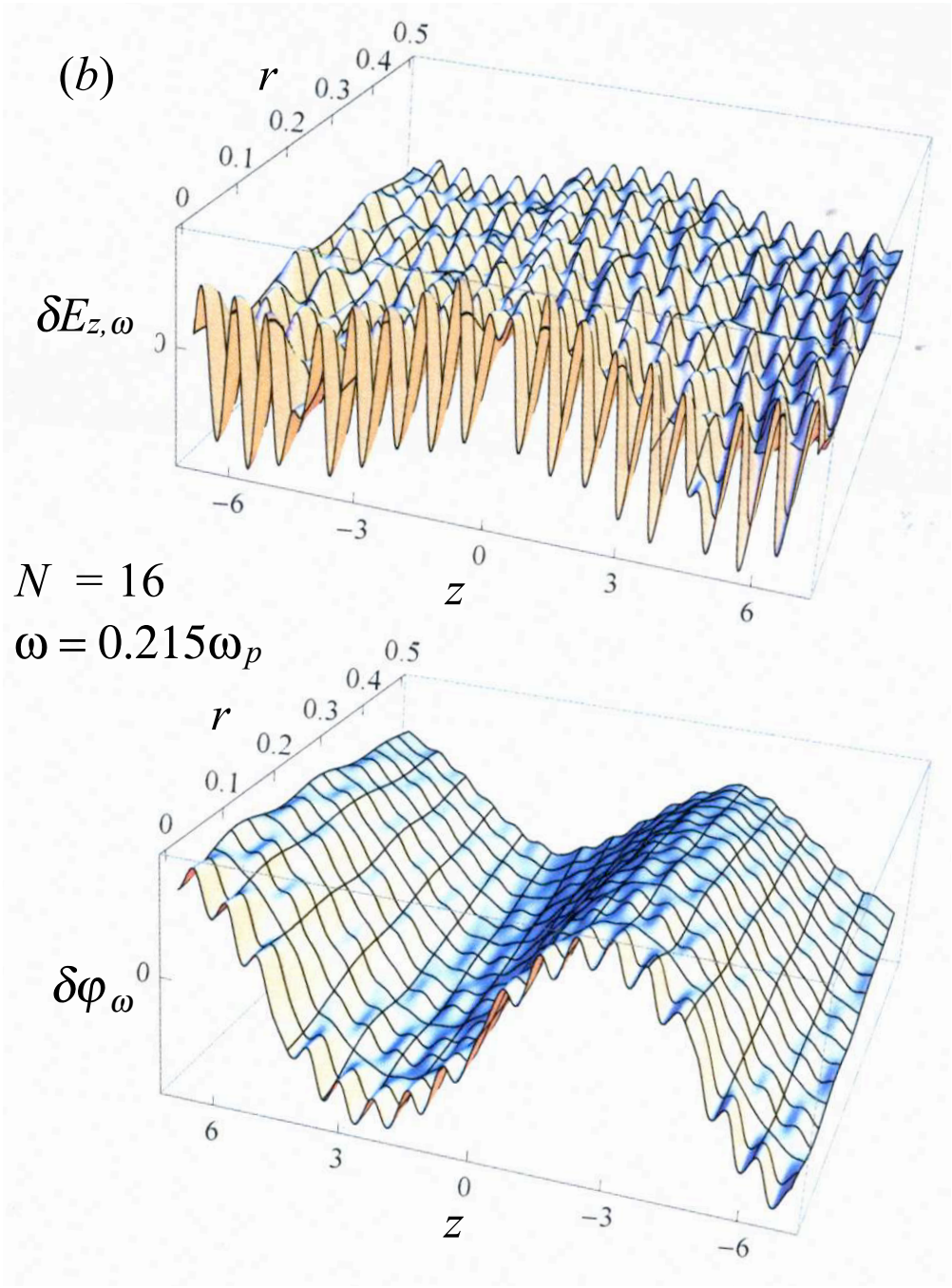

Figure 5.2, continued.

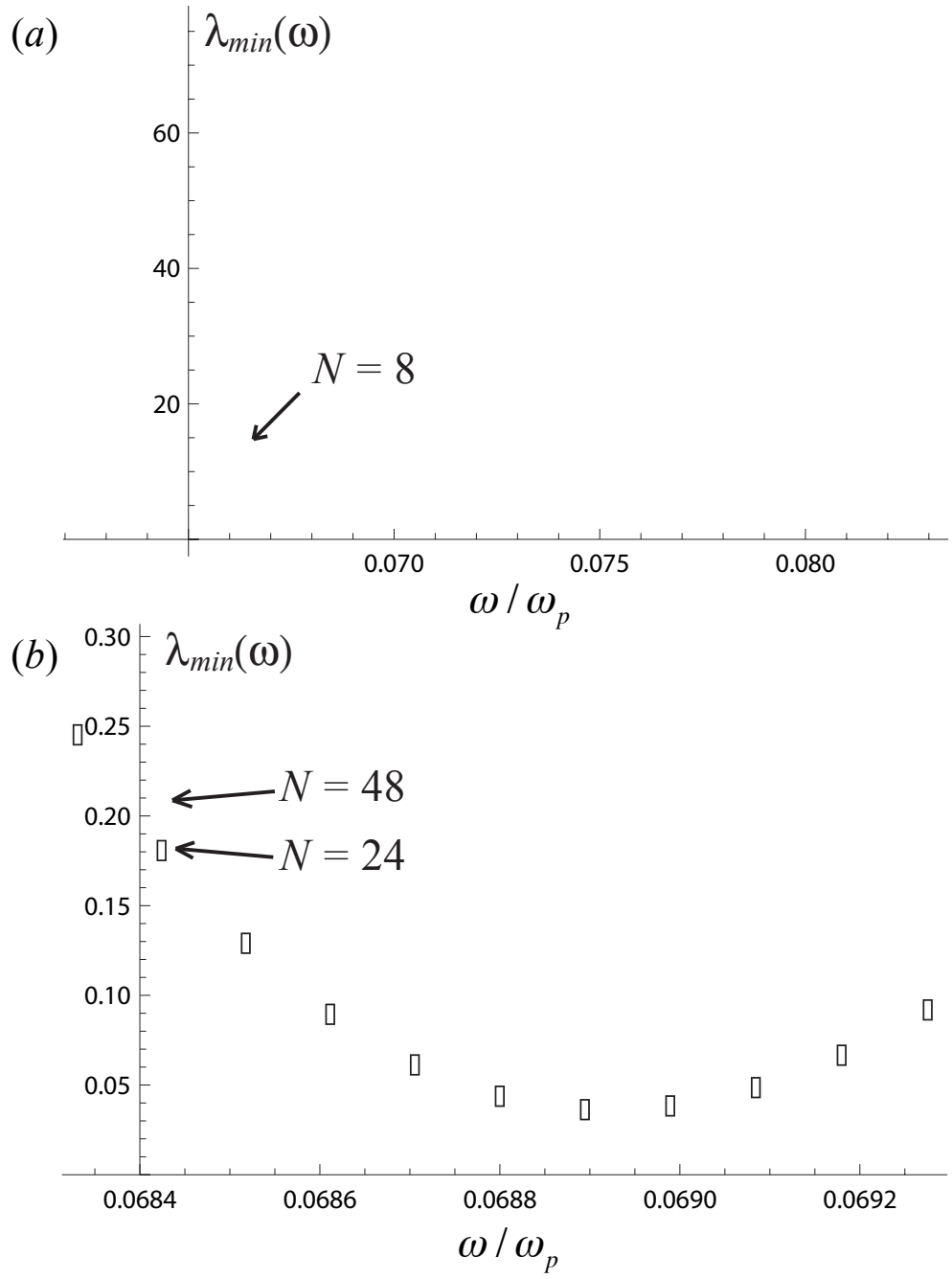

Figure 5.3. (*a*) Evaluation of the function $\lambda_{\min}(\omega)$ at discrete values of ω for $N = 8$ basis functions. The local minima near $\omega = 0.070\omega_p$ and $\omega = 0.078\omega_p$ indicate the frequencies of two low-order modes. (*b*) Evaluation of the function $\lambda_{\min}(\omega)$ on a finer grid in ω for $N = 24$ (open rectangles) and $N = 48$ (solid circles) basis functions.

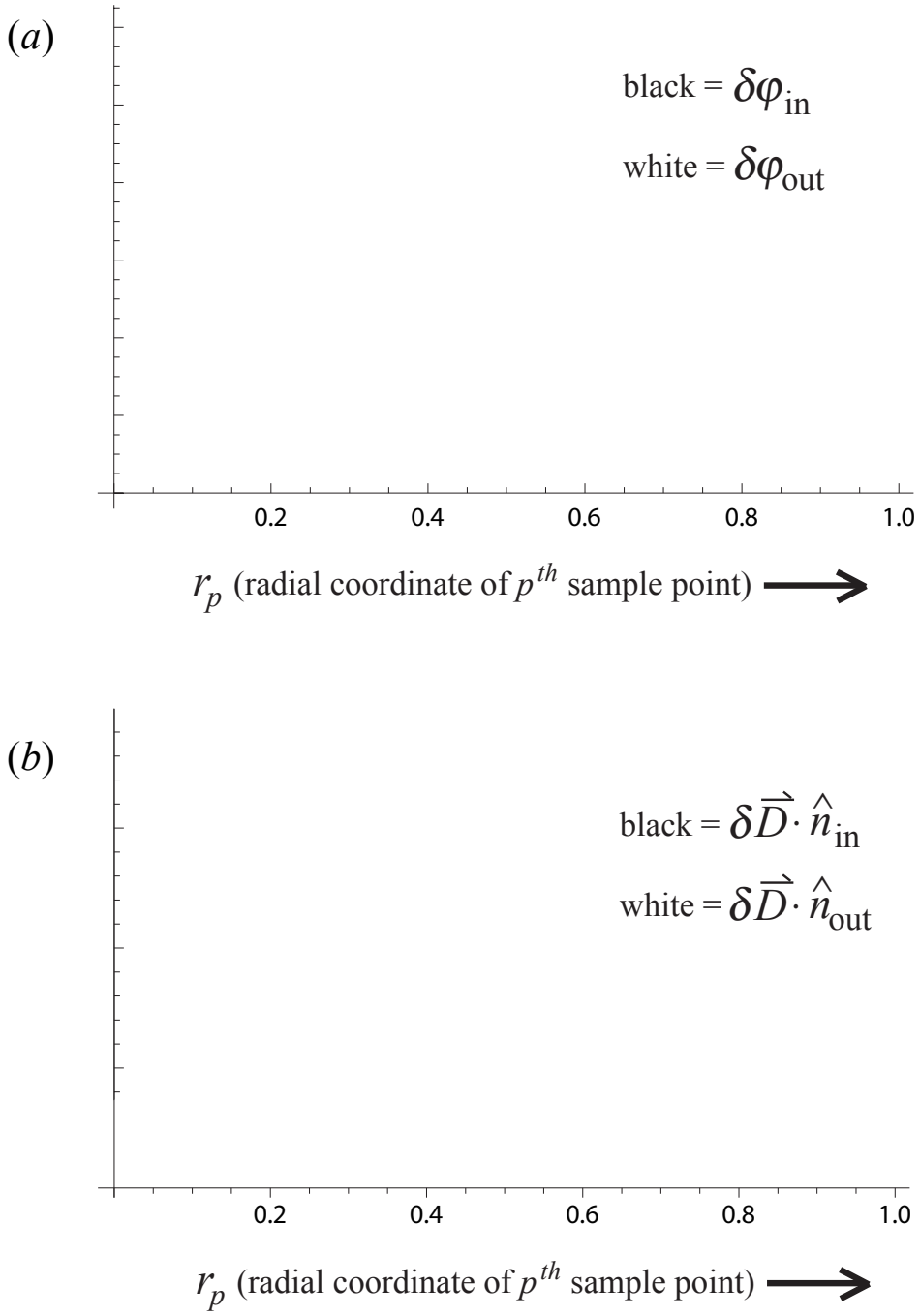

Figure 5.4. An example of the matching of (*a*) the mode potential and (*b*) the normal component of the electric displacement at the sample points along the matching surface. Each black circle/white square gives the value of the electric potential or normal component of the electric displacement as the sample point is approached from inside/outside. Here $N = 48$ and $P = 240$. The spatial dependence of this mode is displayed in Fig. 5.5(*a*).

Figure 5.5. (*a*) The axial electric field, $\delta E_{z,\omega}$, and potential, $\delta\varphi_{\omega}$, of a normal mode of a plasma with length $L + \Delta L_0 = 8.0$, radius $a = 0.33$, and end-shape $\Delta L_0 = a$; note the strong mixing of the $m = 1$ and $m = 2$ components. (*b*),(*c*) Two normal modes of a plasma cylinder with length $L + \Delta L_0 = 14.0$, radius $a = 0.5$, and end-shape given by $\Delta L_0 = 2a$. (*d*),(*e*) Two normal modes of a plasma cylinder with length $L + \Delta L_0 = 14.0$, radius $a = 0.5$ and end shape given by $\Delta L_0 = a$. In (*a*)-(*e*), the domain of each plot is the interior of the plasma, and the radius of the trap is $R = 1.0$.

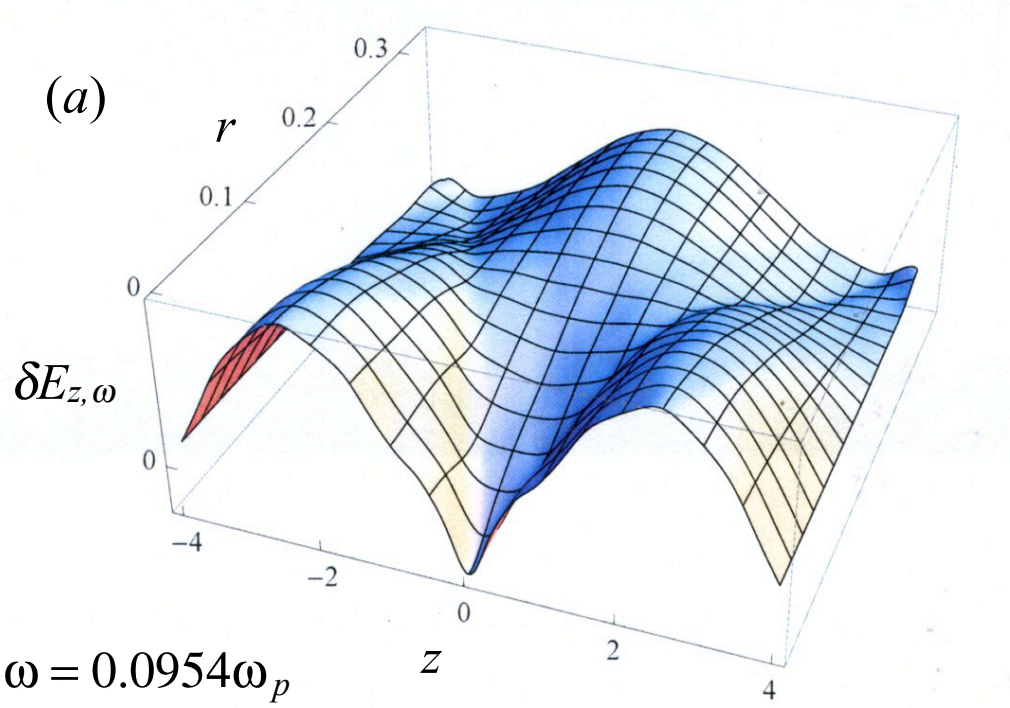

$\omega = 0.0954\omega_p$

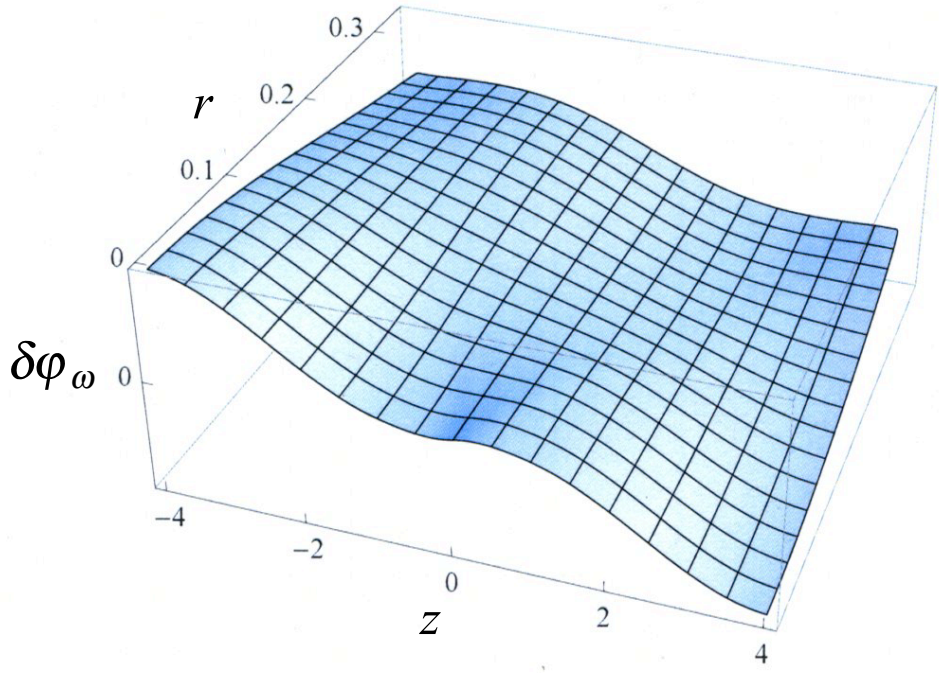

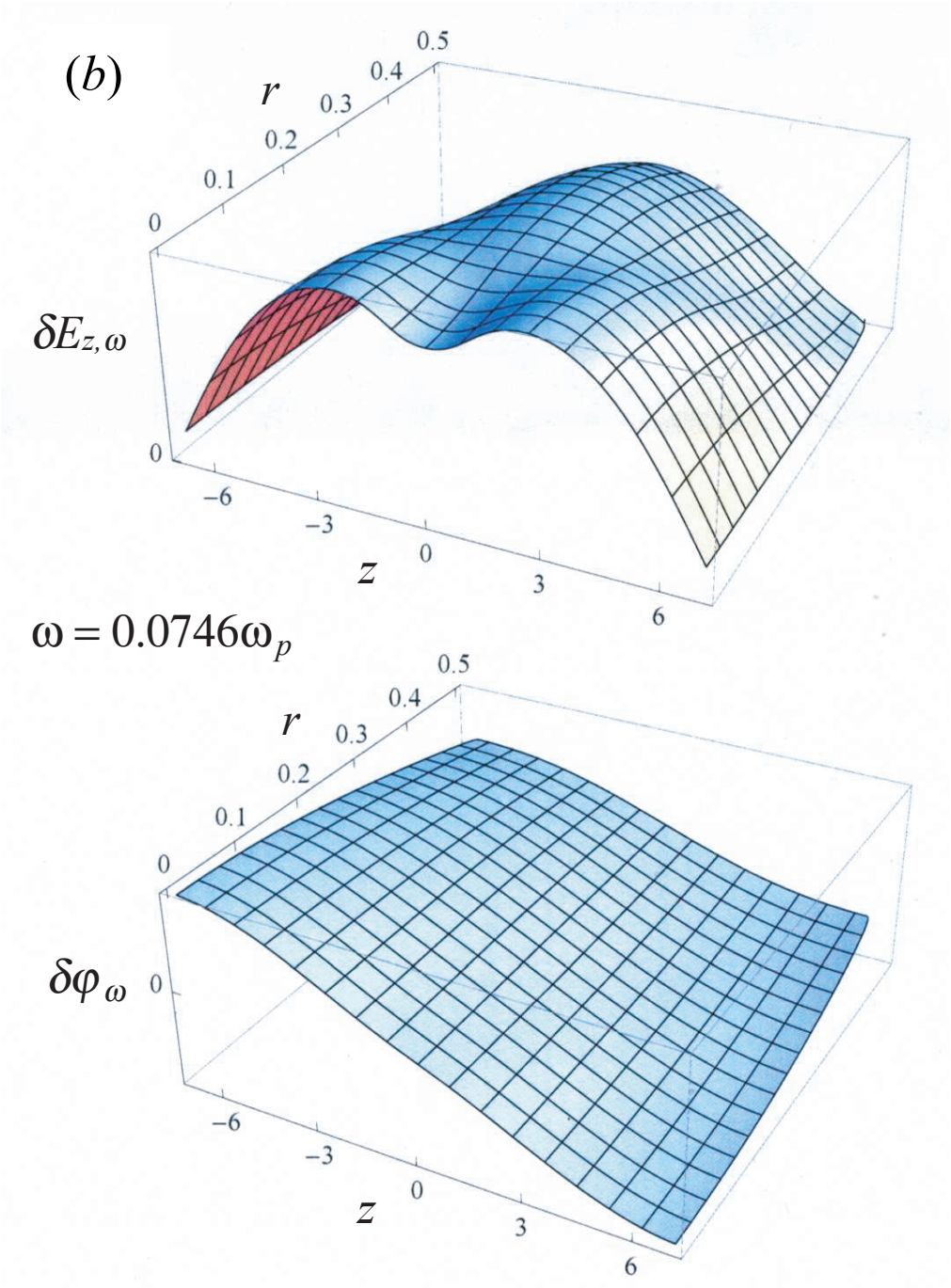

Figure 5.5, continued.

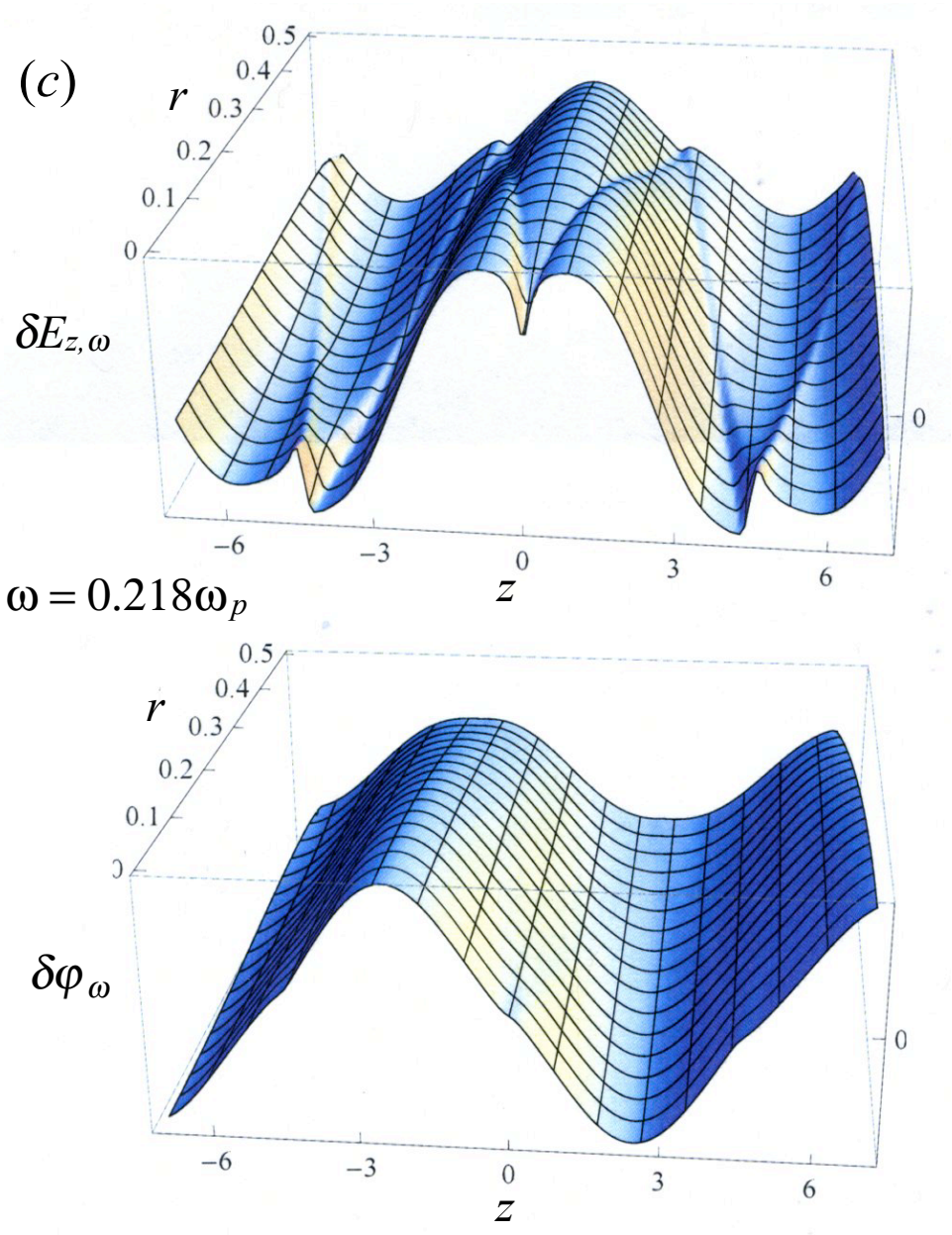

Figure 5.5, continued.

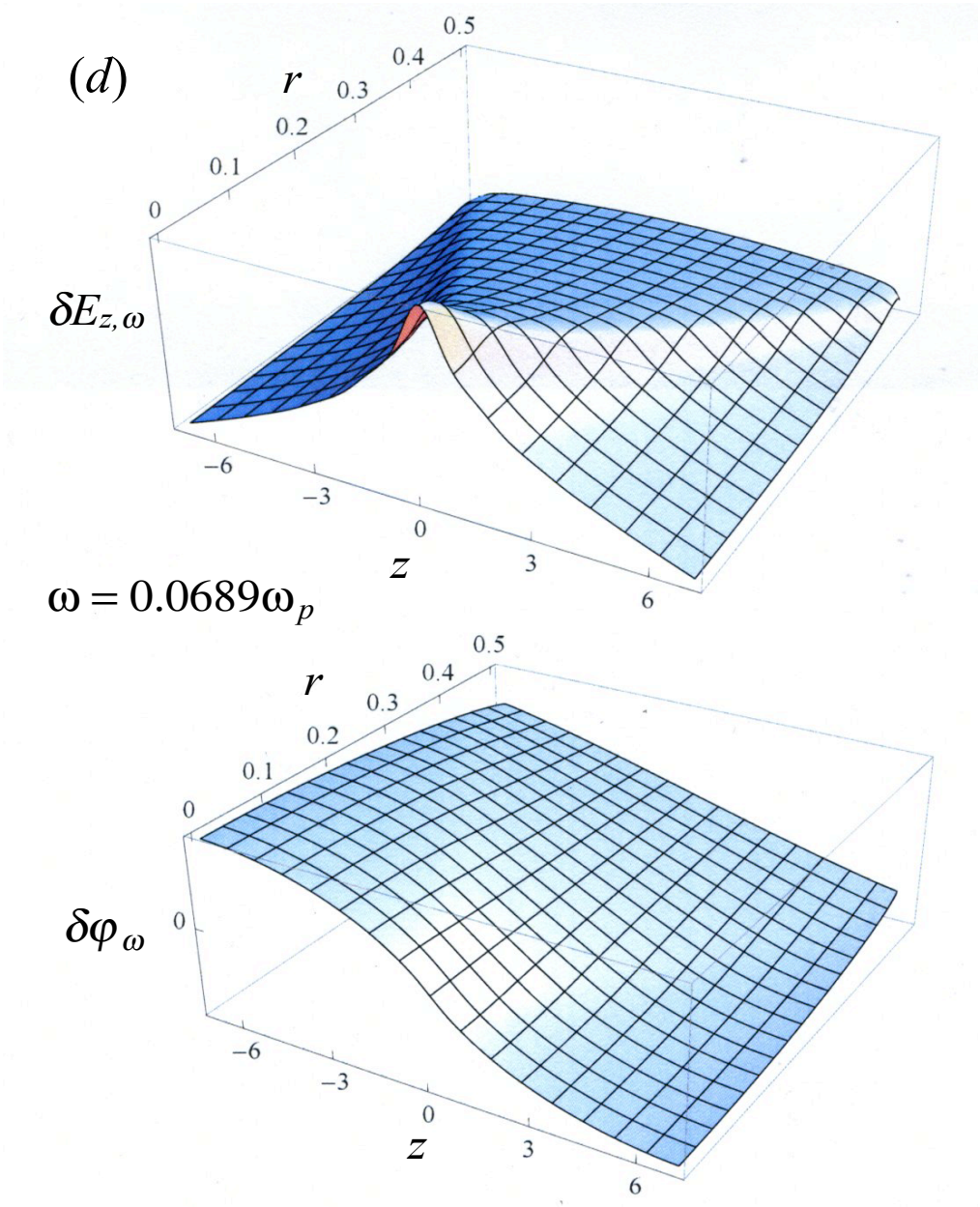

Figure 5.5, continued.

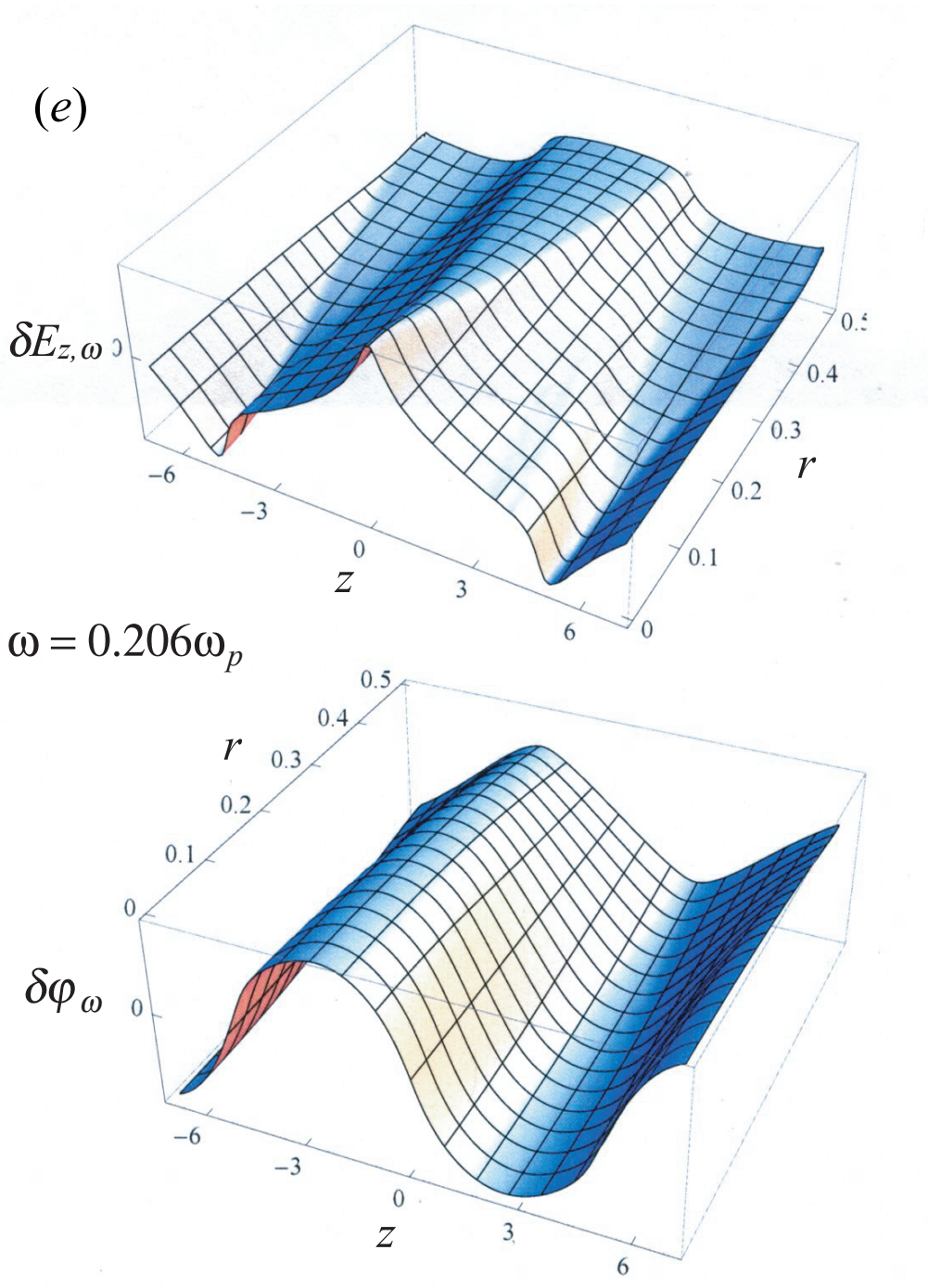

Figure 5.5, continued.

Figure. 5.6. (*a*) The axial electric field, $\delta E_{z,\omega}$, and potential, $\delta\varphi_{\omega}$, of a normal mode of a plasma with length $L + \Delta L_0 = 0.401$, radius $a = 0.200$, and end-shape given by $\Delta L_0 = 2a$. Note that this plasma is nearly spherical; the central cylindrical section of the plasma is only one four-thousandth the length of the plasma at $r = 0$. The radius of the trap is $R = 1.0$. (The convergence in the parameter regime $L << L_0, a << R$ is relatively poor compared with that for long cylindrical plasmas, so the fine-scale ripple in the electric field could be an artifact of the incomplete convergence.) (*b*) One of two $(l = 3, m = 0)$ modes of a perfectly spherical plasma in the limit $R \to \infty$. Note the similarity between these modes.

(a)

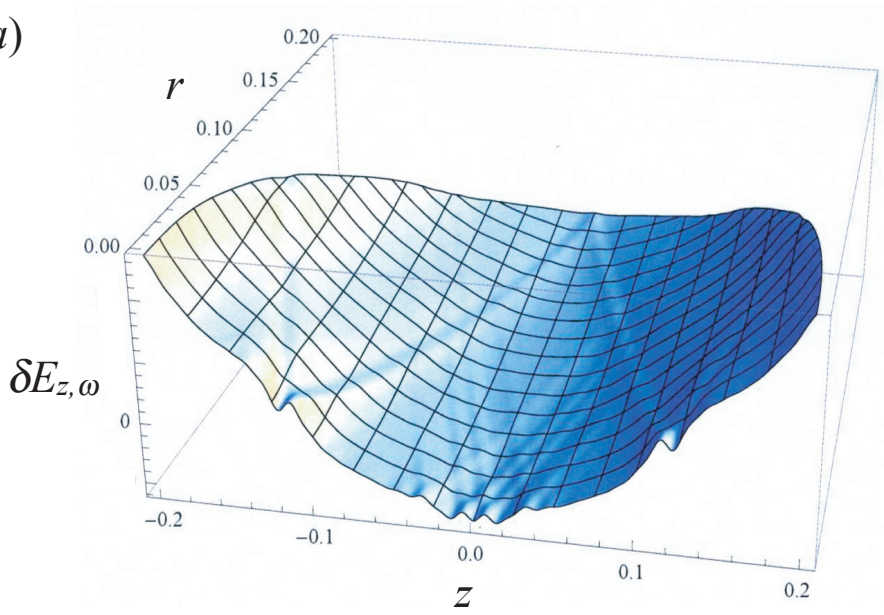

$\omega = 0.860\omega_p$

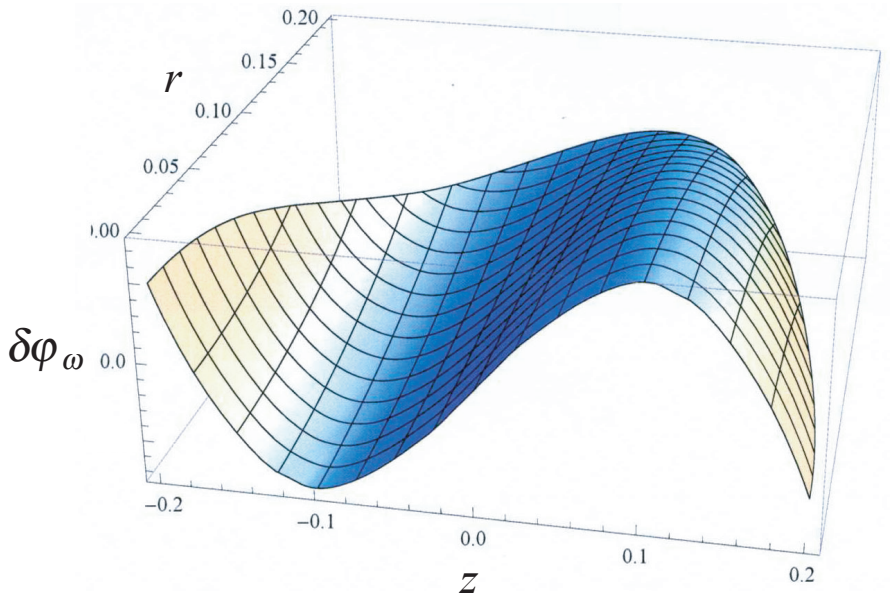

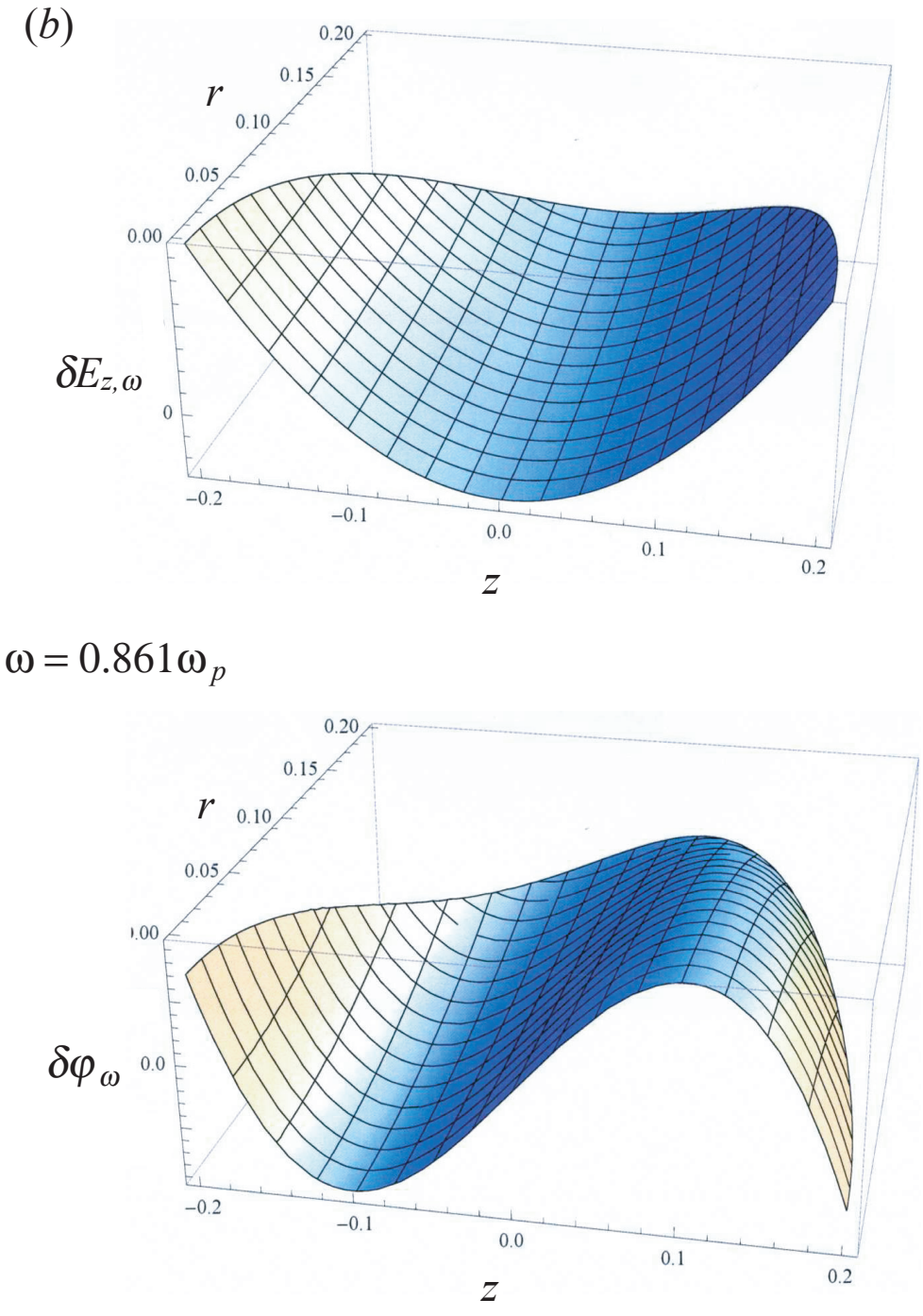

Figure 5.6, continued.

Epilogue

To conclude, we suggest several avenues for building upon the work presented in this dissertation.

First, while the effect of long-range collisions on plasma waves was given a simple treatment using fluid theory, a more satisfactory analysis might incorporate these collisions into the kinetic description of the wave. Dubin and O'Neil derived a collision operator for these non-point-like interactions, which could be employed to this end [23]. Also, as Dubin and O'Neil point out, cross-field transport can be enhanced by interactions over distances of many Debye lengths; in this case, the transport is mediated by the emission and absorption of plasma waves. However, this non-local transport was not considered in this dissertation; in taking the cross-field viscosity to be approximately $\eta \sim mn\nu_c\lambda_D^2$, we implicitly assumed that interactions are cutoff at the Debye length. More fundamentally, the fluid analysis itself presumes that transport is local.

One could also improve upon the mode calculations for the finite-length plasma column by taking a true cold equilibrium as the unperturbed plasma state. The plasma shape assumed in our calculations is only an idealization of the equilibrium shape, but Prasad and O'Neil have shown that the true shape can be calculated numerically. In fact, the mode calculations of Jennings *et al* [8] and Rasband *et al* [9] used true equilibria, but, as discussed in Chapter 5, the authors did not examine the electric fields associated with the modes--only the potentials--so the degree of mixing

between degenerate waves was severely underestimated.

In addition, an improved mode calculation might solve the eigenvalue problem for the mode electric field, yielding a complete set of modes all at once. (Recall that our method yields only one mode at a time.) With a complete set of modes, one could calculate the plasma response to an electrical signal applied to the trap wall, in accord with the standard method for exciting these modes in the laboratory. Since the modes are closely spaced in frequency, any signal that lasts for a finite time will likely excite not just a single mode, but multiple nearly degenerate modes.

Finally, we hope that the predictions described in this dissertation will be tested in the laboratory. In fact, there is an ongoing effort at UCSD to measure the collisional damping of plasma waves in a single-species plasma column. Francois Anderegg has measured the damping rate of longitudinal normal modes of a Mg^+ plasma in the low-temperature regime where Landau damping is negligible. At the time of these experiments, it was thought that the normal modes were simply standing Trivelpiece-Gould waves with axial wavenumbers quantized to fit the length of the plasma column. Thus, it seemed reasonable to compare the measured damping rate with the imaginary part of the complex frequency formula (1.1) for a Trivelpiece-Gould wave, using wavenumbers deduced from the measured wave frequency. However, across several decades in temperature, the measured damping rate exceeded the predicted rate by over an order of magnitude, even though the temperature scaling of the data seemed to agree with that of the formula.

Based on this uniform discrepancy, we concluded that we had identified the correct damping mechanism, but that perhaps the mode structure involved higher wavenumbers than expected, giving rise to the enhanced damping observed in the experiment. Indeed, this interpretation motivated the calculation of modes of a cold finite-length plasma column that forms the second part of this dissertation, and these calculations revealed that each mode involves many degenerate waves. Ironically, in the meantime, the damping rate was re-measured at smaller wave amplitude, and the new data exhibit a different temperature scaling. We now believe that the measured damping is the result of friction against impurities in the plasma, which is masking the far weaker damping associated with like-particle collisions. In order for the damping from like-particle collisions to be observed, the plasma must be rid of impurities.

References

[1] A. W. Trivelpiece and R. W. Gould, J. Appl. Phys. **30**, 1784 (1959).

[2] J. S. deGrassie and J. H. Malmberg, Phys. Rev. Lett. **39**, 1077 (1977).

[3] M. W. Anderson and T. M. O'Neil, Phys. Plasmas **14**, 112110 (2007).

[4] J. P. Dougherty, Phys. Fluids **7**, 1788 (1964).

[5] M. W. Anderson and T. M. O'Neil, Phys. Plasmas **14**, 052103 (2007).

[6] D. H. E. Dubin, Phys. Plasmas **5**, 1688 (1998).

[7] S. A. Prasad and T. M. O'Neil, Phys. Fluids **26**, 665 (1983).

[8] J. K. Jennings, R. L. Spencer, K. C. Hansen, Phys. Plasmas **2**, 2630 (1995).

[9] S. N. Rasband and R. L. Spencer, Phys. Plasmas **10**, 948 (2003).

[10] R. K. Fisher and R. W. Gould, Phys. Rev. Lett. **22**, 1093 (1969).

[11] A. Lenard and I. B. Bernstein, Phys. Rev. **112**, 1456 (1958).

[12] C. S. Ng, A. Bhattachrjee, and F. Skiff, Phys. Rev. Lett. **83**, 1974 (1999).

[13] R. W. Simon and A. Short, Phys. Plasmas **9**, 3245 (2002).

[14] C. S. Ng, A. Bhattacharjee, and F. Skiff, Phys. Rev. Lett. **92**, 065002 (2004).

[15] L. D. Landau, J. Phys (Moscow) **10**, 25 (1946).

[16] N. G. Van Kampen, Physica (Amsterdam) **21**, 949 (1955).

[17] L. Stenflo, J. Plasma Phys. **4**, 145 (1970).

[18] S. DeSouza-Machado, M. Sarfaty, and F. Skiff, Phys. Plasmas **6**, 2323 (1999).

[19] R. C. Davidson, *Theory of Neon-Neeutral Plasmas* (Imperial College and World Scientific, New York, 2001), p. 251.

[20] D. Nicholson, *Introduction to Plasma Theory* (Wiley, New York, 1983), p. 62.

[21] D. Bohm and E. P. Gross, Phys. Rev. **75**, 1851 (1949).

[22] J. D. Huba, *NRL Plasma Formulary* (Naval Research Laboratory, Washington, DC, 2009), p. 33.

[23] D. H. E. Dubin and T. M. O'Neil, Phys. Rev. Lett. **78**, 3868 (1997).

[24] D. H. E. Dubin and T. M. O'Neil, Rev. Mod. Phys. **71**, 87 (1999).

[25] S. A. Prasad and T. M. O'Neil, Phys. Fluids **22**, 278 (1979).

[26] R. W. Gould, *Personal Communication* (2010).

[27] L. R. Brewer, J. D. Prestage, J. J. Bollinger, W. M. Itano, D. J. Larson, and D. J. Wineland, Phys. Rev. A **38**, 859 (1988).

[28] D. H. E. Dubin, Phys. Rev. Lett. **66**, 2076 (1991).

[29] T. B. Mitchell, J. J. Bollinger, X. -P. Huang, and W. M. Itano, Optics Express **2**, 314 (1998).

[30] J. R. Danielson, F. Anderegg, and C. F. Driscoll, Phys. Rev. Lett. **92**, 245003 (2004).

[31] M. N. Rosenbluth, W. M. MacDonald, and D. L. Judd, Phys. Rev. **107**, 1 (1957).

[32] P. Bhatnagar, E. P. Gross, and M. K. Krook, Phys. Rev. **94**, 511 (1954).

[33] S. Chandrasekhar, Rev. Mod. Phys. **15**, 1 (1943).

[34] P. Resibois, J. Stat. Phys. **2**, 21 (1970).

[35] S. I. Braginskii, *Reviews of Plasma Physics, Vol. 1* (Consultants Bureau, New York, 1965), p. 205.

[36] A. W. Hyatt, C. F. Driscoll, and J. H. Malmberg, Phys. Rev. Lett. **59**, 2975 (1987).

[37] D. Montgomery, G. Joyce, and L. Turner, Phys. Fluids **17**, 954 (1974).

[38] L. D. Landau**,** Phys. Z. Sowjetunion **10,** 154 (1936).

[39] B. R. Beck, J. Fajans, J. H. Malmberg, Phys. Plasmas **3**, 1250 (1996).

[40] D. H. E. Dubin, Phys. Plasmas **12**, 042107:1-13 (2005).